MULTIPLE SCATTERING OF ELECTROMAGNETIC WAVES BY DISTRIBUTIONS OF PARTICLES WITH APPLICATIONS TO RADIO WAVE PROPAGATION THROUGH PRECIPITATION

by

Anastasios I. Tsolakis

Dissertation submitted to the Graduate Faculty of the
Virginia Polytechnic Institute and State University
in partial fulfillment of the requirements for the degree of

DOCTOR OF PHILOSOPHY

in

Electrical Engineering

APPROVED: _____

I. M. Besieris, Chairman

_____ _____

W. L. Stutzman C. W. Bostian

_____ _____

W. E. Kohler W. A. Davis

January, 1982

Blacksburg, Virginia

ACKNOWLEDGEMENTS

The author wishes to express his graditude and deep appreciation to Professors I. M. Besieris and W. L. Stutzman for their advice and guidance during the course of this research.

He is also indebted to Professors C. W. Bostian and W. A. Davis for their encouragement and helpful suggestions. Special recognition is due to Professor W. E. Kohler for his close involvement in Chapter 5 of this dissertation. In addition, he is indebted to all the members of the Satellite Communications Group at Virginia Tech, for their help and advice in the measurement aspects of this research.

The patience and understanding of Cynthia Will who typed this dissertation are thankfully acknowledged.

The research embodied in this dissertation was supported in part by the Office of Naval Research under Contract No. N00014-76-C-0056, NASA, Contract No. NAS5-22577, Intelsat Nos. INTEL-123, and INTEL-155.

TABLE OF CONTENTS

Page

CHAPTER I

INTRODUCTION

The study of wave propagation through an ensemble of discrete scattering is of importance in many physical areas. Among them we cite millimeter wave propagation through precipitation, light wave propagation through the atmosphere, and mirowave and light wave propagation through obscurants, such as smoke, dust, chemical clouds, etc.

The study of scattering by distributions of uncorrelated identical scatterers can be traced back to the original work of Rayleigh [1]. This work provided the first quantitative basis for the explanation of the blue color of the sky. A significant limitation of Rayleigh's work is that it cannot accommodate multiple scattering effects. The latter become important when the density of the scatterers is high and their scattering coefficients are large.

Fundamental work on multiple scattering of scalar waves by distributions of uncorrelated scatterers was initiated by Foldy [2] and it has been developed further by Lax [3] and Twersky [4]. Based on these original contributions, a great number of applications have appeared in the literature (cf., for example, Refs. 32-35) involving both the coherent field and the incoherent intensity.

The problem of assessing the multiple scattering effects on scalar and vector waves in the presence of random distributions of correlated scatterers is more challenging. Basic contributions along this direction have been made by Twersky [5] and Bringi *et al.* [6] in

connection with the coherent field, and by Barbanenkov and Finkel'berg [7] and Watson [8] in connection with the incoherent field intensity.

The motivation of the work leading to this thesis was based on the following considerations: (1) Inadequate coupling between available experimental data and theoretical results related to multiple scattering effects on the coherent field in the presence of a random distribution of uncorrelated scatterers; (2) Delineation of the regions of validity of single scattering vis-a-vis multiple scattering theories; (3) Absence of a second-order statistical theory for studying pulse propagation through random distributions of correlated scatterers.

In order to examine the depolarization effects of waves propagating through precipitation channels, a vector-valued Dyson equation for the coherent field in a distribution of uncorrelated scatterers is derived in the first part of the thesis following, essentially, Twersky's procedure. Specific applications of this equation are then made to problems dealing with millimeter wave propagation through ice and rain and the theoretical results are compared with existing experimental data. Finally, the domains of validity of single scattering vis-a-vis multiple scattering theories are ascertained.

Twersky's procedure is extended in the second part of the thesis in order to derive a vector-valued Dyson equation and a tensor-valued two-frequency Bethe-Saltpeter equation for waves propagating in a distribution of spatially pair-correlated absorptive scatterers. These equations are subsequently specialized to the case of a tenuous

medium consisting of a random distribution of pair-correlated isotropic absorptive scatterers, and an analogy is established between the Dyson equation and the Bethe-Saltpeter equation for the discrete case and the corresponding equations associated with a continuous random medium under the assumption of Gaussian statistics.

The last part of the thesis provides a systematic transition from the Dyson equation and the two-frequency Bethe-Saltpeter equation to a two-frequency radiative transfer equation suitable for pulsed scalar waves in the presence of a random distribution of absorptive discrete scatterers with pair correlations. This transition is effected by a continuous stochastic transport theory that was originally introduced by Barabanenkov et al. [9] and subsequently extended to the two-frequency context by Besieris and Kohler [10].

The structure of the thesis is organized as follows: Some preliminary work dealing with single particle scattering is discussed in Chapter II. A vector-valued Dyson equation for the coherent field in a distribution of uncorrelated scatterers is derived in Chapter III using Twersky's procedure. Applications of the main results contained in Chapter III to millimeter wave propagation through ice and rain are discussed in detail in Chapter IV. Chapter V contains three parts: (1) A derivation of a vector-valued Dyson equation and a matrix-valued two-frequency Bethe-Saltpeter equation for a general distribution of pair-correlated absorptive scatterers; (2) A specialization of these two equations to the case of a tenuous medium consisting of pair-correlated isotropic absorptive scatterers;

(3) A systematic transition via a wave-kinetic approach to a two-frequency radiative transfer equation. The main contributions contained in the thesis, as well as several possible extensions and applications, are discussed in Chapter VI.

CHAPTER II

SCATTERING BY A SINGLE PARTICLE

In order to study radio wave or light wave propagation through an ensemble of scatterers, the scattering properties of individual scatterers must first be determined. Knowing the scattering properties of the individual scatterers, the effects of the ensemble of the scatterers to the propagating wave can be studied.

In this chapter, we will present the general formulation for a plane wave scattered by a single scatterer. Since the exact solution to this problem exists only when the scatterer is a sphere (Mie-solution), approximations to the general formulation will be given. After establishing calculation procedures for scattering by a single scatterer, scattering by an ensemble of scatterers will be discussed in the next chapter.

2.1 The Single-Scatterer Problem

Let us consider a scatterer enclosed in volume V' having permittivity ε and permeability μ_o. The medium in which the scatterer is embedded is vacuum, with parameters ε_o, μ_o (see Fig. 2.1). $\vec{E}_o$ is the incident plane wave upon the scatterer. The total electric field $\vec{E}(\vec{r})$ obeys the Fredholm integral equation [11].

$$\vec{E}(\vec{r}) = \vec{E}_o + (\vec{\nabla}\vec{\nabla}\cdot + k_o^2) \frac{1}{4\pi\varepsilon_o} \int_{V'} (\varepsilon - \varepsilon_o) \vec{E}(\vec{r}') \psi(\vec{r}, \vec{r}') \, dV' \quad , \quad (2\text{-}1)$$

where

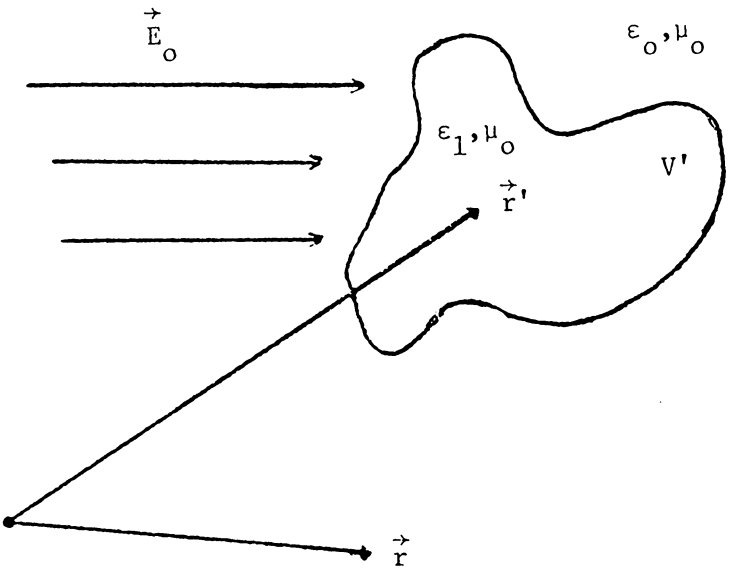

Figure 2.1. Geometry for scattering of a plane wave by a single particle.

$$\psi(\vec{r}, \vec{r}') = \exp\{-jk_o |\vec{r} - \vec{r}'|\}/|\vec{r} - \vec{r}'| \qquad (2\text{-}2a)$$

and k_o is the free space wave number

$$k_o^2 = \omega_o^2 \mu_o \varepsilon_o \quad . \qquad (2\text{-}2b)$$

Equation (2-1) has an exact solution only when the scatterer is a sphere (Mie-Theory). A detailed derivation for the scattered field by a sphere is presented in Ref. [12]. For arbitrary scatterers, different approximations exist to equation (2-1). In most practical situations, and especially in propagation through precipitation, we are interested in the scattered field in the far zone. At a large distance $\vec{r}$ from the scatterer the scalar Green's function $\psi(\vec{r}, \vec{r}')$ may be approximated as

$$\psi(\vec{r}, \vec{r}') \sim \exp\{-jk_o(\vec{r} - \hat{r} \cdot \vec{r}')\}/r \quad , \qquad (2\text{-}3a)$$

where

$$r = |\vec{r}| \qquad (2\text{-}3b)$$

and

$$\hat{r} = \frac{\vec{r}}{|\vec{r}|} \quad . \qquad (2\text{-}3c)$$

Under this approximation the total field in the far zone may be written as

$$\vec{E}(r) \simeq \vec{E}_o + \frac{k_o^2 e^{-jk_o r}}{4\pi\varepsilon_o r} \int_{V'} (\varepsilon - \varepsilon_o)\, \vec{E}(\vec{r}') \cdot (\bar{I} - \hat{r}\hat{r})\, e^{jk_o \hat{r} \cdot \vec{r}'}\, dV' \quad , \qquad (2\text{-}4a)$$

where $\bar{I}$ is the unit dyadic. The field scattered by the scatterer in the far zone is given by

$$\vec{E}_s(\vec{r}) \simeq \frac{k_o^2 e^{-jk_o r}}{4\pi\varepsilon_o r} \int_{V'} (\varepsilon - \varepsilon_o)\, \vec{E}(\vec{r}') \cdot (\bar{I} - \hat{r}\hat{r})\, e^{jk_o \hat{r} \cdot \vec{r}'}\, dV' \,. \tag{2-4b}$$

Depending on the scatterer size relative to wavelength and its dielectric constant, different approximations can be made to equation (2-4). In the following, three important approximations will be discussed: Rayleigh scattering, Rayleigh-Gans scattering and the WKB approximation.

a) Rayleigh Scattering [13]:

When the dimensions of the scatterer are very small relative to wavelength, in other words, when $k_o|\underline{r}'| << 1$, the exponential within the integrand of Eq. (2-4) may be replaced by unit. Then,

$$\vec{E}(\vec{r}) = \frac{k_o^2 e^{-jk_o r}}{4\pi\varepsilon_o r} \{\vec{p} - (\vec{p} \cdot \hat{r})\hat{r}\} \quad , \tag{2-5a}$$

where

$$\vec{p} = \varepsilon_o \int_{V'} (\varepsilon_r - 1)\, \vec{E}(\vec{r}')\, dV' \quad . \tag{2-5b}$$

The scatterer in this case radiates as an electric dipole of moment $\vec{p}$.

Equation (2-5) holds under two assumptions [14]. Let ℓ be the maximum dimension of the scatterer. Then, $k_o \ell$ must be much less than unity ($k_o \ell << 1$), and $|k_o\, \varepsilon_r \ell| << 1$. The first assumption, i.e.,

$k_o \ell << 1$, justifies the derivation of (2-5) and also indicates that the scatterer may be regarded as placed in a uniform external field. The assumption that $|k_o \varepsilon_r \ell| << 1$ implies that the field inside the scatterer follows the external field instantaneously, so that the phase changes are of no consequence.

The problem is thus reduced to a static one. We have to determine the internal field of the scatterer induced by a uniform electrostatic external field. By using Eq. (2-5b), the dipole moment of the scatterer can be calculated from the internal field. In Ref. [15], the dipole moments of an oblate and prolate spheroid are calculated under the Rayleigh scattering assumptions. These results are used to calculate the scattering matrix of an ice-needle (prolate spheroid with eccentricity equal to one), and an ice plate (oblate spheroid with unity eccentricity). In Chapter IV, these scattering matrices are used in studying wave propagation through ice clouds.

b) Rayleigh-Gans Scattering:

The index of refraction of the scatterer is given by $\eta = \sqrt{\varepsilon_r}$, where ε_r is the relative permittivity of the scatterer. In Rayleigh scattering, no specific assumptions about η were made. When η is approximately equal to unity, the scatterer is called diaphanous [14]. For a diaphanous scatterer with $k_o \ell \, |\eta^2 - 1| << 1$, the Rayleigh-Gans [16] or Born [17] approximation holds.

In the Rayleigh-Gans approximation the field $\vec{E}(\vec{r})$ inside the scatterer is approximated with the incident field $\vec{E}_o$. Under this

assumption, the far-zone scattered field $\vec{E}_s(\vec{r})$ from Eq. (2-4) becomes

$$\vec{E}_s(\vec{r}) = \frac{k_o^2 e^{-jk_o r}}{4\pi\varepsilon_o r} \int_{V'} (\varepsilon - \varepsilon_o) (\vec{E}_o - (\vec{E}_o \cdot \hat{r})\hat{r}) e^{+jk_o \hat{r} \cdot \vec{r}'} dV' \quad . \tag{2-6}$$

For a homogeneous diaphanous sphere (see Fig. 2.2) the scattered field takes the form

$$\vec{E}_s(\vec{r}) = k_o^2 \frac{e^{-jk_o r}}{4\pi\varepsilon_o r} (\varepsilon - \varepsilon_o) \{\vec{E}_o - (\vec{E}_o \cdot \hat{r})\hat{r}\}$$

$$\int_o^{2\pi} d\phi' \int_o^{\pi} \sin\theta' \, d\theta' \int_o^{a} r'^2 \exp\{2j \, k_o \sin(\theta/2) \cos\theta'\} \, dr' \tag{2-7a}$$

$$= \frac{k_o^2 e^{-jk_o r}}{\varepsilon_o r} (\varepsilon - \varepsilon_o) \{\vec{E}_o - (\vec{E}_o \cdot \hat{r})\hat{r}\} \left[\frac{\sin(2 k_o \sin(\theta/2)a)}{2 k_o \sin(\theta/2)}\right.$$

$$\left. - \frac{a \cos(2 k_o \sin(\theta/2)a)}{(2 k_o \sin(\theta/2))^2}\right] \quad , \tag{2-7b}$$

where a is the radius of the sphere and θ is the angle between $\vec{r}$ and the z-axis, assuming that the origin is the center of the sphere. For more complicated shapes of scatterers the volume integral in Eq. (2-7a) cannot be calculated analytically and numerical solutions must be used. Exact evaluation of the volume integral can be done for ellipsoids [ ].

c) High Frequency Scattering; The WKB Method:

The WKB approximation is applicable to cases where the Rayleigh or the Rayleigh-Gans approximations cannot be applied. Specifically the WKB approximation holds when

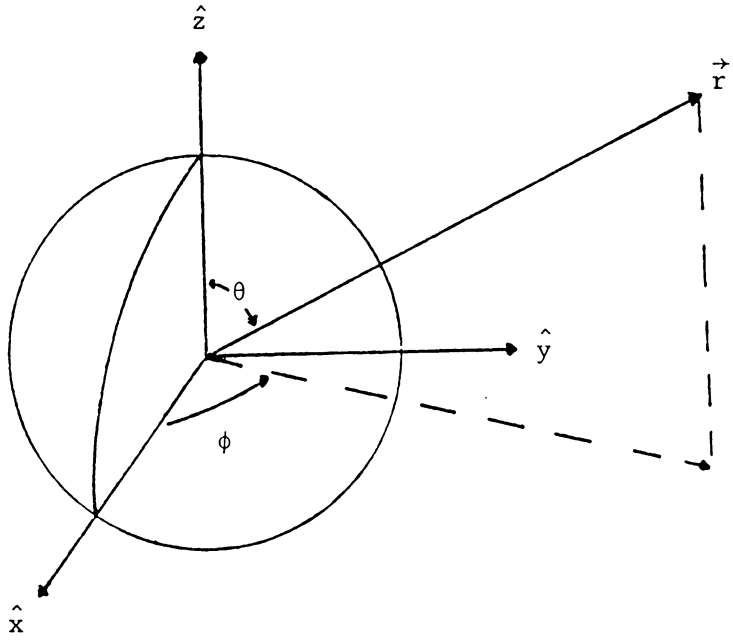

Figure 2.2. Geometry for scattering by a diaphanous sphere.

$$|\eta^2 - 1|\ k_o \ell >> 1 \quad \text{and} \quad |\eta^2 - 1| < 1 \quad . \tag{2-8}$$

In the WKB approximation the field $\vec{E}(\vec{r})$ inside the volume V' is approximated by a plane wave propagating in the same direction as the indicent field, with propagation constant equal to

$$k^2 = \omega^2 \mu_o \varepsilon_o = (\eta k_o)^2 \quad . \tag{2-9}$$

Under these assumptions equation (2-4) takes the form

$$\vec{E}(r) \simeq k_o^2 \frac{e^{-jk_o r}}{4\pi\varepsilon_o r} \int_{V'} \frac{2(\varepsilon - \varepsilon_o)}{\eta + 1} \vec{E}_o\, e^{-j[k_o z_1 + k_o \eta(z' - z_1)]} \times e^{jk_o \hat{r} \cdot \vec{r}'} dV' \quad . \tag{2-10}$$

The incident plane wave is assumed to be propagating in the z-direction. z_1 is the value of z' associated with $\vec{r}'$ for points lying on the surface of the scatterer as shown in Fig. 2.3. The factor $\frac{2}{\eta + 1}$ is the normal incidence transmission coefficient from vacuum to the medium of the scatterer.

The WKB approximation is part of a general mathematical method developed by Wentzel, Kramers, and Brillouin [18]. According to the WKB method the field inside the scatterer is expanded in the series

$$\vec{E}(r) = e^{-jk_o f(\vec{r})} \{\vec{E}_o + \frac{\vec{E}_1}{k_o} + \frac{\vec{E}_2}{k_o^2} + \ldots\} \quad . \tag{2-11}$$

Using the above equation in conjunction with Eq. (2-2) and collecting together like powers of k_o, a set of equations can be obtained for

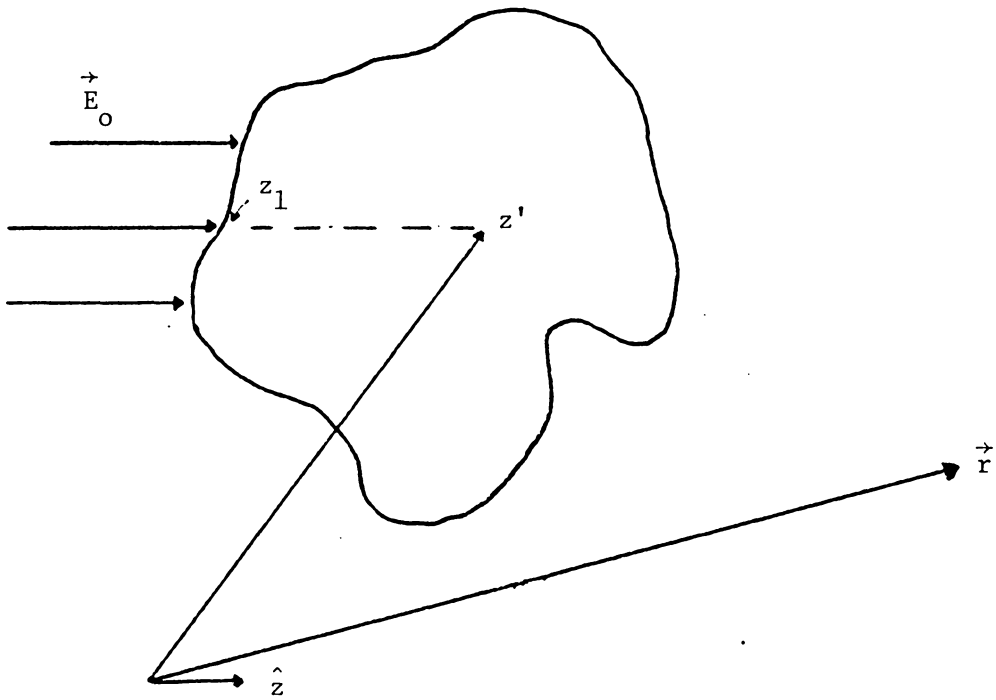

Figure 2.3. Geometry in calculating the scattered field by WKB approximation.

$f(\vec{r})$, $\vec{E}_o$, $\vec{E}_1$, $\vec{E}_2$, ... , etc.. For high frequencies, $k_o(\eta^2 - 1)\ell >> 1$. In this case $\vec{E}(\vec{r})$ can be approximated by

$$\vec{E}(\vec{r}) \simeq e^{-jk_o f(\vec{r})} \vec{E}_o \quad , \tag{2-12}$$

and equation (2-10) is obtained.

The three approximations discussed so far are valid only in specific cases when certain assumptions hold. However, in many scattering problems it is necessary to calculate the scattered field when none of the aforementioned approximations hold. For these specific problems exact analytical results do not exist. Most of the work in this area is based on numerical techniques and the use of fast computational machines. In the next few paragraphs we will summarize the most commonly used methods to calculate the scattered field by a dielectric body with complex permittivity. The majority of these methods have been used to calculate the scattering coefficients of a spheroidal or ellipsoidal scatterer.

i) Point-Matching Technique:

In the point-matching solution the incident field, the scattered field, and the field inside the scatterer are expanded in terms of spherical wave functions. The infinite modal summations of the expansions are truncated at some modal index (M, N), and boundary conditions are applied to the same number of points as the number of unknown expansion coefficients. The coefficients are then calculated by inverting a square M*N matrix that is formulated by the boundary

conditions at M*N points.

The method described above has been used by Oguchi [13]. Morrison and Cross [20] also used the point-matching technique with a least squares fit. In the latter case the number of boundary points is larger than the number of unknown coefficients and the fields are matched at these points in the sense of least squares. The least squares fit technique converges much faster than the one used by Oguchi.

ii) Spheroidal Wave Function Expansions:

The scattering properties of a spheroidal scatterer are obtained by expanding the fields in spheroidal vector wave functions and truncating the infinite summation of the expansion to a finite sum. The unknown coefficients of the expansion functions are evaluated by applying boundary conditions. Usually, spheroidal wave function expansion methods require the boundary conditions to be applied to fewer points than the point matching technique, especially when the scatterer is a spheroid. This method has been applied by Oguchi [21].

iii) Waterman's T Matrix Formulation (Extended Boundary Condition):

This technique has been used extensively for scattering by perfectly conducting bodies. Recently, the technique has been applied to dielectrics. The scattered field is expressed in terms of electric and magnetic surface currents. These currents are expanded in terms

of M_{rnm}, N_{rnm} [22] spherical harmonics. Boundary conditions are applied on an inscribed sphere inside the scatterer. By truncating the infinite expansion of the currents, the expansion coefficients can be obtained by matrix inversion.

iv) Fredholm Integral Equation Method:

This method was introduced by Holt, Uzunoglou and Evans [23]. Starting with the integral equation for scattering (see Eq. 2-1), it is shown that the Fourier transform of the field inside the scatterer is the solution of two coupled integral equations. The integrations are reduced by numerical quadrature methods to matrix equations, whose solution can be easily obtained. It is important to notice that the scattering amplitude obtained by this method satisfies the Schwinger variational principle, and thus the method is stable.

Of these numerical methods the most favorable are Waterman's method and the Fredholm Integral Equation method, since both converge rapidly over a wide range of scatterer sizes. It should be noted though that the latter needs a large amount of computer storage when the shape of the scatterer has a complicated structure.

2.2 The Scattering Tensor

In the previous section it was discussed that the far zone scattered field may be calculated by either an analytical or numerical method. Assuming that the incident field $\vec{E}_o$ is a plane wave propagating in the z direction the far-zone scattered field that is given by

equation (2-4) has components perpendicular to the direction of propagation and can be expressed in the vector form

$$\vec{E}_s(r) = \frac{e^{-jkr}}{r} \bar{f}(\vec{r})\, \vec{E}_o \quad , \tag{2-13}$$

where $\bar{f}(\vec{r})$ is the scattering tensor of the scatterer. For Rayleigh-Gans scattering it is clear from Eq. (2-6) that the scattering tensor is given by

$$\bar{f}(\vec{r}) = \frac{k_o^2}{4\pi\varepsilon_o} \int_{V'} (\varepsilon - \varepsilon_o)\, (\bar{I} - \hat{r}\hat{r})\, e^{+jk_o \hat{r} \cdot \vec{r}'}\, dV' \quad . \tag{2-14}$$

Equation (2-13) may be written in a matrix form

$$\begin{bmatrix} E_{x_s} \\ \\ \\ E_{y_s} \end{bmatrix} = \frac{e^{-jkr}}{r} \underline{f}(\vec{r}) \begin{bmatrix} E_{ox} \\ \\ \\ E_{oy} \end{bmatrix} \quad , \tag{2-15}$$

where $\underline{f}(\vec{r})$ is a 2×2 matrix corresponding to the scattering tensor

$$\underline{f}(\vec{r}) = \begin{bmatrix} f_{11} & f_{12} \\ \\ \\ f_{21} & f_{22} \end{bmatrix} \quad . \tag{2-16}$$

In most scattering problems the goal is to calculate the scattering matrix of the scatterer. In this thesis the scattering matrix of ice particles and raindrops will be used to study radio wave propagation through ice clouds and rain. The scattering matrix of

the ice-particles (needles, plates) was calculated using the Rayleigh approximation, since ice particles are Rayleigh scatterers up to 50 GHz [24]. For the calculation of the raindrop scattering matrix the Fredholm Integral Equation method was used. The size of the raindrops is of the order of the wavelength in the microwave region, and the Rayleigh or the Rayleigh-Gans approximations do not hold. It was necessary then to use a numerical method to compute the scattering matrix.

In this chapter we discussed, in summary, scattering by one particle, and the different approximations used in the computation of the scattered field. Our major goal is to study wave propagation through distribution of scatterers and apply the results of our study to radio wave propagation through precipitation (ice, rain). In the next chapter we will treat wave propagation through an ensemble of scatterers incorporating the single scatterer results.

CHAPTER III

SCATTERING BY A DISTRIBUTION OF SCATTERERS

It was shown in Chapter II that the field scattered by one particle obeys an integral equation that may be solved numerically or by using approximations. Problems that involve more than one scatterer are more complicated, and in general, cannot be solved analytically. In these cases, it is necessary to make certain assumptions in order to simplify them. A commonly used assumption is that the scatterers are randomly distributed, and that they are infinite in number. Also, it is assumed that each scatterer is in the far zone of all others.

Scattering by random distributions of scatterers was first studied by Rayleigh [1]. In Rayleigh's work all the scatterers are identical and aligned, and the single scattering approximation is used. A detailed derivation of the Rayleigh results is presented in Ref. [25]. The single scattering approximation does not hold when the density of scatterers is large or the carrier frequency of the propagating wave is high. In order to derive the equation for the coherent field propagating through the distribution of scatterers under these conditions, first order multiple scattering or complete multiple scattering must be used. The first order multiple scattering approximation has been used by different authors in the past [26]. The basic work on multiple scattering by random distributions has been carried out by Foldy [2], Lax [3], and Twersky [4].

Our intent in this chapter is to derive equations for the average vector electric field $\langle \vec{E}(\vec{r}) \rangle$ in the presence of a random distribution of scatterers using, first the single-scattering approximation, and secondly the multiple scattering approach. In Section 3.1 the single-scattering approximation is used to derive expressions for the coherent electric field in an ensemble of scatterers with random distributions in space, size, shape and orientation angle. In Section 3.2 the single-scattering approximation results are used to treat an ensemble of scatterers under the first-order multiple scattering approximation. The Foldy-Twersky scattering procedure is used in Section 3.3 to derive an integral equation for the vector coherent field in a ensemble of scatterers including all orders of multiple scattering. Finally, in Section 3.4 the multiple scattering results are applied to a plane wave propagating through a slab of scatterers.

3.1 Scattering by a slab of scatterers; Single-Scattering Approximation

Under the single-scattering approximation, the electric field $\vec{E}$ is scattered only once by the scatterers. Let us consider specifically the slab of scatterers of thickness L shown in Figure 3.1, with a plane wave incident upon it. Each scatterer (say the pth one) can have a random position $\vec{r}_p$, size as measured by the equivolumetric radius a_p, shape as represented by the shape parameter s_p, and orientation angle represented by ϕ_p. The field at point $\vec{r}$, where the receiving antenna is located, is the incident field plus the field

scattered by particles in the "active" region of the slab; the latter coincides with the central few Fresnel zones seen by r. Summing over the particle contributions, we obtain

$$\vec{E}(\vec{r}) = \vec{E}^{i} + \sum_{p=1}^{N} \frac{e^{-jk_o(x_p^2 + y_p^2)/2r_p}}{r_p} \bar{f}_p(\vec{r}) \cdot \vec{E}^{i}(\vec{r}) \quad , \tag{3-1}$$

where $\bar{f}_p(\vec{r})$ is the scattering tensor of the pth scatterer and $r_p = |\vec{r}_p|$.

In order to compute the average field at point $\vec{r}$ we assume that the scatterers are randomly distributed in space, size, shape and orientation angle, and that all of them have the same particle distribution

$$\frac{n(\vec{\omega}_p)}{N} \quad , \tag{3-2}$$

where $\vec{\omega}_p$ represents the random parameters of position $\vec{r}_p$, size a_p, shape s_p, and orientation angle ϕ_p. $n(\vec{\omega}_p)$ is the number of scatterers per unit volume for particles in class $\vec{\omega}_p$.

Equation (3-1) is averaged using the distribution given in Eq. (3-2):

$$\langle \vec{E}(\vec{r}) \rangle = [\bar{I} + \int_{\vec{r}', \vec{\omega}} \bar{f}(\vec{r}') \frac{e^{-jk_o(x'^2 + y'^2)/2r'}}{r'} n(\vec{r}', \vec{\omega})\, d\vec{r}'\, d\vec{\omega}] \cdot \vec{E}^{i} \tag{3-3}$$

Here, $d\vec{r}' = dx'dy'dz'$ is the elemental volume of space, and $\vec{\omega}$ encompasses the distribution parameters for the particle size, shape, and

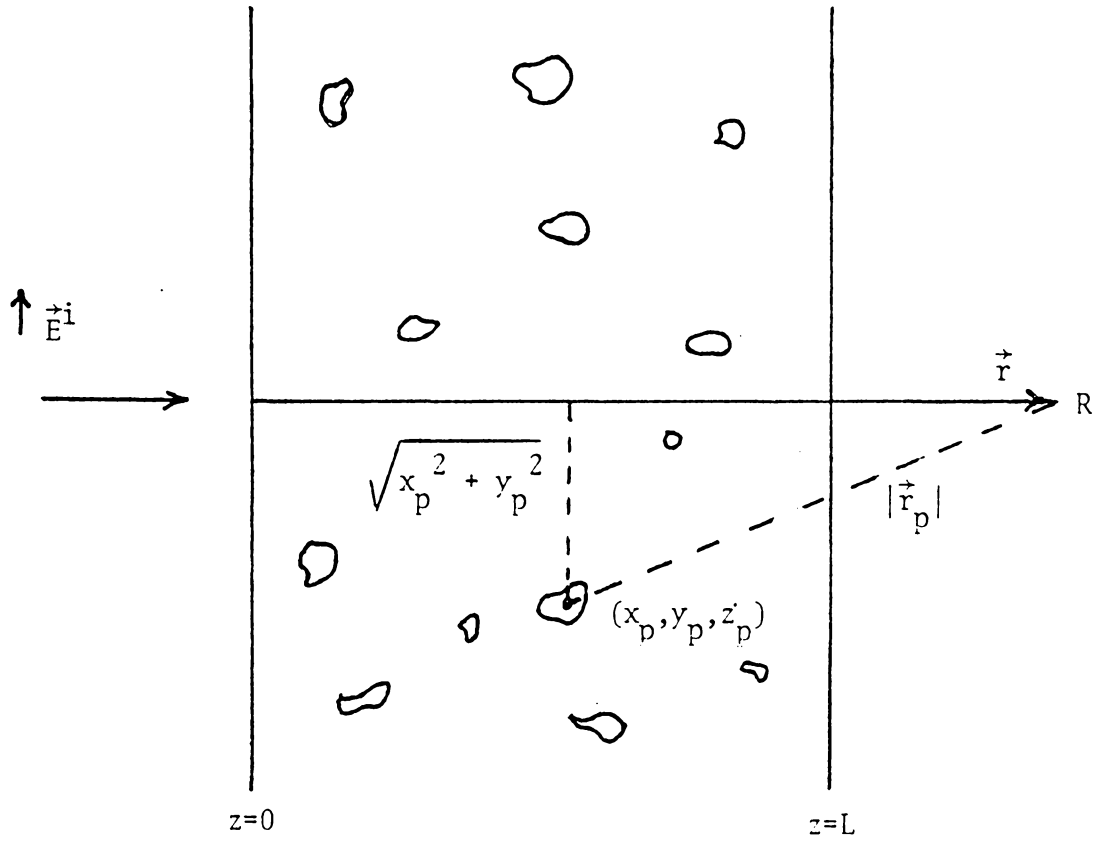

Figure 3.1. Plane wave propagating through a slab of scatterers.

orientation [$\vec{\omega} = (a, s, \phi)$].

Since major contributions arise from particles in the first few Fresnel zones, r' is nearly independent of x', and y' in the integral appearing in Eq. (3-3). We can make then the substitutions

$$x_1 = \frac{jk_o}{2r'} x' \quad , \quad y_1 = \frac{jk_o}{2r'} y' \quad , \quad z_1 = z' \quad , \tag{3-4}$$

giving

$$\langle \vec{E}(\vec{r}) \rangle = [\bar{I} + \frac{2}{jk_o} \int_{\vec{\omega}} d\vec{\omega} \int_{z_1} dz_1 \int_{-\infty}^{\infty} dx_1 \int_{-\infty}^{\infty} d\, y_1 \, e^{-(x_1^2 + y_1^2)}$$

$$\times \bar{f}\, n(\vec{r}_1, \vec{\omega})] \cdot \vec{E}^i(\vec{r}) \quad . \tag{3-5}$$

Using the relationship

$$\int_{-\infty}^{+\infty} e^{-u^2} du = \sqrt{\pi} \quad , \tag{3-6}$$

and assuming that $n(\vec{r}_1, \vec{\omega})$ varies only in the direction of propagation z, Eq. (3-5) gives

$$\langle \vec{E}(\vec{r}) \rangle = [\bar{I} + \frac{2\pi}{jk_o} \iint_{z_1 \vec{\omega}} \bar{f}\, n(z_1, \vec{\omega})\, dz_1\, d\vec{\omega}] \cdot \vec{E}^i(\vec{r}) \equiv [\bar{I} - j\,\bar{k}] \cdot \vec{E}^i(\vec{r}) \quad , \tag{3-7}$$

where

$$\bar{k} = \frac{2\pi}{k_o} \iint \bar{f}\, n(z_1, \vec{\omega})\, dz_1\, d\vec{\omega} \quad . \tag{3-8}$$

If the elements of the tensor $\bar{k}$ are small, the quantity $[\bar{I} - j\,\bar{k}]$

may be approximated by an exponential. This step is further motivated by our knowledge that the exponential form includes multiple scattering effects, as will be shown in later sections. Within the framework of this approximation Eq. (3-7) can be written in the matrix form

$$\langle \underline{E}(r) \rangle = e^{-j\underline{k}} \underline{E}^{i}(\vec{r}) \tag{3-9}$$

Here, $\langle \underline{E}(\vec{r}) \rangle$ is the column matrix corresponding to the vector $\langle \vec{E}(\vec{r}) \rangle$. In the same reasoning $\underline{E}^{i}(\vec{r})$ is the column matrix associated with $\vec{E}^{i}(\vec{r})$ and $\underline{k}$ the matrix corresponding to the tensor $\bar{k}$. A detailed evaluation of Eq. (3-9) using an eigenvalue-eigenvector method is described in Chapter IV.

The coherent field scattered by a slab of scatterers under the single scattering approximation has been found to be given by

$$\langle \vec{E}^{s}(\vec{r}) \rangle = \bar{D} \cdot \vec{E}^{i}(r) \tag{3-10}$$

where $\bar{D}$ is the scattering tensor of the slab and depends on the scattering properties of the individual scatterers and their random distribution in space, shape, size and orientation angle. Specifically,

$$\bar{D} = [\bar{I} - j\frac{2\pi}{k_o} \int_{z_1,\vec{\omega}} \bar{f}(\vec{\omega}) n(z_1, \vec{\omega})\, dz d\vec{\omega}] \tag{3-11}$$

In the derivation of this result the assumption was made that the plane wave is scattered only once by the particles. The above assumption is unrealistic, since the wave may be scattered once, twice, etc., by the particles before reaching the point P at position $\vec{r}$. When the scattering coefficients of the particles and the particle density are

small, contributions to the scattered wave by second, third and higher order scattering may be ignored. There care cases, however, where the scattering coefficients of the scatterer are large (e.g., for raindrops above 30 GHz), and the multiple scattering contributions cannot be ignored. Starting with the next section we will take into considueration multiple-scattering contributions.

3.2 First-Order Multiple Scattering by a Slab of Particles

Under the first-order multiple scattering approximation the slab of particles is divided into n thin subslab (see Figure 3.2). In each individual subslab the single scattering approximation is assumed to hold. The coherent field at point P is then given by

$$\langle \vec{E}(\vec{r}) \rangle = \bar{D}_1 \cdot \bar{D}_2 \cdot \ldots \cdot \bar{D}_n \cdot \vec{E}^i(\vec{r}) \quad , \tag{3-12}$$

where $\bar{D}_i$ is the scattering tensor of the ith subslab and is defined by Equation (3-11).

This approach, called the first-order multiple scattering approximation, has been used by researchers in different areas of wave propagation. In radio wave propagation through precipitation, for example, Persinger and Stutzman [27] have used a computerized code to evaluate Eq. (3-13) in order to calculate attenuation and isolation of a wave propagating through a medium consisting of ice particles and rain.

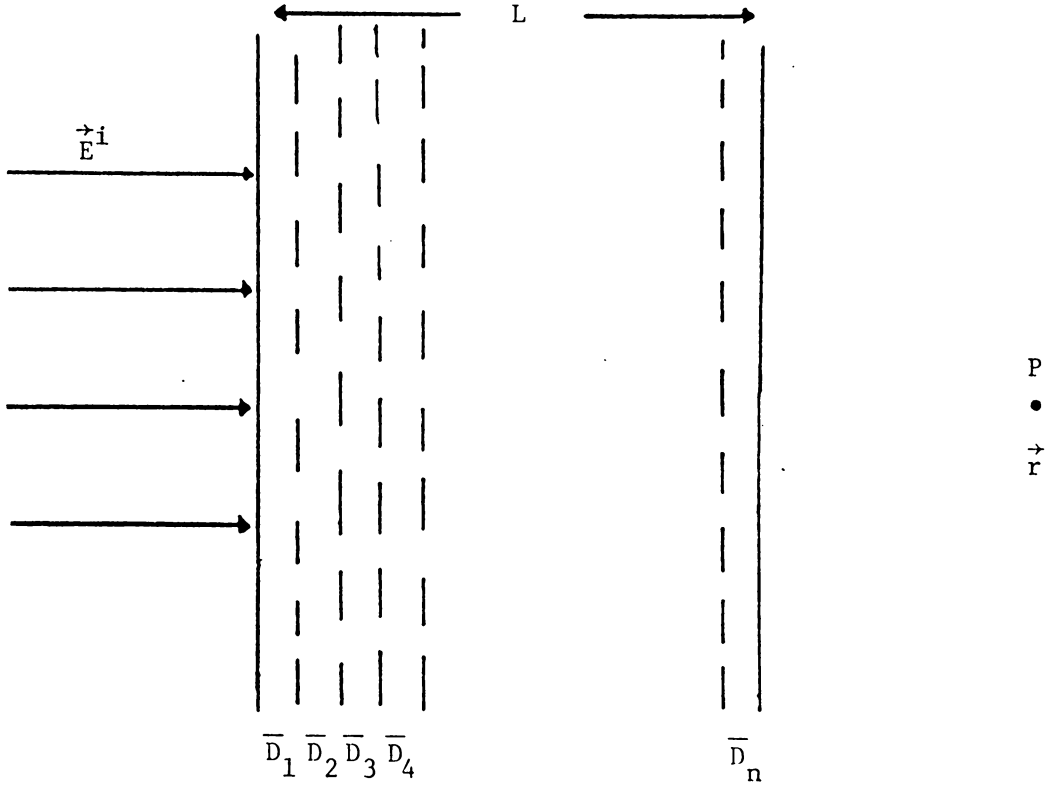

Figure 3.2. First order multiple scattering by a slab of particles.

3.3 Multiple Scattering by Random Distributions of Particles

So far, the scattered coherent electric field by a slab of randomly distributed particles has been calculated using the single scattering and the first-order multiple scattering approximations. The first approximation results in a simple form for the coherent field, but it holds only when the scattering coefficients and the density of the particles are small. The second one holds for any forward scattering propagation provided that the thickness of each subslab is kept infenitesimally small. As shown in Eq. (3-12), the coherent field in this case contains the dot products of an infinite number of tensors. Its evaluation can be done only by fast digital machines.

In order to include both forward and backward multiple scattering, we will use an approach first introduced by Foldy [2] and developed further by Twersky [4] and Lax [3]. In our formulation we will assume that the medium is anisotropic, and will derive the Dyson equation for the coherent vector electric field in terms of the scattering tensor of the individual scatterers and their distribution in space, size, shape and orientation.

Let us assume that N scatterers are randomly distributed in space, and that they have random orientation, size, and shape. The medium between any two scatterers is free space (see Figure 3.3). The vector electric field $\vec{E}(\vec{r})$ between the scatterers satisfies the Helmholtz equation

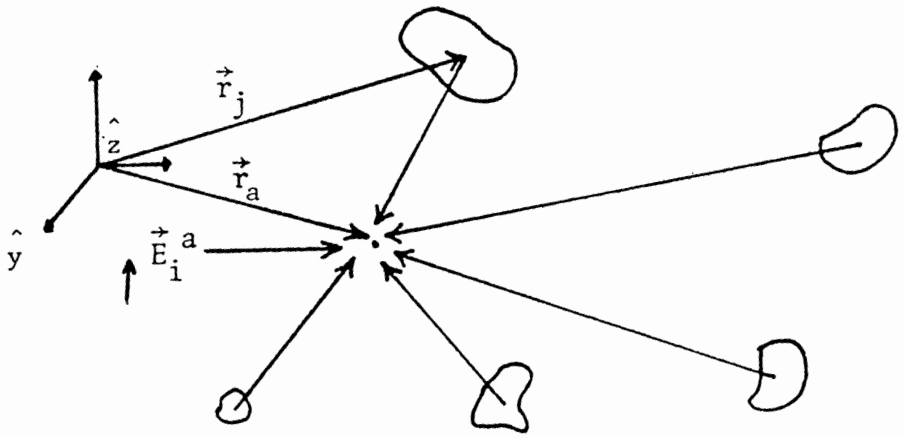

Figure 3.3. The field at $\vec{r}_a$ as the sum of the incident wave and the scattered fields.

$$(\nabla^2 + k_o^2)\ \vec{E}(\vec{r}) = 0 \quad , \tag{3-13}$$

where k_o is the free space propagation constant.

The incident field $\vec{E}^a$ at the point $\vec{r}_a$ is the sum of the incident electric field E_i^a and the field scattered by the N scatterers, specifically, we have

$$\vec{E}^a = \vec{E}_i^a + \sum_{j=1}^{N} \vec{G}_j^a \quad , \tag{3-14}$$

where $\vec{G}_j^a$ is the field at position $\vec{r}_a$ that is scattered by the jth scatterer. The latter is a function of the scattering properties of the jth scatterer $\vec{r}_j$ and the position $\vec{r}_a$, niz.,

$$\vec{G}_j^a = \bar{g}_j^a \cdot \vec{E}^j \quad . \tag{3-15}$$

$\bar{g}_j^a$ is operating on the incident field upon the jth scatterer, $\vec{E}^j$, to result in $\vec{G}_j^a$. A similar equation for the field $\vec{E}^j$ may be written as

$$\vec{E}^j = \vec{E}_i^j + \sum_{k=1,k\neq j}^{N} \vec{G}_k^j \quad . \tag{3-16}$$

Substituting (3-16) into (3-15) we obtain

$$\vec{G}^j = \bar{g}_j^a \cdot [\vec{E}_i^j + \sum_{k=1,k\neq j}^{N} \vec{G}_k^j] \quad . \tag{3-17}$$

Using (3-17) and (3-14), we have

$$\vec{E}^a = \vec{E}_i^a + \sum_{j=1}^{N} \bar{g}_j^a \cdot E_i^j + \sum_{j=1}^{N} \sum_{k=1,k\neq j}^{N} g_j^a \cdot g_k^j\ \vec{E}^k \quad . \tag{3-18}$$

By iterating the above process it follows that

$$\vec{E}^a = \vec{E}_i^a + \sum_{j=1}^{N} \bar{g}_j^a \cdot \vec{E}_i^j + \sum_{j=1}^{N} \sum_{k=1,k\neq j}^{N} \bar{g}_j^a \cdot \bar{g}_k^j \cdot \vec{E}_i^k +$$

$$\sum_{j=1}^{N} \sum_{k=1,k\neq j}^{N} \sum_{\ell=1,\ell\neq k}^{N} \bar{g}_j^a \cdot \bar{g}_k^j \cdot \bar{g}_\ell^k \cdot \vec{E}_i^\ell + ... + ... \qquad (3\text{-}19)$$

The triple summation in Eq. (3-19) may be written as

$$\sum_{j=1}^{N} \sum_{k=1,k\neq j}^{N} \sum_{\ell=1,\ell\neq k}^{N} \bar{g}_j^a \cdot \bar{g}_k^j \cdot \bar{g}_\ell^k \cdot \vec{E}_i^\ell = \sum_{j=1}^{N} \sum_{k=1,k\neq j}^{N} \sum_{\ell=1,\ell\neq k,\ell\neq j}^{N}$$

$$\bar{g}_j^a \cdot \bar{g}_k^j \cdot \bar{g}_\ell^k E_i^\ell + \sum_{j=1}^{N} \sum_{k=1}^{N} \bar{g}_j^a \cdot \bar{g}_k^j \cdot \bar{g}_j^k \vec{E}_i^j \quad . \qquad (3\text{-}20)$$

Figure (3.4a) shows a graphical representation of the first summation on the right-hand side of Eq. (3-20), and Figure (3.4b) of the second one.

Assuming that backscattering is smaller than forward scattering, the second summation in Eq. (3-20) may be ignored, and Eq. (3-19) may be written as

$$\vec{E}^a = \vec{E}_i^a + \sum_{j=1}^{N} \bar{g}_j^a \cdot \vec{E}_i^j + \sum_{j=1}^{N} \sum_{k=1,k\neq j}^{N} \bar{g}_j^a \cdot g_k^j \cdot \vec{E}_i^k +$$

$$\sum_{j=1}^{N} \sum_{k=1,k\neq j}^{N} \sum_{\ell=1,\ell\neq k,\ell\neq j}^{N} \bar{g}_j^a \cdot \bar{g}_k^j \cdot \bar{g}_\ell^k \cdot \vec{E}_i^\ell + \ldots \quad . \qquad (3\text{-}21)$$

In deriving Eq. (3-21) we have ignored triple scattering between two scatterers. By a similar reasoning we will ignore fourth order scattering between three scatterers and so on. The above procedure

was first introduced by Twersky [ ] in order to obtain a closed form equation for the coherent field.

We make next the assumption, as in Section 3.1, that each scatterer has the same space, shape, size, and orientation distribution, and that there are no correlations between scatterers. The particle distribution may be defined as

$$p(\vec{\omega}_j) = \frac{n(\vec{\omega}_j)}{N} \quad , \tag{3-22}$$

where $\vec{\omega}_j$ represents the random parameters of position $\vec{r}_j$, size a_j, shape s_j, andorientation ϕ_j. The quantity $n(\vec{\omega}_j)$ is the number of scatterers per unit volume for particles in class $\vec{\omega}_j$.

Taking the ensemble average of (3-21), we obtain an expression for the coherent field at point $\vec{r}_a$:

$$\begin{aligned}
\langle \vec{E}^a \rangle = \vec{E}_i^a &+ \sum_{j=1}^{N} \int_{\vec{\omega}_j} \bar{\bar{g}}_j^a \cdot \bar{\bar{E}}_i^j \frac{n(\vec{\omega}_j)}{N} d\vec{\omega}_j + \sum_{j=1}^{N} \sum_{k=1, k\neq j}^{N} \\
&\int_{\vec{\omega}_j} \int_{\vec{\omega}_k} \bar{\bar{g}}_j^a \cdot \bar{\bar{g}}_k^j \cdot \vec{E}_i^k \frac{n(\vec{\omega}_j) n(\vec{\omega}_k)}{N^2} d\vec{\omega}_j \, d\vec{\omega}_k + \sum_{j=1}^{N} \sum_{k=1, k\neq j}^{N} \sum_{\ell=1, \ell\neq k, \ell\neq j}^{N} \\
&\int_{\vec{\omega}_j} \int_{\vec{\omega}_k} \int_{\vec{\omega}_\ell} \bar{\bar{g}}_j^a \cdot \bar{\bar{g}}_k^a \cdot \bar{\bar{g}}_\ell^k \cdot \vec{E}_i^\ell \frac{n(\vec{\omega}_j) n(\vec{\omega}_k) n(\vec{\omega}_\ell)}{N^3} d\vec{\omega}_j \, d\vec{\omega}_k \, d\vec{\omega}_\ell \\
&+ \cdots\cdots + \cdots\cdots
\end{aligned} \tag{3-23}$$

or

$$\langle \vec{E}^a \rangle = \vec{E}_i^{\,a} + \int_{\vec{\omega}_j} \vec{g}_j^{\,a} \cdot \vec{E}_i^{\,j}\, n(\vec{\omega}_j)\, d\vec{\omega}_j + \frac{N-1}{N} \int_{\vec{\omega}_j, \vec{\omega}_k} \bar{g}_j^{\,a} \cdot \bar{g}_k^{\,j} \cdot \vec{E}_i^{\,k}$$

$$n(\vec{\omega}_j) n(\vec{\omega}_k)\, d\vec{\omega}_j\, d\vec{\omega}_k + \frac{N-2}{N} \int_{\vec{\omega}_j, \vec{\omega}_k, \vec{\omega}_\ell} \bar{g}_j^{\,a} \cdot \bar{g}_k^{\,j} \cdot \bar{g}_\ell^{\,k} \cdot \vec{E}_i^{\,\ell}$$

$$n(\vec{\omega}_j) n(\vec{\omega}_k) n(\vec{\omega}_\ell) d\vec{\omega}_j\, d\vec{\omega}_k\, d\vec{\omega}_\ell + \ldots. + \ldots. \qquad (3\text{-}24)$$

By letting N tend to infinity, the ratios $\frac{N-1}{N}$, $\frac{N-2}{N}$, etc., tend to unity, and the infinite summation in Eq. (3-24) can be presented by the integral equation

$$\langle \vec{E}^a \rangle = \vec{E}_i^{\,a} + \int_{\vec{\omega}_j} \bar{g}_j^{\,a} \cdot \langle \vec{E}^j \rangle\, n(\vec{\omega}_j)\, d\vec{\omega}_j \quad . \qquad (3\text{-}25)$$

This is the Dyson equation for the coherent field in an ensemble of raondomly distributed scatterers, and it is often called the Foldy-Lax-Twersky equation. It has been derived on the basis of the Twersky procedure. The same equation may also be obtained using Lax's polycrystalline approximation [3].

The Dyson equation (3.25) is more general than the equations for the coherent field derived by the single scattering or first-order multiple scattering approximations, and it includes backscattering. Evaluation of equation (3-25) is very difficult and depends on the complexity of the operator $\bar{g}_j^{\,a}$. If the medium is tenuous (this means that the average distance d between any two arbitrary scatterers is much greater than the free space wavelength, i.e., $k_o d >> 1$), each

scatterer is in the far zone of all other scatterers, and $\bar{\bar{g}}_j^{\,a}$ may be replaced by

$$\bar{\bar{g}}_j^{\,a} = \frac{e^{-jk_o|\vec{r}_a - \vec{r}_j|}}{|\vec{r}_a - \vec{r}_j|} \bar{\bar{f}} \quad , \tag{3-26}$$

where $\bar{\bar{f}}$ is the scattering tensor of the scatterer.

In the next section we will apply the multiple scattering results to the case of a plane wave incident upon a tenuous slab of scatterers.

3.4 The Coherent Field in a Slab of Scatterers; Multiple Scattering Solution

Let us consider a slab of a random distribution of scatterers (see Fig. 3.5) that has length L. The scatterers have random size, shape and orientation, and are described by the probability density function $p(\vec{\omega})$ given in Eq. (3-20). A plane wave propagating in the z direction is incident upon the slab. The incident vector field $\vec{E}_i$ is given by

$$\vec{E}_i = \vec{E}_o e^{-jk_o z} \quad . \tag{3-27}$$

The average field $\langle\vec{E}\rangle$ inside the slab obeys the vector Foldy-Lax-Twersky integral equation from (3-25) is

$$\langle\vec{E}^a\rangle = \vec{E}_i^{\,a} + \int_{\vec{\omega}_j} \bar{\bar{g}}_j^{\,a} \langle\vec{E}^j\rangle \, n(\vec{\omega}_j) \, d\vec{\omega}_j \quad . \tag{3-28}$$

The medium of the scatterers is assumed to be tenuous, so that the scattering operator $\bar{\bar{g}}_j^{\,a}$ can take the form shown in Eq. (3-26), viz.,

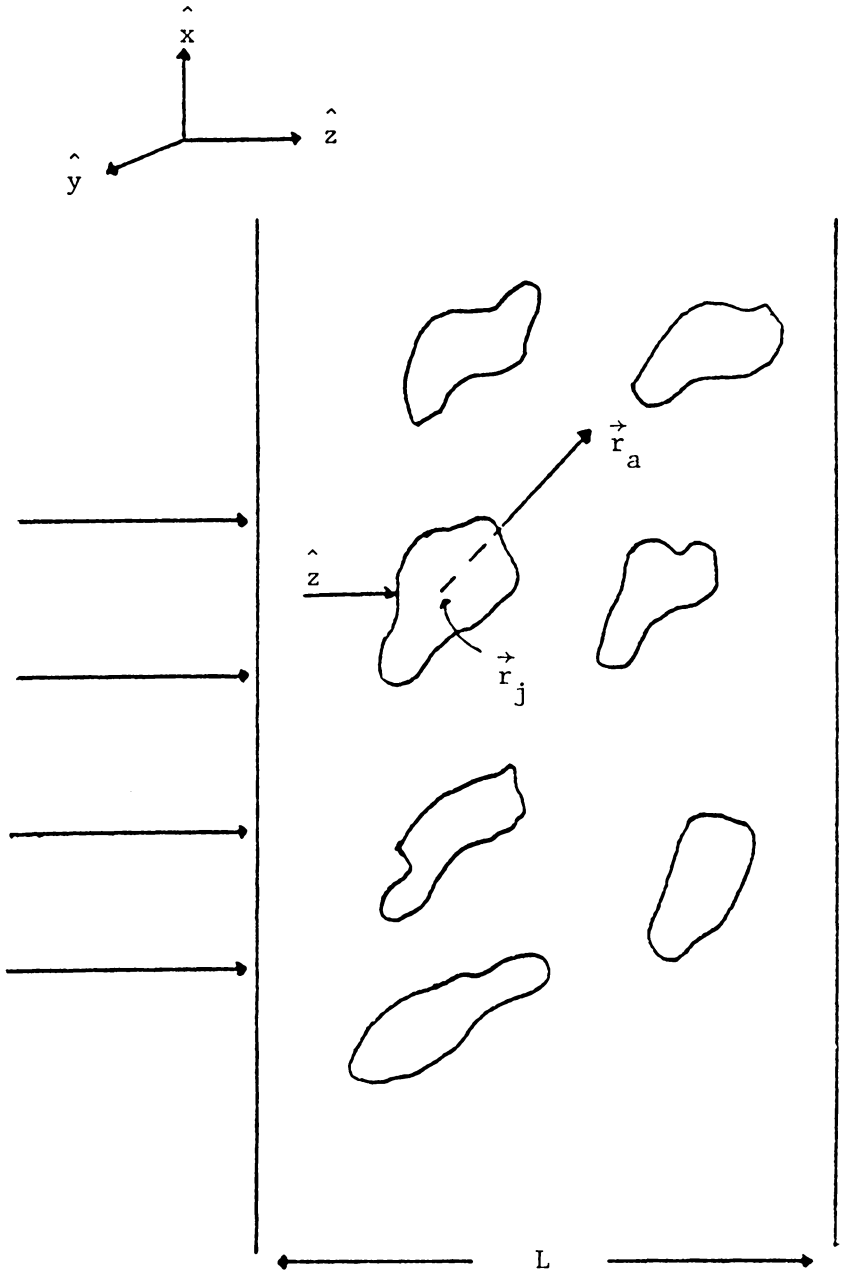

Figure 3.5. Plane wave incident on a slab of scatterers.

$$\bar{g}_j^{\,a} \langle \vec{E}^j \rangle = \bar{f}_j(\hat{z}, \vec{r}_a - \vec{r}_j) \langle \vec{E}^j \rangle \frac{e^{-jk_o|\vec{r}_a - \vec{r}_j|}}{|\vec{r}_a - \vec{r}_j|} \quad . \tag{3-29}$$

Substituting equation (3-30) into (3-29) results in the expression

$$\langle \vec{E}^a \rangle = \vec{E}_i^{\,a} + \int_{\vec{\omega}_j} \bar{f}_j(\hat{z}, \vec{r}_a - \vec{r}_j) \langle \vec{E}^j \rangle \frac{e^{-jk_o|\vec{r}_a - \vec{r}_j|}}{|\vec{r}_a - \vec{r}_j|} n(\vec{\omega}_j)\, d\vec{\omega}_j \quad . \tag{3-30}$$

We assume that $n(\vec{\omega}_j)$ varies only in the direction of propagation. Because of the existing symmetry, the average field is a function only of z. We have, then,

$$\langle \vec{E}(z) \rangle = \vec{E}_o\, e^{-jk_o z} + \int_{\vec{\omega}_j} \bar{f}_j(\hat{z}, \vec{r}_a - \vec{r}_j) \langle \vec{E}^j \rangle \frac{e^{-jk_o|\vec{r} - \vec{r}_j|}}{|\vec{r} - \vec{r}_j|} n(\vec{\omega}_j)\, d\vec{\omega}_j \quad , \tag{3-31}$$

where

$$|\vec{r} - \vec{r}_j| = [(x - x_j)^2 + (y - y_j)^2 + (z - z_j)^2]^{1/2} \tag{3.32}$$

and

$$\vec{\omega}_j = (\vec{r}_j, a_j, s_j, \phi_j) \quad . \tag{3.33}$$

In order to evaluate equation (3.32) we make a further assumption: that the effects to the coherent field over the x,y plane are not of great significance since it is propagating in the z direction. The integral of equation (3.32) may then be evaluated over the x,y variables by the method of stationary phase. The stationary phase points are $(x_j, y_j)^{sp} = (x, y)$. Thus,

$$\langle \vec{E}(z) \rangle = \vec{E}_o \, e^{-jk_o z} + \frac{2\pi j}{k_o} \int_{\vec{\omega}} \bar{f}_j \, (\hat{z}, \hat{z}) \, \langle \vec{E}(z_j) \rangle \, e^{-jk_o (z - z_j)} \, n(\vec{\omega}_j) \, d\vec{\omega}_j \tag{3-34}$$

where

$$\vec{\omega}_j = (z_j, y_j, a_j, s_j) \quad , \tag{3-35}$$

z_j varying between 0 and z.

Let us assume that the coherent field has the matrix form

$$\langle \underline{E}(z) \rangle = e^{-j\underline{k}'(z)} \quad \underline{A} \quad . \tag{3-36}$$

Substituting (3-36) into (3-34), we obtain values for $\underline{k}'(z)$ and $\underline{A}$; specifically,

$$\underline{A} = \underline{E}_o \tag{3-37}$$

and

$$\underline{k}'(z) = k_o \, \underline{I} \, z + \frac{2\pi j}{k_o} \int_{\vec{\omega}_j} \underline{f}(\hat{z}, \hat{z}) \, n(\vec{\omega}_j) \, d\vec{\omega}_j \tag{3-38}$$

or

$$\langle \underline{E}(z) \rangle = \underline{e}^{-j\underline{k}(z)} \cdot \underline{E}_o \, e^{-jk_o z} \tag{3-39}$$

where

$$\underline{k}(z) = \frac{2\pi j}{k_o} \int_{\vec{\omega}_j} \underline{f} \, n(\vec{\omega}_j) \, d\vec{\omega}_j \quad , \tag{3-40}$$

$\underline{f}$ being the forward scattering tensor of the individual scatterer.

Comparing equations (3-40) and (3-8) we realize that they are exactly the same. We conclude, then, that when the imaginary elements of $\underline{k}(z)$ are much smaller than unity the single scattering approximation and the multiple scattering approach produce identical results. On the other hand, when the density of the scatterers $n(\vec{\omega}_j)$ increases, and/or the scattering coefficients of the individual scatterer are large, multiple scattering becomes very important.

The quations derived for the coherent vector electric field in this section will be used to study radio wave propagation through an ice-cloud and rain at frequencies from 10-30 GHz. Ice particles and raindrops are nonspherical and cause depolarization to the propagating wave. Therefore, it is essential to use equations for the vector field. In the next chapter we will first formulate the problem for radio wave propagation through an ice-cloud. The theoretically predicted values for depolarization will then be compared with existing data that has been collected at the VPI&SU Tracking Station. Also, the multiple scattering predicted values for isolation in a rain medium will be compared with the ones of Persinger and Stutzman which are based on a first-order multiple scattering model.

CHAPTER IV

APPLICATION OF MULTIPLE-SCATTERING RESULTS TO PROPAGATION THROUGH PRECIPITATION

Since the early 1960's, a lot of theoretical work has been done in studying radio wave propagation through precipitation in the microwave regions. Raindrops cause attenuation and depolarization of the propagating waves. On the other hand, ice particles in the upper atmosphere cause only depolarization.

Early theoretical works by Oguchi [28], Evans [29] and Watson [30] formulate the problem within the framework of the single scattering approximation, with all particles (raindrops, ice crystals) having the same shape, size and orientation. Experimental data [31], however, have demonstrated that not all precipitation particles have the same size and shape; instead, there exist distributions in size, shape and orientation.

Lately, different models have appeared in the literature [32-35] that take into account multiple scattering effects, as well as distributions in size, shape, and orientation. All of them are lacking, however, in one respect: they assume uniform particle density across the propagation path; also, that the random parameters of the particles (position, size, etc.) are statistically independent.

In this chapter we will study ice depolarization and rain attenuation and isolation using the Dyson equation for the coherent field derived in Section 3.4. Specifically, we will calculate the

coherent field inside an ice-cloud and a rain medium. These calculations are the same, except for the differences in the scattering matrices for ice-particles or raindrops, and the differences in their size, shape and orientation distributions.

First, we will discuss theoretical predictions for ice-depolarization and compare them to experimental data. Then, we will formulate the rain problem using the multiple scattering approach, and compare the predicted values to the ones determined on the basis of the first-order multiple scattering approach [27].

4.1 Ice Depolarization

Since the middle 1970's, it has been recognized that high-altitude ice crystals can cause depolarization of millimeter radio signals (above 1 GHz) along an earth-space path. Several measurements have been reported, indicating that the formation of "ice clouds" is not a rare event. Also, some theoretical models have been proposed for use in calculations on ice-crystal depolarization. The review article by Bostian and Allnutt [31] provides a concise summary of "ice depolarization". In this section we will present a theoretical formulation of this problem, and we will compare our predictions with earth-space link measurements.

4.1.1 Formulation of the Ice Depolarization Problem

We choose a rectangular coordinate system so that z is the propagation direction, and the electric field vector associated with

the transmitted signal has components E_x^i and E_y^i. The x-direction is usually taken to be parallel to local horizontal. The electric field arriving at the receive antenna is

$$\underline{\vec{E}} = \underline{D}\,\underline{\vec{E}}^i \quad , \tag{4-1}$$

where $\underline{D}$ is the ice depolarization matrix defined by equation (3-11), viz.,

$$\underline{D} = \begin{bmatrix} D_{xx} & D_{xy} \\ D_{yx} & D_{yy} \end{bmatrix} \quad , \tag{4-2}$$

and

$$\underline{\vec{E}} \quad \begin{bmatrix} E_x \\ E_y \end{bmatrix} \quad , \quad \underline{\vec{E}}^i = \begin{bmatrix} E_x^i \\ E_y^i \end{bmatrix} \quad . \tag{4-3}$$

The field $\underline{E}^i$ incident upon the ice medium is phase referenced to the receiver. Then $\underline{D}$ represents only changes introduced by the ice medium, and is the identity matrix for clear air conditions.

A dual-polarized receiving antenna produces voltages V_c' and V_x' at the co- and cross-polarized output ports during an ice event, and V_c and V_x during clear air conditions. The receive voltages are computed using

$$\underline{V}' = \begin{bmatrix} V_c' \\ \\ V_x' \end{bmatrix} = \underline{A}_R \vec{\underline{E}} \quad , \tag{4-4}$$

with the receive antenna response matrix given by

$$\underline{A}_R = \begin{bmatrix} a_{11} & a_{12} \\ \\ a_{21} & a_{22} \end{bmatrix} = \begin{bmatrix} \cos \gamma_c & \sin \gamma_c \, e^{-j\delta_c} \\ \\ \cos \gamma_x & \sin \gamma_x \, e^{-j\delta_x} \end{bmatrix} \quad , \tag{4-5}$$

where (γ_c, δ_c) and (γ_x, δ_x) are the conventional polarization parameters [36].

We make the customary assumption that ice media introduce no attenuation. Our attention is then on depolarization. To study this we define the complex cross polarization ratio

$$C = \frac{V_x'}{V_c'} \quad . \tag{4-6}$$

Parameters which follow directly from this are ice depolarization ratio CPR = $|C|^2$, or isolation I = $1/|C|^2$, and relative phase shift (or just "phase"), which is given by $\angle C = \angle V_x' - V_c'$. In practice, the phase during an ice event is relative to that during clear weather; that is, the clear weather phase value is subtracted from the phase measured during an event.

4.1.2 Some Basic Concepts in Ice Depolarization

In this subsection several simplifying assumptions will be made about ice media which will enable us to use previously derived theoretical results.

We assume first that the ice medium is homogeneous, with all particles aligned at a tilt angle θ in a plane perpendicular to the propagation direction. In this case the propagation constant model yields a depolarization matrix with the following entires [15, 26]:

$$\begin{aligned} D_{xx} &= d_h(\cos^2\theta + g\sin^2\theta) \quad , \\ D_{xy} &= D_{yx} = d_h(g-1)\sin\theta\cos\theta \quad , \\ D_{yy} &= d_h(\sin^2\theta + g\cos^2\theta) \quad . \end{aligned} \tag{4-7}$$

Here,

d_v, d_h = propagation factors for polarization along the minor and major axis,

$$g = \frac{d_v}{d_h} = e^{-(a_y - a_h)L}\, e^{-j(\beta_v - \beta_h)L} \quad , \tag{4-8}$$

being the ice medium thickness along the path. Cox *et al.* have presented a similar formulation [37, eq. (A26)].

Assuming the attenuation to be zero ($a_v = a_h = 0$), we have

$$g = 1\, e^{j\phi'} \quad , \tag{4-9}$$

where $\phi' = (\beta_h - \beta_v)L$ is the differential phase along the principal

axes of the medium. For not too severe depolarization the differential phase shift experienced will be small, and then,

$$g \simeq 1 \quad . \tag{4-10}$$

In this case, the depolarization matrix entries in (4-5) reduce to

$$\begin{aligned} D_{xx} &= D_{yy} = d_h \quad , \\ D_{xy} &= D_{yx} = d_h(g - 1) \sin\theta \cos\theta \quad . \end{aligned} \tag{4-11}$$

For a linearly polarized incident field, with the electric field vector forming an angle θ with respect to the major axes of the particles, $E_x^i = 1$ and $E_y^i = 0$. Equations (4-1) and (4-4) lead to $V_c' = E^i D_{xx}$ and $V_x' = -E^i D_{yx}$ for an ideal receive antenna which has $a_{11} = 1$, $a_{12} = a_{21} = 0$, $a_{22} = -1$. The corresponding complex cross polarization ratio in eq. (4-6) becomes

$$C_L = -\frac{D_{yx}}{D_{xx}} = \frac{(1 - g)\tan\theta}{1 + g\tan^2\theta} \quad . \tag{4-12}$$

For an ice medium, the quantities D_{xx}, D_{yx} obey equation (4-11) which when used in conjunction with (4-12) result in the cross polarization ratio

$$C_L \simeq (1 - g)\sin\theta\cos\theta = \frac{1 - g}{2}\sin 2\theta \quad . \tag{4-13}$$

We assume that the medium differential phase is much smaller than unity ($\phi' << 1$). Under this restriction, the following approximation holds:

$$1 - g = 1 - e^{j\phi'} = 1 - (1 + j\phi' - \phi'^2/2) = \frac{\phi'^2}{2} - j\phi' \quad . \tag{4-14}$$

Introducing this result into (4-13) yields

$$C_L \simeq (\phi'/2 - j)\,\frac{\phi'}{2} \sin 2\theta \quad , \tag{4-15}$$

from which, finally, we obtain

$$CPR_L = |C_L|^2 \simeq [\phi'/2 \sin 2\theta]^2 \quad , \tag{4-16}$$

$$\angle C_L \simeq \pi/2 \quad . \tag{4-17}$$

Thus, the induced cross-polarized signal in a weakly differential phase-shifting medium is nearly in phase-quadrature with the co-polarized signal in the linearly polarized case independently of the angle between the incident electric vector field and the medium axes [37].

For a right-handed circularly polarized incident wave, $E_x^i = E^i/\sqrt{2}$ and $E_y^i = -E^i/\sqrt{2}$. An ideal receive antenna matched to the incident wave has $a_{11} = a_{21} = 1$, $a_{12} = j$, $a_{22} = -j$. The cross polarization is given for this specific case as

$$C_c = \frac{D_{xx} - D_{yy} - j\,(D_{yx} + D_{xy})}{D_{xx} + D_{yy} + j\,(D_{yx} - D_{xy})} \quad . \tag{4-18}$$

Following the same reasoning as for the linearly polarized wave, C_c may be approximated as [31]

$$CPR_c = |C_c|^2 \simeq (\frac{\phi'}{2})^2 \quad , \tag{4-19}$$

$$\angle C_c = -\pi/2 + \frac{\phi'}{2} + 2\theta \quad . \tag{4-20}$$

As expected, the circular depolarization magnitude is independent of θ and equals the linear depolarization magnitude for $\theta = 45°$ in the linear case. Furthermore the phase for circular polarization is dependent upon the phase shift and medium orientation angle.

4.1.3 The Ice-Particle Scattering Matrix

In order to use the results of Section 3.4 where no restrictions were made about the alignment of the particles and their distributions, it is necessary to compute the scattering matrix of a single ice particle.

Forward scattering from ice crystals can be computed using the Rayleigh scattering approximation discussed in Section 2.2, since the particles are small relative to a wavelength. The Rayleigh scattering approach is considered to be valid up to at least 30 GHz [31] or even 50 GHz [24].

Complete details are found in [15, Chap. 6], and only the main results are presented here.

The field scattered from a single ice particle in the far zone is governed by eq. (2-5), viz.,

$$\vec{E}_s^s = \frac{k_o^2}{4\pi\varepsilon_o} \{\vec{p} - (\vec{p} \cdot \hat{r})\hat{r}\} \frac{e^{-jk_o r}}{r} \quad , \tag{4-21}$$

where $\vec{p}$ is the electric dipole moment for the particle. Static field techniques are used to solve for $\vec{p}$. Furthermore, as it is customary, the ice particle shapes are assumed to be either ice plates approximated as flat oblate spheroids, or ice needles approximated by long

narrow prolate spheroids. Also, the solutions are evaluated in the limit as the eccentricity approaches unity.

The single particle scattered field is representable as

$$\begin{bmatrix} E_x^s \\ \\ E_y^s \end{bmatrix} = \underline{f} \begin{bmatrix} E_x^i \\ \\ E_y^i \end{bmatrix} \frac{e^{-jk_o r}}{r} \quad , \tag{4-22}$$

where $\underline{f}$, the scattering matrix, is different for plates and needles. For ice plates (oblate spheroids with unity eccentricity),

$$\underline{f}_{plate} = \frac{k_o^2 V}{4\pi} (m^2 - 1) \begin{bmatrix} 1 + \frac{1-m^2}{m^2} \cos^2 \delta \cos^2 \theta & \frac{1-m^2}{m^2} \cos^2 \delta \sin 2\theta \\ \\ \frac{1-m^2}{m^2} \cos^2 \delta \sin 2\theta & 1 + \frac{1-m^2}{m^2} \cos^2 \delta \sin^2 \theta \end{bmatrix} \tag{4-23}$$

and for ice needles (prolate spheroids with unity eccentricity)

$$\underline{f}_{needle} = \frac{k_o^2 V}{4\pi} \frac{2(m^2 - 1)}{m^2 + 1} \begin{bmatrix} q_{xx} & q_{xy} \\ \\ q_{yx} & q_{yy} \end{bmatrix} \quad , \tag{4-24}$$

where

$$q_{xx} = 1 + \frac{m^2-1}{4} [\cos 2\phi(\sin^2 \theta - \sin^2 \delta \cos^2 \theta) + \sin^2 \theta + \sin^2 \delta \cos^2 \theta$$

$$+ \sin 2\theta \sin 2\phi \sin \delta] ,$$

$$q_{yy} = 1 + \frac{m^2-1}{4} [\cos 2\phi[\cos^2 \theta - \sin^2 \delta \sin^2 \theta) + \cos^2 \theta + \sin^2 \delta \sin^2 \theta$$

$$- 2 \sin 2\theta \sin 2\phi \sin \delta] ,$$

$$q_{xy} = q_{yx} = \frac{m^2-1}{8} [\sin 2\theta \cos^2 \delta - \sin 2\theta \cos 2\phi(1 + \sin^2 \delta)$$

$$- 2 \sin \delta \sin 2\phi \cos 2\theta] .$$

In these expressions V is the volume of the spheroid, m is the complex index of refraction of ice, δ is the satellite elevation angle, θ is the projection of the tilt angle of the particle onto the xy-plane (for both plates and needles), and ϕ is the azimuthal rotation angle of the axis of symmetry for ice needles. The geometry used for ice needles and ice plates is presented respectively in Figures 4.1, 4.2, and has been explained in more detail by Bostian and Allnutt [31].

4.1.4 Computations for a Realistic Ice Medium

In Section 4.1.2 it was assumed that all the ice particles were identical and alligned. An ice cloud, however, may be composed of ice plates, ice needles, or both. From experimental data it is believed that ice-needles are alligned only for a short time period. For most ice events the needles are distributed around an average

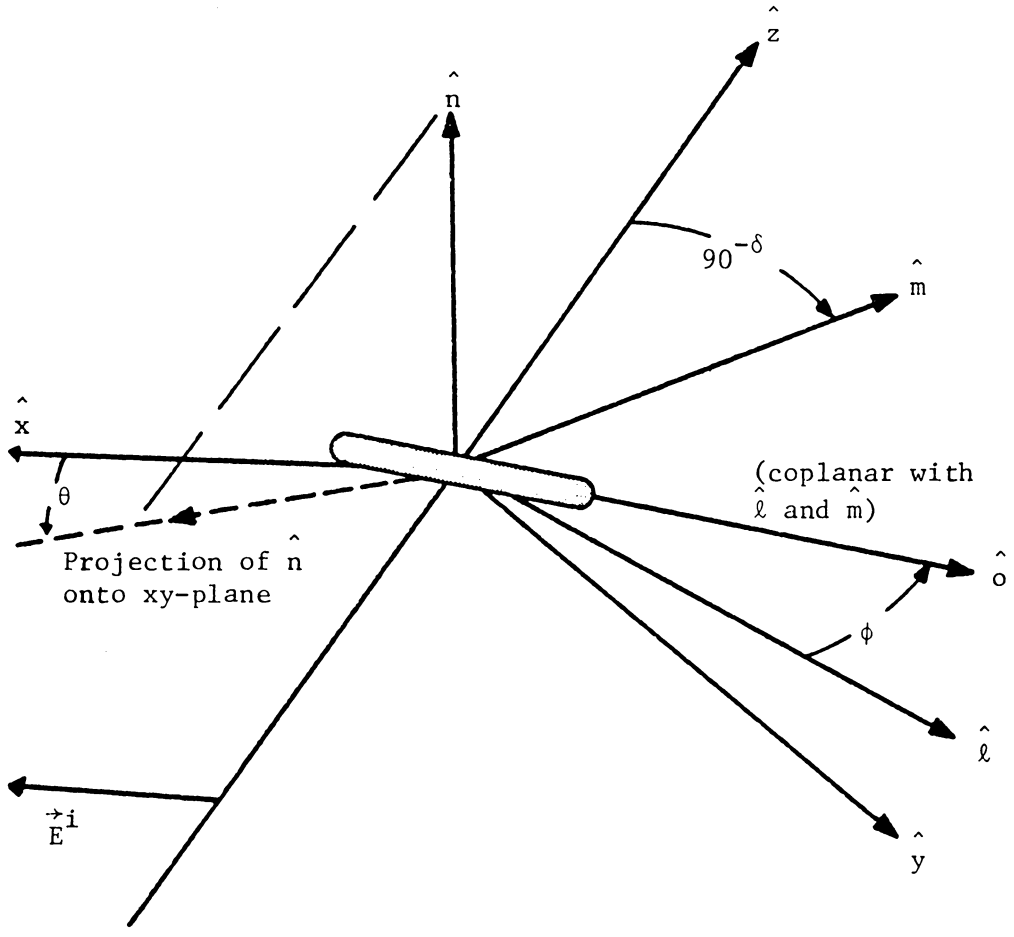

Figure 4.1a. Geometry for depolarization calculations in scattering by a prolate spheroid repressing an ice needle.

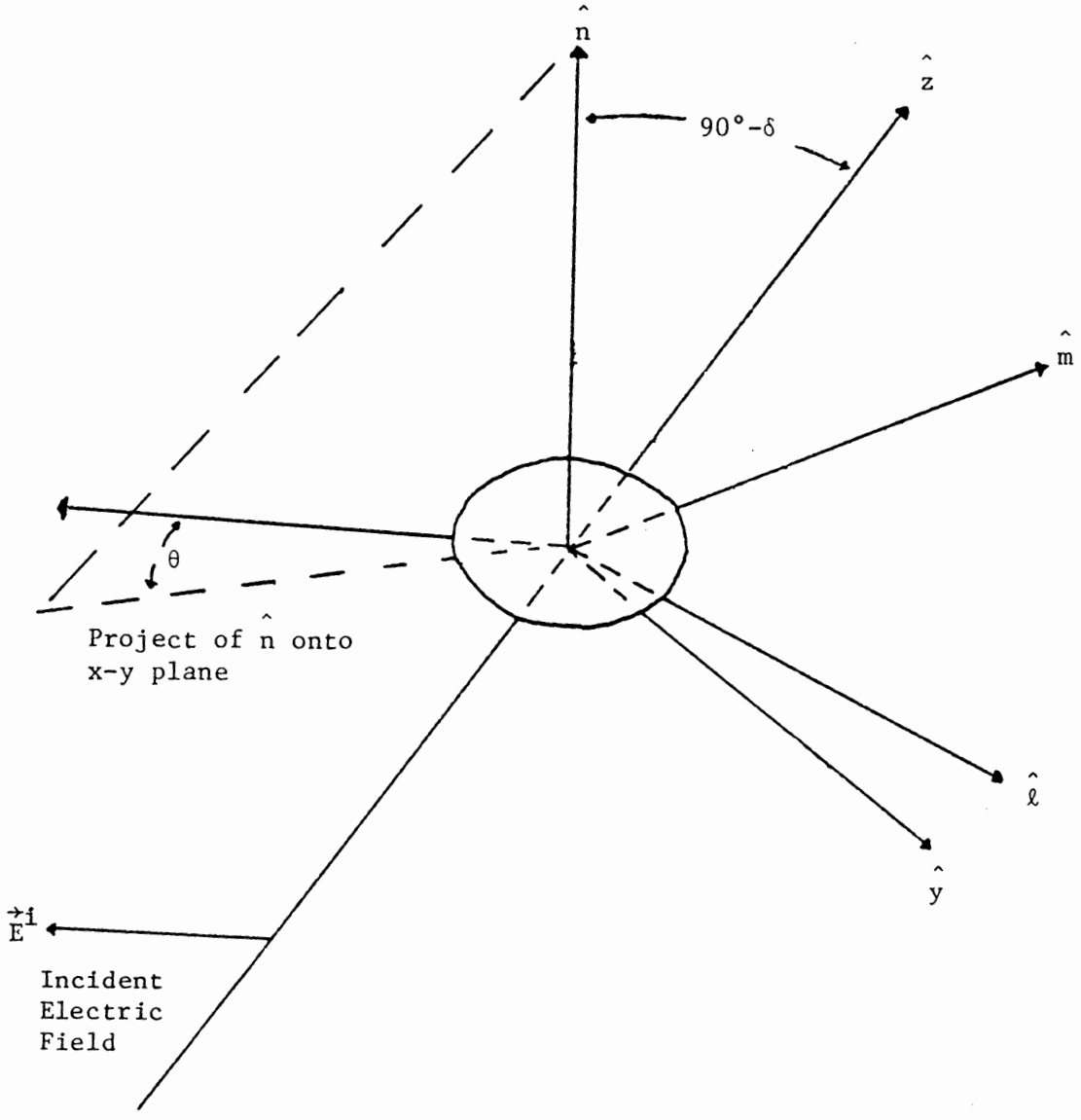

Figure 4.1b. Geometry for depolarization calculations in scattering by an oblate spheroid representing an ice plate.

orientation angle. Also, they have size distribution of an exponential form [38].

In order to calculate the depolarization effects of a realistic ice cloud, we will use the results of Section 3.3. The ice-cloud is modeled by a slab of ice particles of length L. The ice particles may be ice plates, ice needles, or both. The spatial distribution of the ice crystals is assumed to be uniform.

We consider a plane wave $\vec{E}_o$ propagating in the z direction to be incident on a slab. The coherent field propagating inside the slab obeys equation (3-40), viz.,

$$\langle \underline{E}(z) \rangle = e^{-j\underline{k}(z)} \underline{E}_o e^{-jk_o z} \quad , \tag{4-25}$$

with

$$\underline{k}(z) = \frac{2\pi}{k_o} \int_{\vec{\omega}} d\vec{\omega} \int_o^z dz' \, \underline{f}(\vec{\omega}, z) n(z, \omega) \, dz' d\omega \quad . \tag{4-26}$$

Here, z is the spatial variable along the direction of propagation, and $\vec{\omega}$ represents the particle random parameters [size, shape and orientation: $\vec{\omega} = (a, s, \phi)$]. For a homogeneous distribution of particles, $n(z, \vec{\omega})$ is independent of z. Also, the density function $n(z, \vec{\omega})$ is independent of z. Also, the density function $n(z, \vec{\omega})$ is assumed to be composed of statistically independent distribution functions of ϕ, s, and a; thus,

$$n(z, \vec{\omega}) = \rho \, p_1(a) p_2(s) p_3(\phi) \quad , \tag{4-27}$$

where ρ is the number of particles per unit volume.

It will subsequently be shown that the distribution of particle sizes need not be specified. The shape distribution is bimodal, with p denoting the fraction of plates, and 1-p the fraction of needles. The orientation angle ϕ in the azimuth plane is assumed to be Gaussian distributed, with average $\langle\phi\rangle$ and standard deviation σ_ϕ. Then,

$$p_3(\phi) = \frac{1}{\sqrt{2\pi}\,\sigma_\phi} \; e^{-(\phi - \langle\phi\rangle)^2/2\sigma_\phi^2} \quad , \tag{4-28}$$

and (4-26) becomes

$$\underline{k} = \frac{2\pi\rho}{k_o} \int f(a, s, \phi)\, p_2(s)\, p_3(\phi)\, dadsd\phi dz$$

$$= \frac{2\pi\rho L}{k_o} \int \underline{f}\, p_1(a) p_2(s) p_3(\phi)\, dadsd\phi \quad , \tag{4-29}$$

where L is the thickness of the uniformly dense ice cloud along the propagation path.

Averaging (4-29) over shape results in the expression

$$\underline{k} = \frac{2\pi\rho L}{k_o} \int \{p\, \underline{f}_{plate} + (1-p)\, \underline{f}_{needle}\}\, p_1(a) p_3(\phi)\, dad\phi \quad . \tag{4-30}$$

Examination of (4-23) and (4-24) reveals that the Rayleigh scattering formulation of the single-particle scattering coefficients renders them independent of size, other than volume dependence. Therefore, integrations in (4.30) over size lead to an average volume.

Only averaging over orientation angle remains. To do this we substitute (4-23) and (4-24) into (4-30). The final result is

$$\underline{k} = \frac{k_o}{2} L_p \rho \langle v \rangle \{ p \, \underline{f}'_{plate} + (1-p) \int \underline{f}'_{needle} \, p_1(\phi) d\phi \} \quad , \tag{4-31}$$

where ice plates and needles are assumed to have the same average volume, and the constants in the single particle scattering coefficients have been adjusted so that

$$f'_{plate} = m^2 - 1 \begin{bmatrix} 1 + \frac{1-m^2}{m^2} \cos^2 \delta \cos^2 \theta & \frac{1-m^2}{m^2} \cos^2 \delta \sin 2\theta \\ \frac{1-m^2}{m^2} \cos^2 \delta \sin 2\theta & 1 + \frac{1-m^2}{m^2} \cos^2 \delta \sin^2 \theta \end{bmatrix} \tag{4-32}$$

and

$$\underline{f}'_{needle} = 2 \frac{m^2-1}{m^2+1} \begin{bmatrix} q_{xx} & q_{xy} \\ q_{xy} & q_{yy} \end{bmatrix} \quad . \tag{4-33}$$

The equations q_{xx}, q_{xy}, and q_{yy} in (4-33) are functions of ϕ of the form cos 2ϕ and sin 2ϕ. The averaging over ϕ in (4-31), then, reduces to averaging cos 2ϕ and sin 2ϕ. We illustrate the procedure with cos 2ϕ, viz.,

$$\langle \cos 2\phi \rangle = \int_{\langle \phi \rangle - \alpha}^{\langle \phi \rangle + \alpha} \cos 2\phi \; p_1(\phi) d\phi \quad , \tag{4-34}$$

where α is the maximum variation of the orientation angle.

In most practical situations the standard deviation is rather

tight around the mean relative to the possible 180° excursion. Because of this, the limits in the integral (4-34) may be extended to infinity; that is

$$\langle \cos 2\phi \rangle = \frac{1}{\sqrt{2\pi}\,\sigma_\phi} \int_{-\infty}^{\infty} \cos 2\phi \; e^{-(\phi-\langle\phi\rangle)^2/2\sigma_\phi^2} \, d\phi \quad . \tag{4-35}$$

Making the change of variables $u = \phi - \langle\phi\rangle$ yields

$$\langle \cos 2\phi \rangle = \frac{1}{\sqrt{2\pi}\,\sigma_\phi} \cos(2\langle\phi\rangle) \int_{-\infty}^{\infty} \cos 2u \; e^{-u^2/2\sigma_\phi^2} \, du \; . \tag{4-36}$$

The remaining integral can be evaluated using the known result

$$\int_{-\infty}^{\infty} e^{-b^2x^2} \cos mx = \frac{\sqrt{\pi}}{2} e^{-m^2/4b^2} \quad . \tag{4-37}$$

Finally, we obtain

$$\langle \cos 2\phi \rangle = e^{-2\sigma_\phi^2} \cos(2\langle\phi\rangle) \quad . \tag{4-38}$$

In a similar fashion, it can be shown that

$$\langle \sin 2\phi \rangle = e^{-2\sigma_\phi^2} \sin(2\langle\phi\rangle) \quad . \tag{4-39}$$

Introducing (4-38) and (4-39) into (4-31) yields

$$\underline{k} = \frac{k_o}{2} \rho \, L \langle V \rangle \{ p \, \underline{f}'_{plate} + (1-p) \langle \underline{f}'_{needle} \rangle \} \quad , \tag{4-40}$$

where $\langle \underline{f}'_{needle} \rangle$ is found by replacing $\sin 2\phi$, $\cos 2\phi$ by $\langle \sin 2\phi \rangle$, $\langle \cos 2\phi \rangle$ respectively in (4-33).

It is convenient to define ice content for the ice cloud as

$$I_c = \rho \, L \langle V \rangle \quad . \tag{4-41}$$

This is the average volume of ice per unit volume of our times the thickness of the ice cloud. It is a measure of the total ice encountered by a wave passing through the cloud. Introduction of this parameter combines three unknowns into one, reducing the complexity of the problem. The value of I_c is open to question, but can be estimated. Choosing an average volume of 10^{-12} m^3 (from an average radius of about 0.1 mm [31]), a particle density of 10^{-6} m^{-3}, and a cloud thickness of 1 to 5 km, gives

$$I_c \sim 10^{-3} \text{ to } 5 \times 10^{-3} \ m^4/m^3 \quad . \tag{4-42}$$

In order to evaluate the coherent field at the slab, z=L, we must evaluate the exponential $e^{-j\underline{k}(z)}$. Evaluation of the exponential matrix begins by finding the eigenvalues of the matrix

$$\underline{k}(L) = \underline{k} = \begin{bmatrix} k_{11} & k_{12} \\ k_{12} & k_{22} \end{bmatrix} \quad . \tag{4-43}$$

The eigenvalues λ_1, λ_2 obey the equation

$$\det\{\lambda \underline{I} - \underline{k}\} = 0 \tag{4-44}$$

which gives

$$\lambda_1, \lambda_2 = \frac{1}{2}\{k_{11} + k_{12} \pm [(k_{11} - k_{22})^2 + (2 k_{12})^2]^{1/2}\} \quad . \tag{4-45}$$

The eigenvectors of $\underline{k}$ for distinct eigenvalues λ_1, λ_2 are

$$\begin{bmatrix} k_{22} - \lambda_i \\ \\ -k_{12} \end{bmatrix} \quad ; \quad \text{where} \quad i = 1, 2 \ . \tag{4-46}$$

Forming the matrix

$$\underline{M} = \begin{bmatrix} k_{22} - \lambda_1 & k_{22} - \lambda_2 \\ \\ -k_{12} & -k_{12} \end{bmatrix} \tag{4-47}$$

allows the evaluation of the matrix exponential [39]

$$e^{-j\underline{k}} = \underline{M} \begin{bmatrix} e^{-j\lambda_1} & 0 \\ \\ 0 & e^{-j\lambda_2} \end{bmatrix} \underline{M}^{-1} \ , \tag{4-48}$$

where

$$\underline{M}^{-1} = \frac{1}{k_{12}(\lambda_1 - \lambda_2)} \begin{bmatrix} -k_{12} & -k_{22} + \lambda_2 \\ \\ k_{12} & k_{22} - \lambda_1 \end{bmatrix} \ . \tag{4-49}$$

Performing the matrix multiplication in (4-48) leads to

$$e^{-j\underline{k}} = \frac{1}{\lambda_1-\lambda_2}\begin{bmatrix} (k_{22}-\lambda_2)e^{-j\lambda_2}-(k_{22}-\lambda_1)e^{-j\lambda_1} & k_{12}(e^{-j\lambda_1}-e^{-j\lambda_2}) \\ k_{12}(e^{-j\lambda_1}-e^{-j\lambda_2}) & (k_{22}-\lambda_2)e^{-j\lambda_1}-(k_{22}-\lambda_1)e^{-j\lambda_2} \end{bmatrix}. \quad (4\text{-}50)$$

Comparing (4-1) to (4-25) we see that $[e^{-j\underline{k}}]$ is simply the depolarization matrix $\underline{D}$ for calculating the received field averaged over the distribution of ice particles. Computation of the depolarization matrix is summarized as follows: Calculate $\underline{k}$ from (4-40); compute the eigenvalues λ_1, λ_2 from (4-45); evaluate the depolarization matrix in (4-50).

The ice computation algorithm as desdribed in this section has been coded in computer program form. This program is described in Appendix B. Inputs to the program are: frequency, elevation angle, mean and standard deviation of azimuth angle, ice content, and fraction of ice plates. Either circular or linear polarization can be used as incident polarization states.

Computations have been performed for the SIRIO system (right-hand circular polarization, 11.6 GHz, 11.7° elevation angle). (Previous computations in [, Chapter 6] were based on single scattering.) Computation results are presented in the form of two types of plots: isolation versus phase (of cross polarized relative to co-polarized outputs signal) and isolation versus mean orientation

angle.

The effect of tilt angle θ on circular polarization is only that of shifting the phase reference point and, in theory, should be unimportant. As a check on the computer program, we present the isolation versus phase plots in Figure 4- . Isolation values are shown for various mixtures of plates and needles.

P is the fraction of ice plates; the remaining ice particles are needles. All are oriented in the horizontal plane. The needles have a Gaussian distribution of orientation angle with standard deviation $\delta_\phi = 5°$ and varying mean $\langle\phi\rangle$. The symbos ○, △, +, and x represent P values of 0, 0.4, 0.6, and 0.8 (the fraction of plates) and are positioned for every 10° increment in $\langle\phi\rangle$. For example, for all needles the plot forms a large vee. The mid point of the vee is a low isolation case that occurs for $\langle\phi\rangle = 0°; 180°$: i.e., the long axis of the needles are nearly perpendicular to the propagation path giving maximum depolarization.

In Fig. 4-2a θ is 45° and in Fig. 4-2b θ is 0°. The results are exactly the same, except for a reduction of a constant 90° in phase. This is supported by the simple results derived earlier. In Eq. (4-23) phase is proportional to 2θ, so if θ were reduced by 45°, phase would decrease by 90° as observed.

Next, we demonstrate the effect of the azimuth angle standard deviation, σ_ϕ. Figure 4-3 shows isolation versus phase for an ice content of 0.002 and σ_ϕ values of 0° and 15°. These, together with Figure 4-2b ($\sigma_\phi = 5°$ case), show that the effect of σ_ϕ is relatively

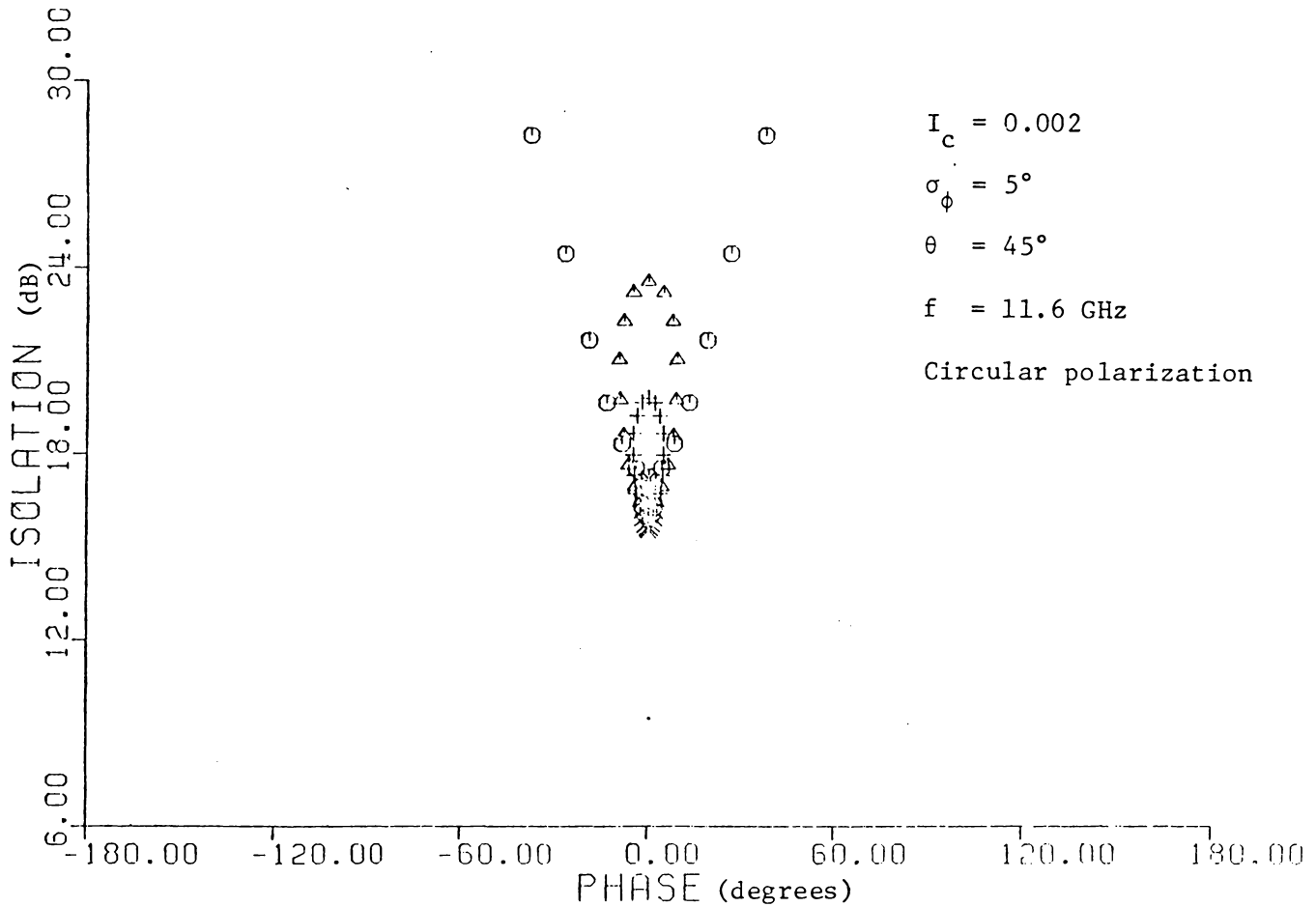

Figure 4.2a. θ = 45°.

Figure 4.2. Isolation versus phase for the following fractions of ice plates: p = 0.8 (x), 0.6 (+), 0.4 (△), and 0.0 (□). The effect of polarization angle θ is demonstrated.

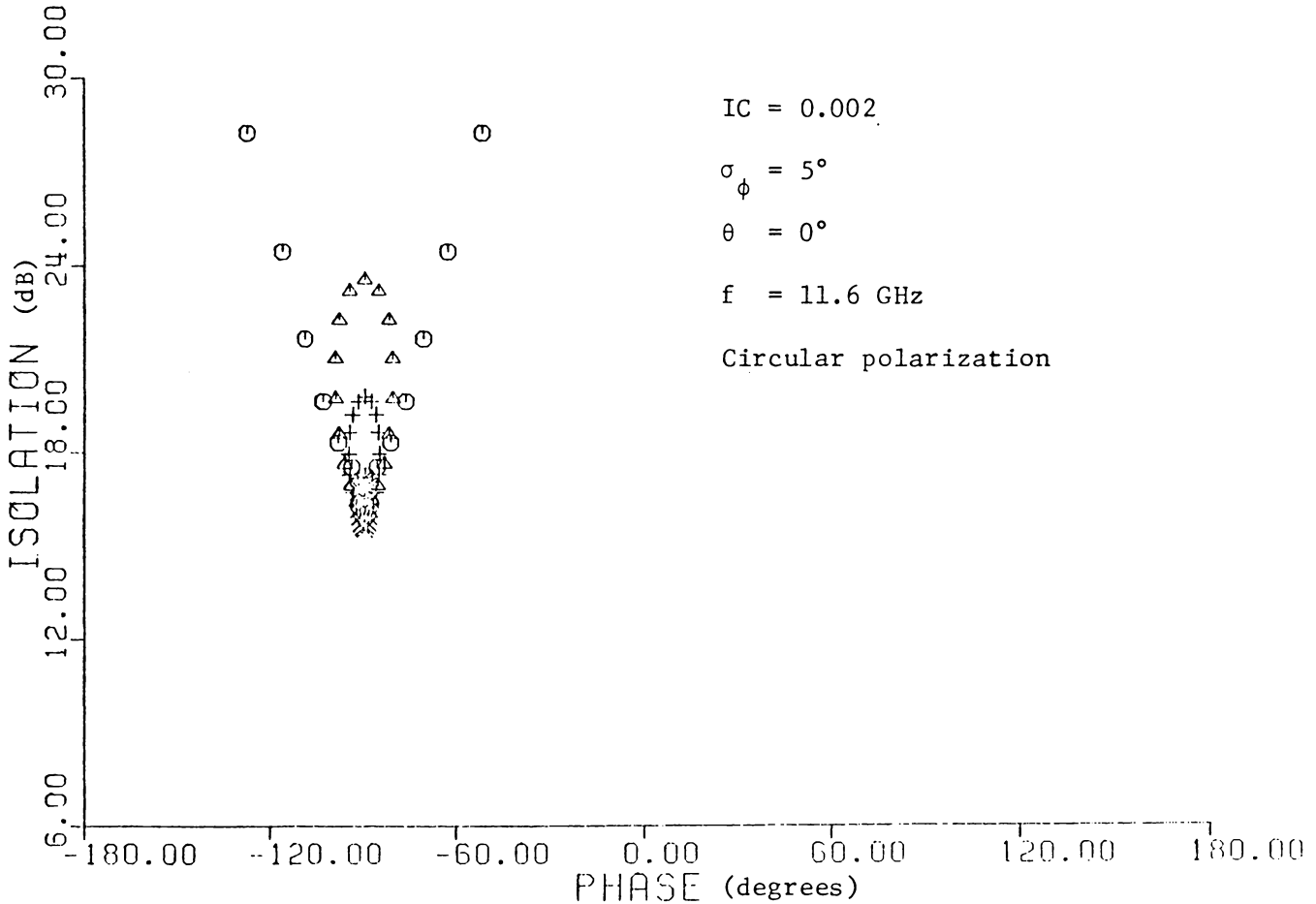

Figure 4.2b. $\theta = 0°$.

Figure 4.2. Isolation versus phase for the following fractions of ice plates: p = 0.8 (x), 0.6 (+), 0.4 (△), and 0.0 (□). The effect of polarization angle θ is demonstrated.

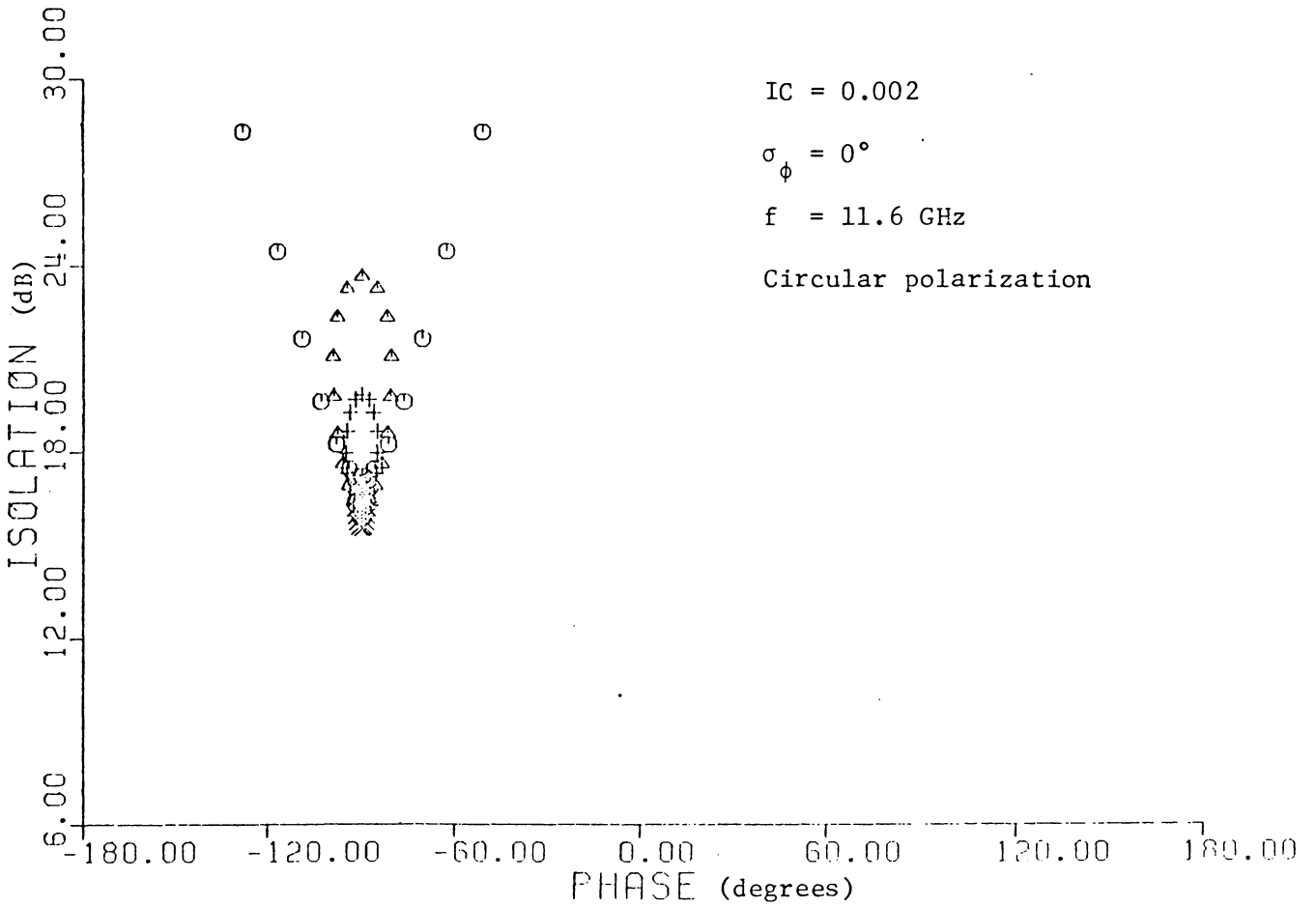

Figure 4.3a. $\sigma_\phi = 0°$.

Figure 4.3. Isolation versus phase for the following fractions of ice plates: p = 0.8 (x), 0.6 (+), 0.4 (△), and 0.0 ( ). The effect of the orientation angle standard deviation σ_ϕ is demonstrated.

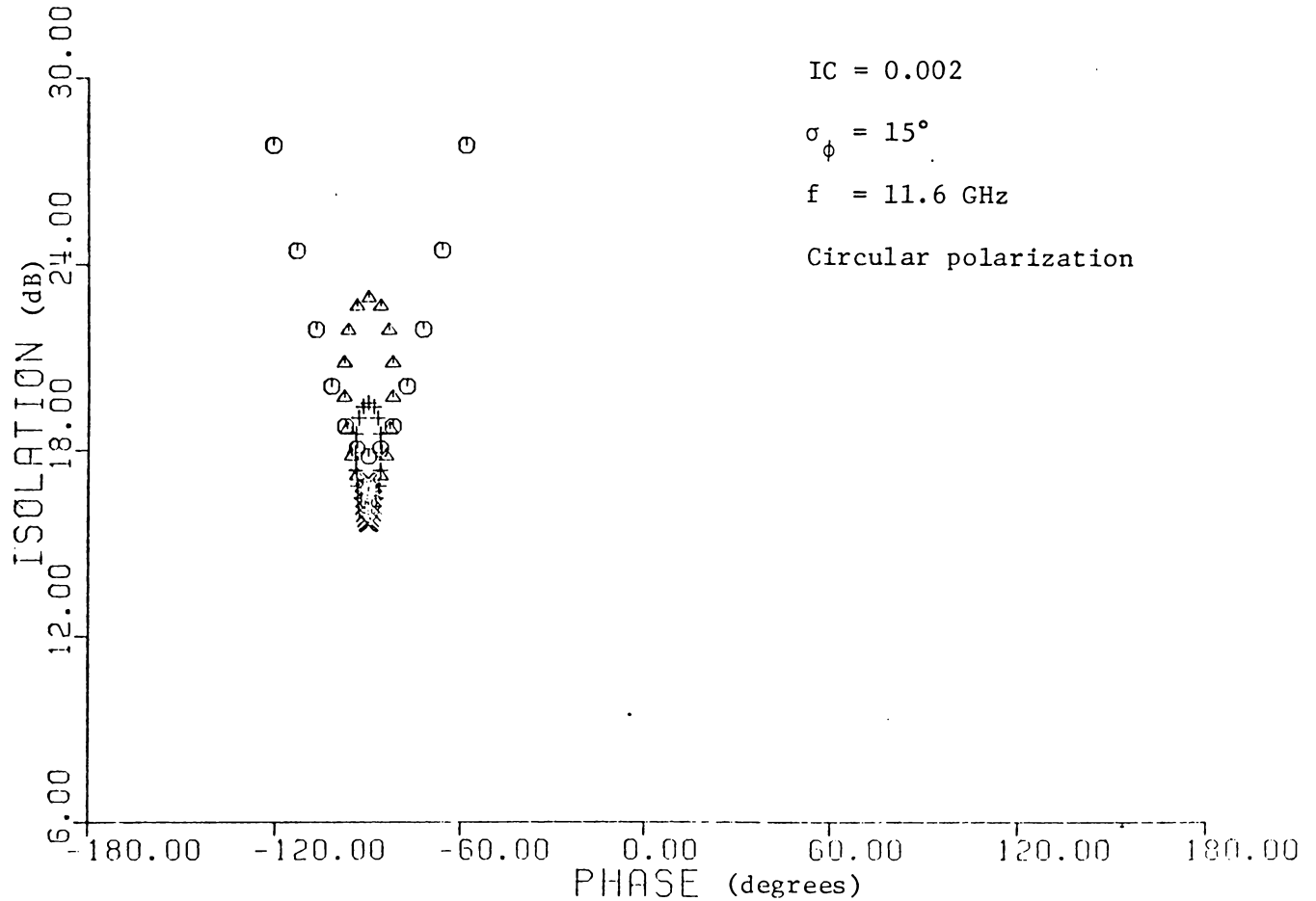

Figure 4.3b. σ_ϕ = 15°.

Figure 4.3. Isolation versus phase for the following fractions of ice plates: p = 0.8 (x), 0.6 (+), 0.4 (Δ), and 0.0 ( ). The effect of the orientation angle standard deviation σ_ϕ is demonstrated.

minor. As σ_ϕ is increased, the isolation values for ice with needles present increases.

The effect of ice quantity is significant. Figure 4-4 shows isolation versus phase for ice quantities of 0.001 and 0.004. These, together with Fig. 4-2b (IC = 0.002), show that isolation values vary greatly over this range of ice quantity variation.

Isolation is also dependent upon mean azimuth angle $<\phi>$ when needles are present. This is illustrated in Fig. 4-5 for various values of σ_ϕ and IC with plate fraction as a parameter.

4.1.5 Comparisons with Data

The data measured at Blacksburg on the SIRIO diversity system for the period July 15 to December 31, 1980, are plotted in Figure 4-6. These can be compared to the predictions for the Blacksburg SIRIO systems presented in Figs. 4-2 to 4-4.

Before comparing data to predictions, it is helpful to reexamine the simple relationships developed earlier. From (4-19) we see that $\frac{\phi'}{2} = \sqrt{CPR_c} = 1/\sqrt{I_c}$, where ϕ' is the medium differential phase shift in the differential propagation constant model. The phase from (4-20), $\angle C_c = -\frac{\pi}{2} + \frac{\phi'}{2} + 2\theta$, can then be used to determine θ. Computing $\frac{\phi'}{2}$ for isolation values of 25, 20, 15, and 10 dB gives values of $\frac{\phi'}{2} = 3.2°$, 5.7°, 10.1°, and 18.1°, respectively. This gives an idea of expected phase variation with isolation due to medium differential phase shift fluctuations. The remaining variation in phase, 2θ, is not directly related to isolation. Changes in θ can

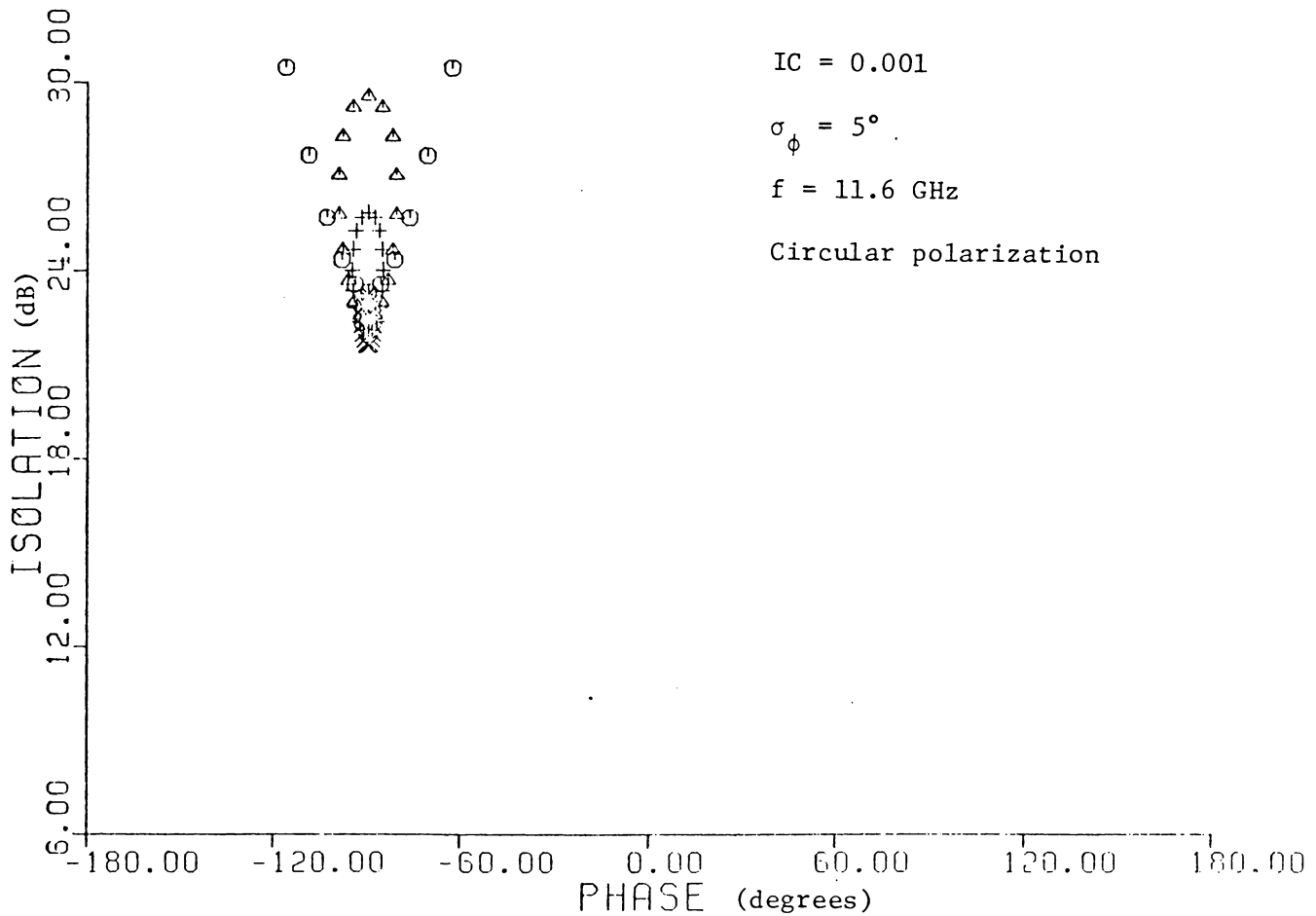

Figure 4.4a. IC = 0.001

Figure 4.4. Isolation versus phase for the following fractions of ice plates: p = 0.8 (x), 0.6 (+), 0.4 (△), and 0.0 ( ). The significance of the ice quantity IC is demonstrated.

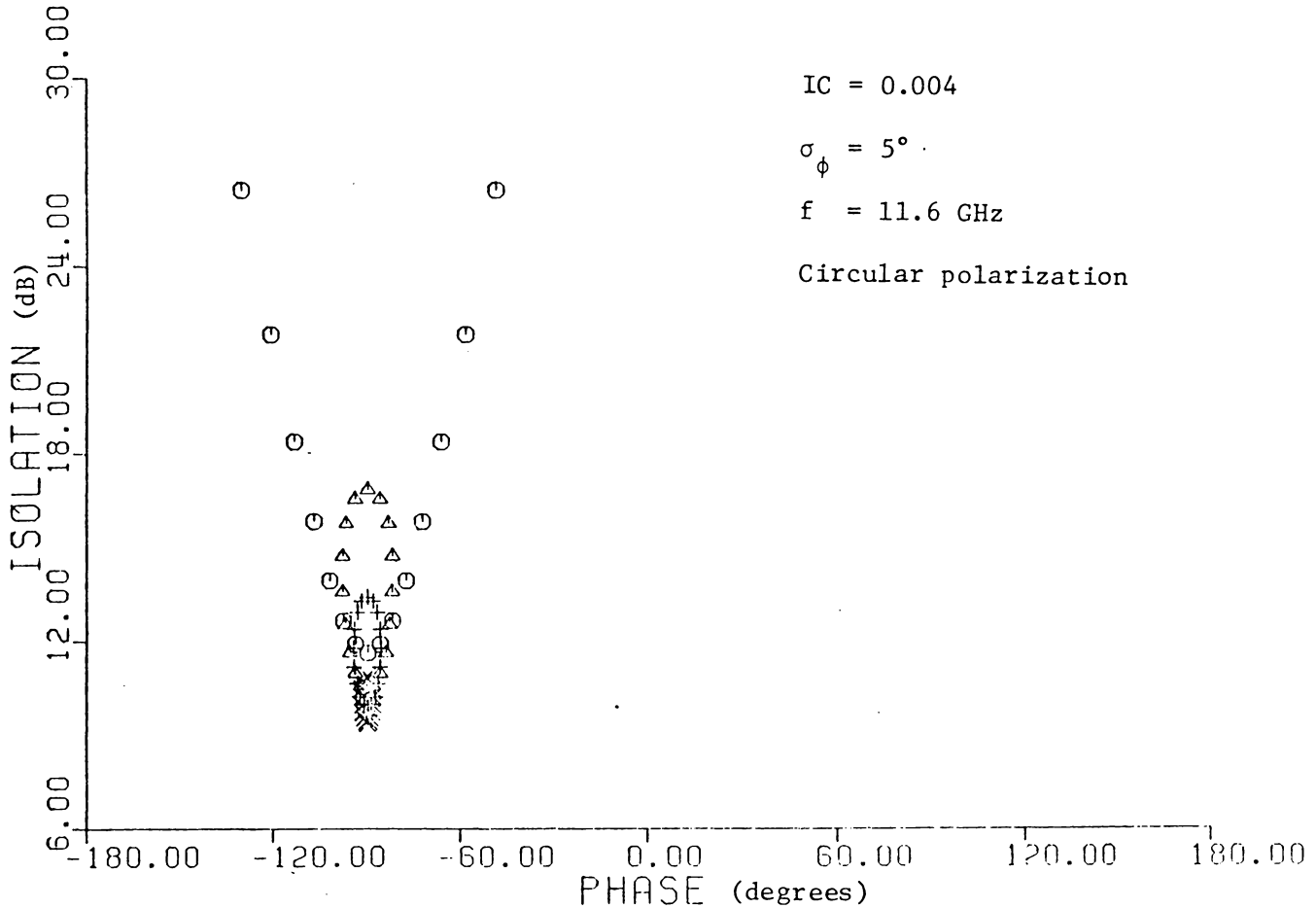

Figure 4.4b. IC = 0.004.

Figure 4.4. Isolation versus phase for the following fractions of ice plates: p = 0.8 (x), 0.6 (+), 0.4 (△), and 0.0 ( ). The significance of the ice quantity IC is demonstrated.

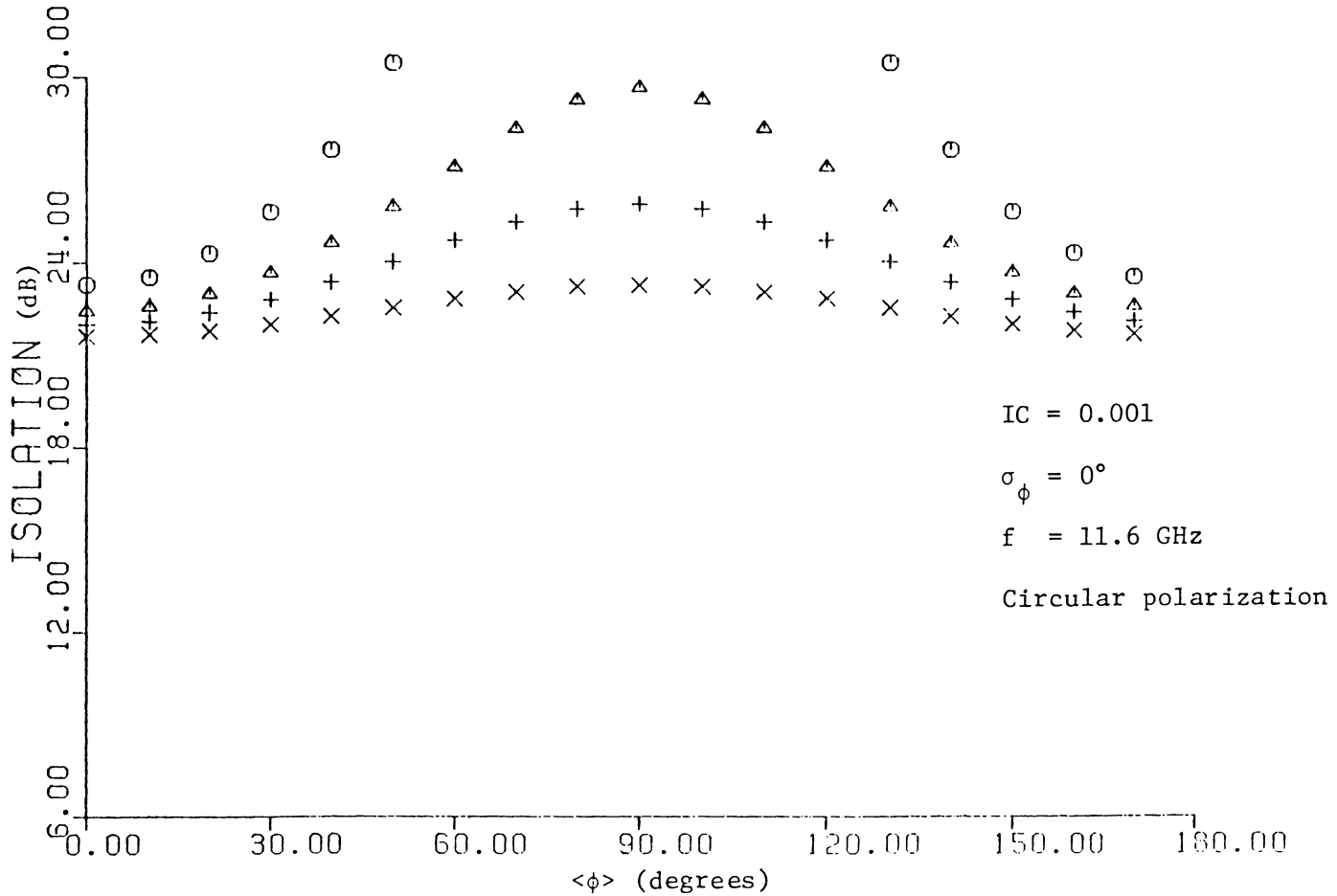

Figure 4.5. Isolation versus mean orientation angle <φ>.
a) IC = 0.001 , σ_ϕ = 0°.

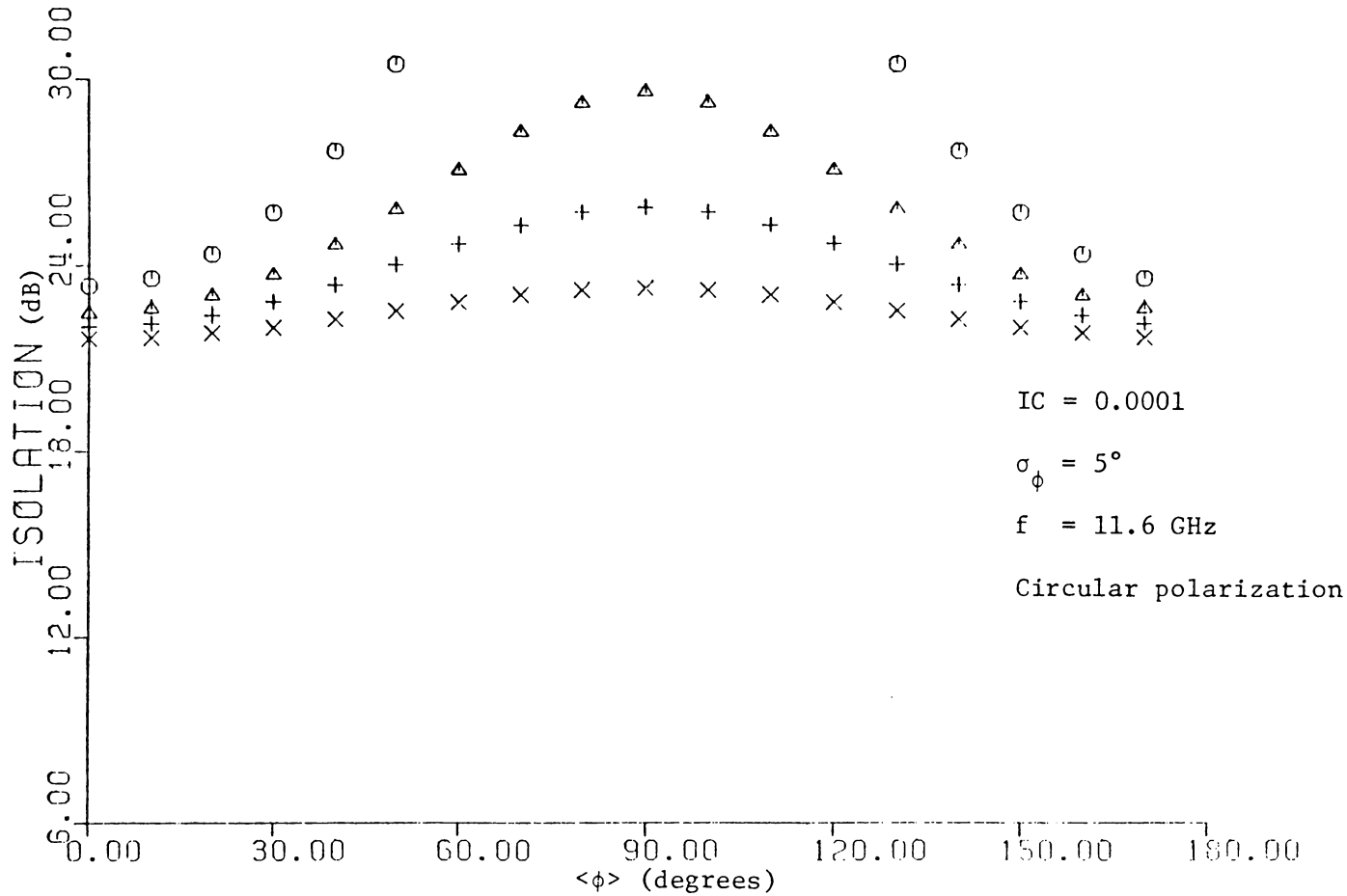

Figure 4.5. Isolation versus mean orientation angle
b) IC = 0.001 , σ_ϕ = 5°.

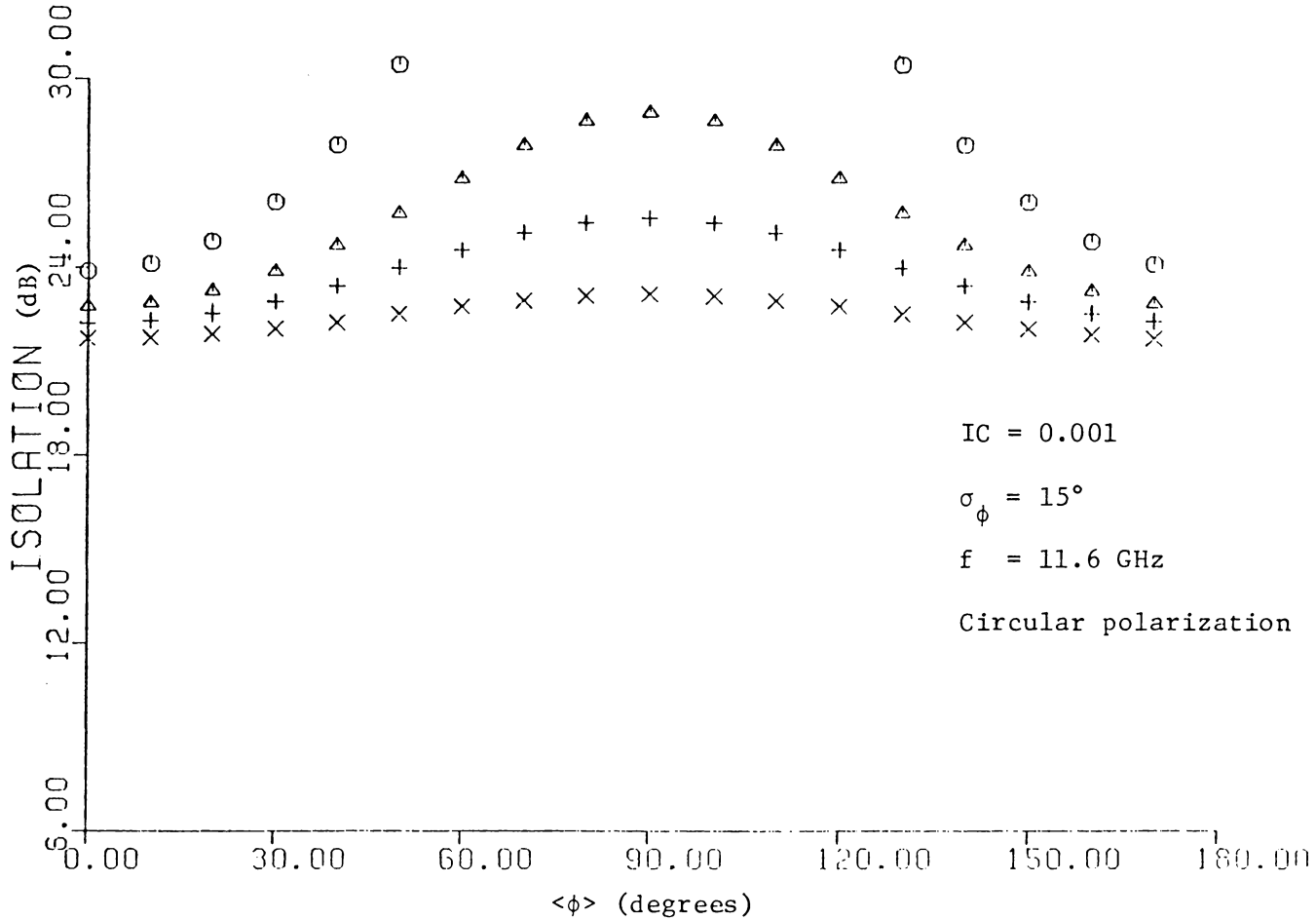

Figure 4.5. Isolation versus mean orientation angle <φ>.
c) IC = 0.001 , σ_ϕ = 15°.

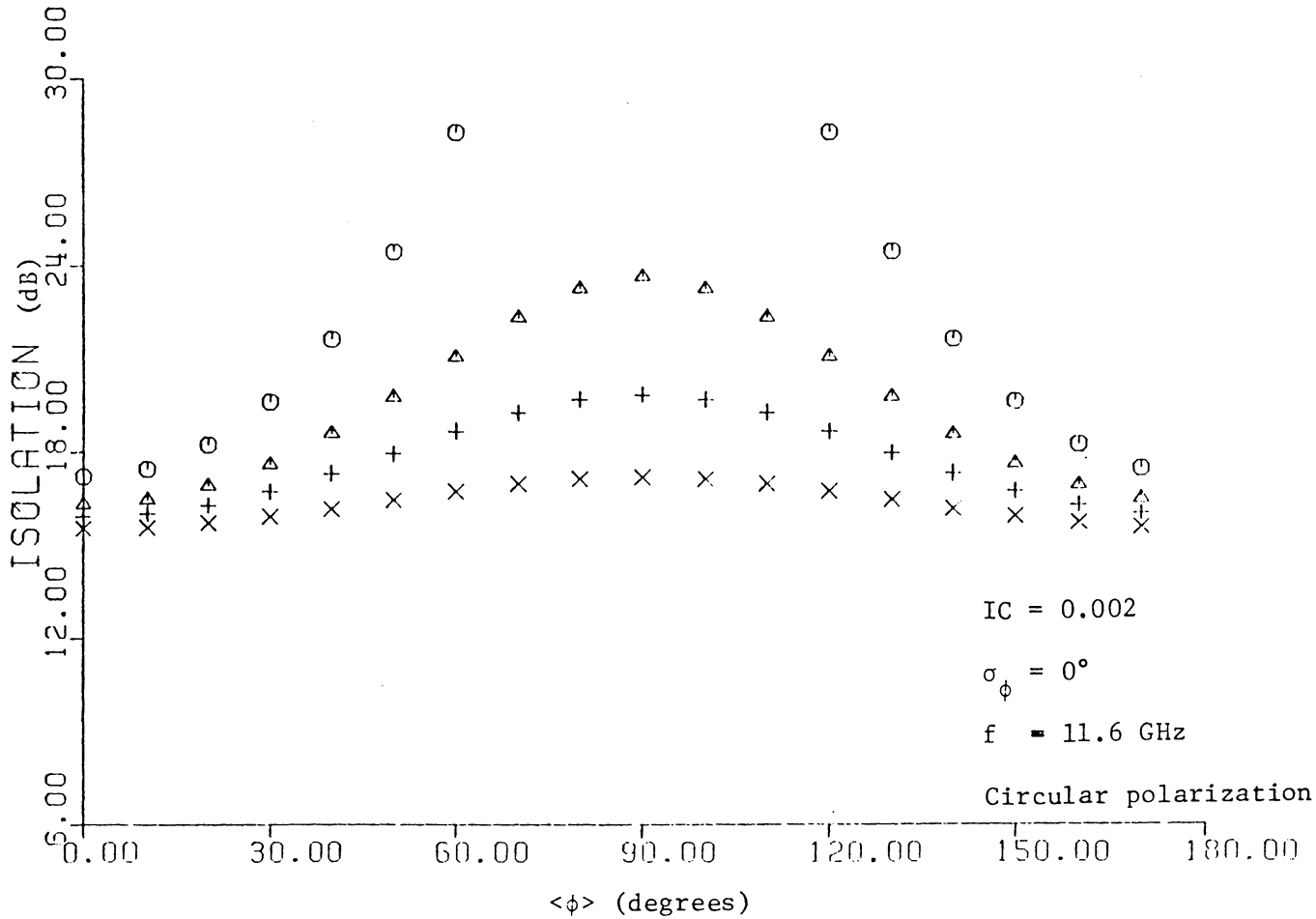

Figure 4.5. Isolation versus mean orientation angle <φ>.
d) IC = 0.002 , σ_ϕ = 0°.

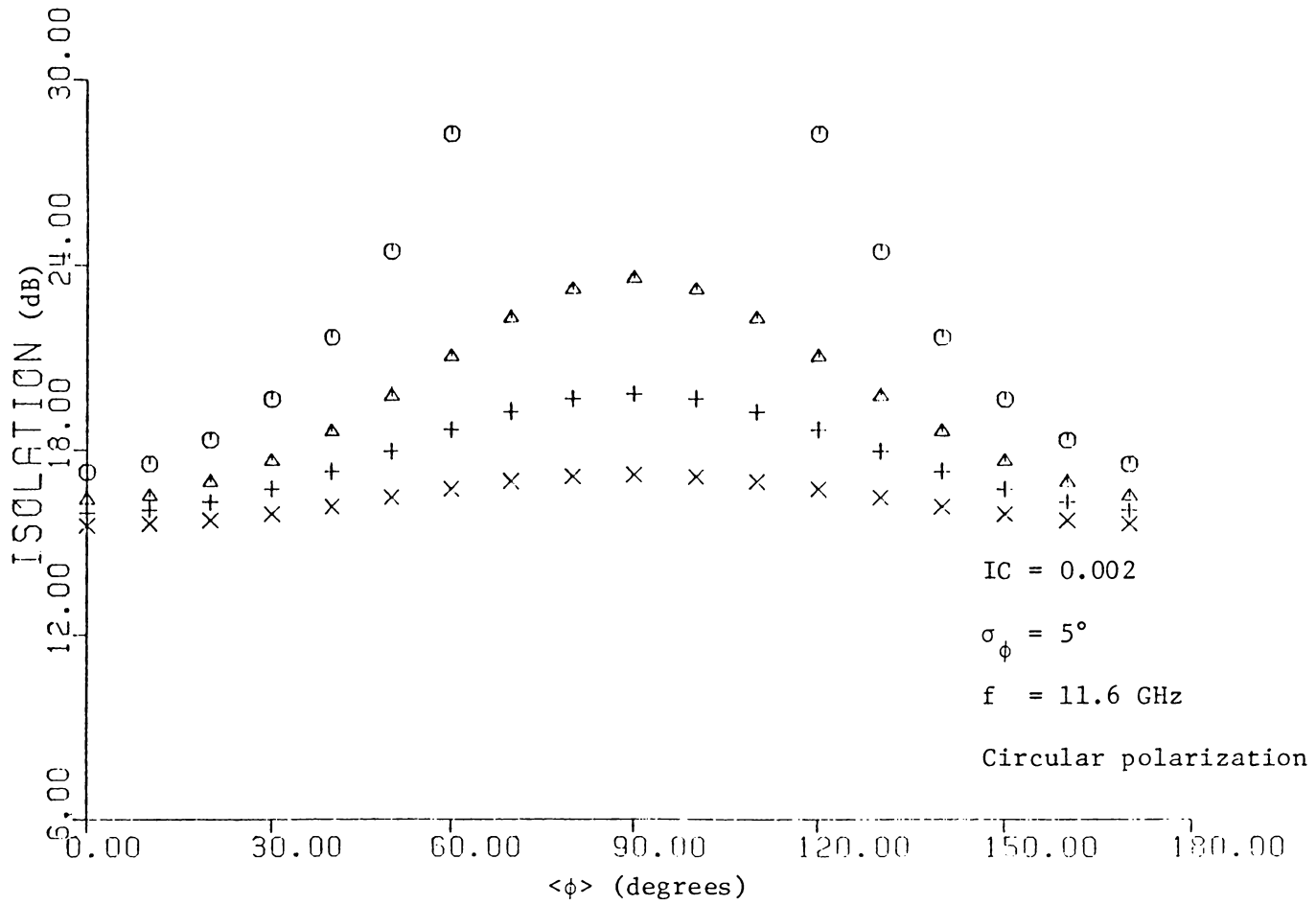

Figure 4.5. Isolation versus mean orientation angle <φ>.
e) IC = 0.002 , σ_ϕ = 5°.

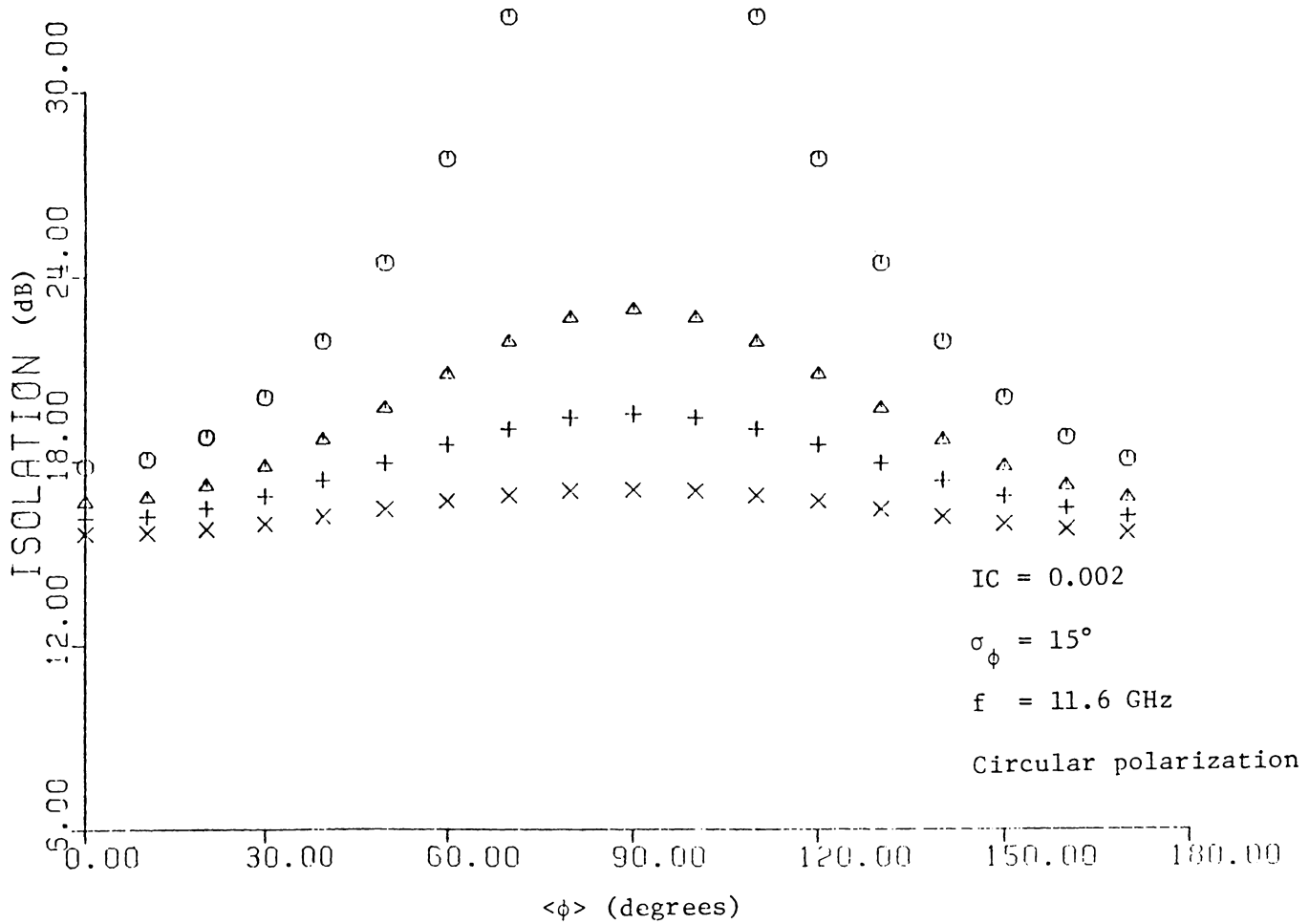

Figure 4.5. Isolation versus mean orientation angle <φ>.
f) IC = 0.002 , σ_ϕ = 15°.

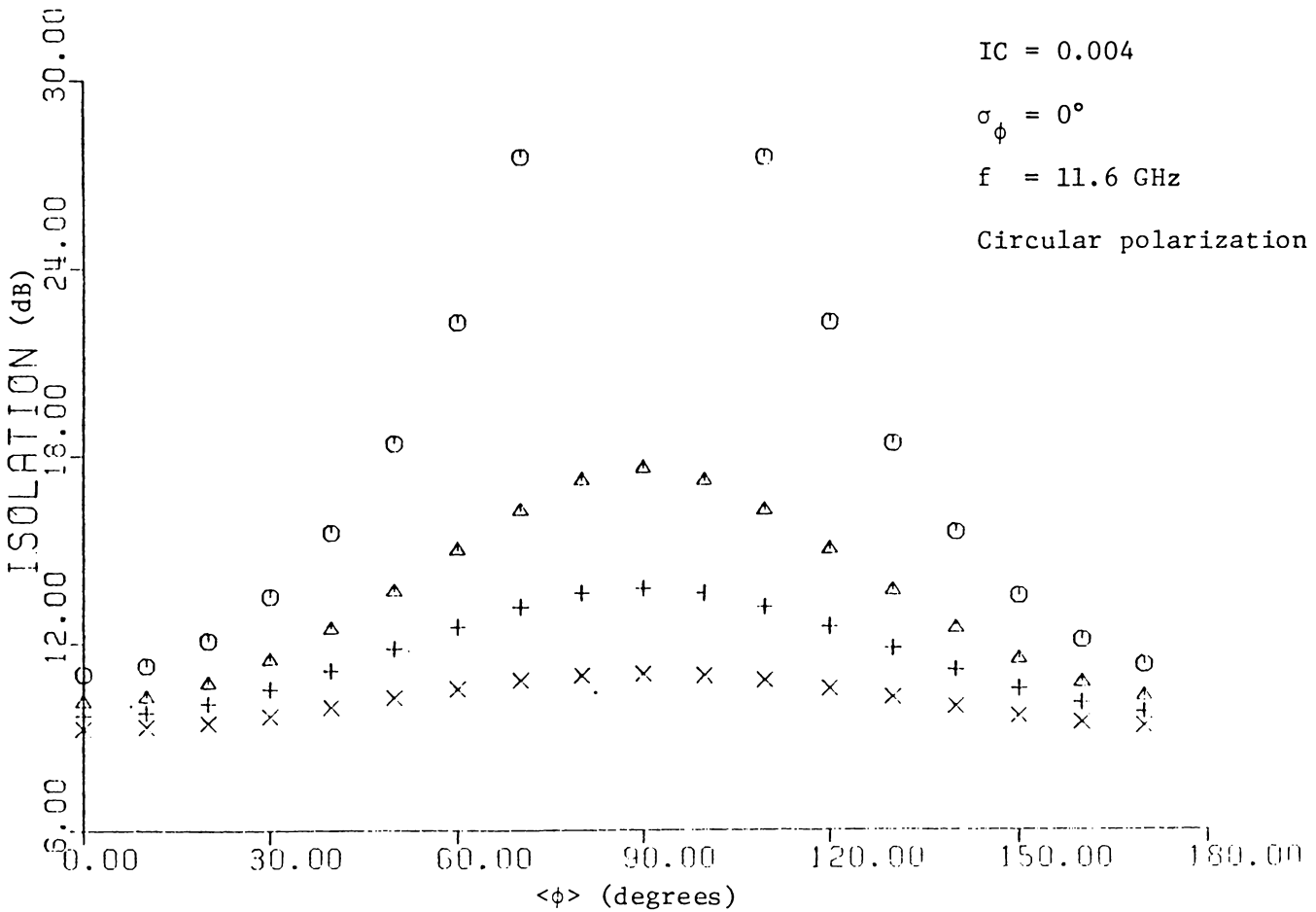

Figure 4.5. Isolation versus mean orientation angle <φ>.
g) IC = 0.004 , σ_ϕ = 0°.

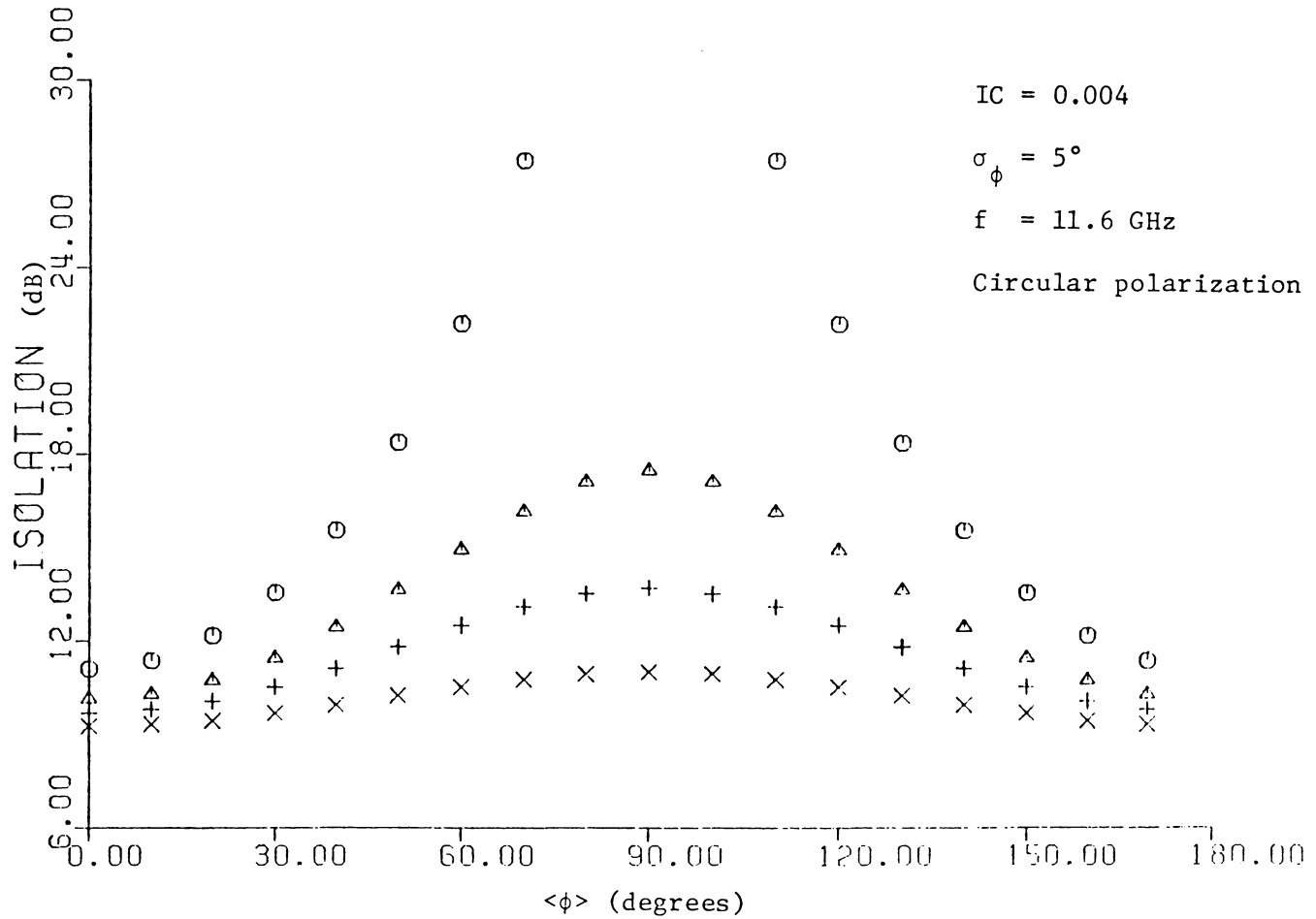

Figure 4.5. Isolation versus mean orientation angle $\langle\phi\rangle$.
h) IC = 0.004 , σ_ϕ = 5°.

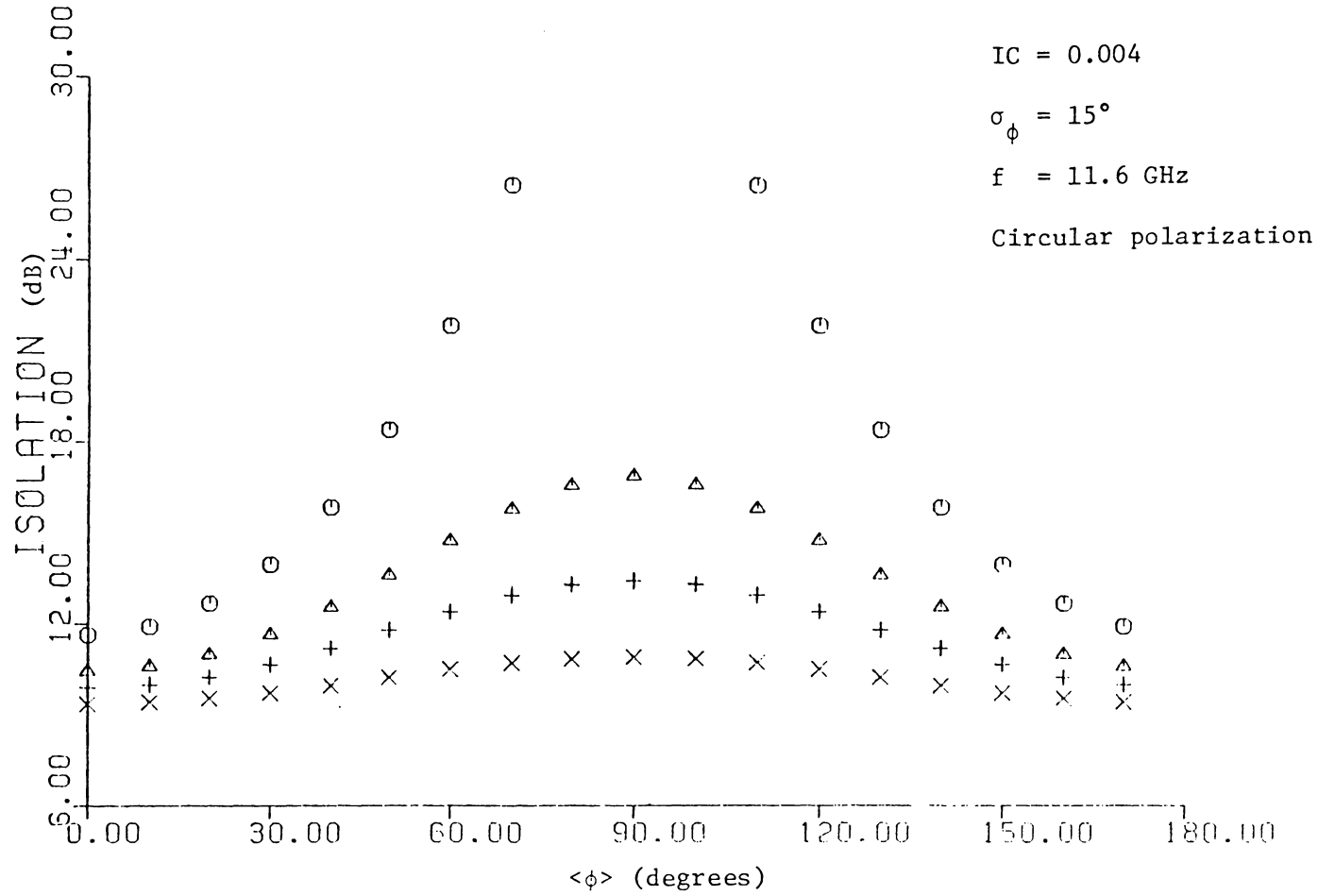

Figure 4.5. Isolation versus mean orientation angle <φ>.
i) IC = 0.004 , σ_ϕ = 15°.

arise due to medium orientation angle changes [ ]. Thus, an average out-of-horizontal-plane tilt of ice particles would lead to a phase change of twice that amount. It is not clear what to expect here but, as discussed in Sec. 4.1.1, $\theta = 25°$ or so would be an extreme case. Therefore, a phase angle fluctuation of 68° would occur for low isolation (10 dB) and extreme canting angles, but typical angle variations would be much less.

This phase angle discussion assumes that no instrument effects are present. In other words, additional phase deviations arise from inaccuracies in establishing a "clear weather" reference angle to which the event value can be compared. Such inaccuracies are caused by small propagation effects which are present but are unresolvable by subtracting the residuals.

On the other hand, large variations in isolation values are created by variations in the ice content, shape distribution, and azimuth angle distribution of ice needles. All these parameter variations are given in Fig. 4.5. Even with the simple medium model adopted, there are still more parameters than the data can resolve. However, we can bound the variations. The data of Fig. 4.6 varies from 26 to 12 dB isolation. This range of values can be matched by the calculated values in Fig. 4.5.

4.2 Rain Attenuation and Depolarization

Rain causes depolarization to the propagating wave as ice clouds do, but, at the same time, the wave is attenuated. Most of the

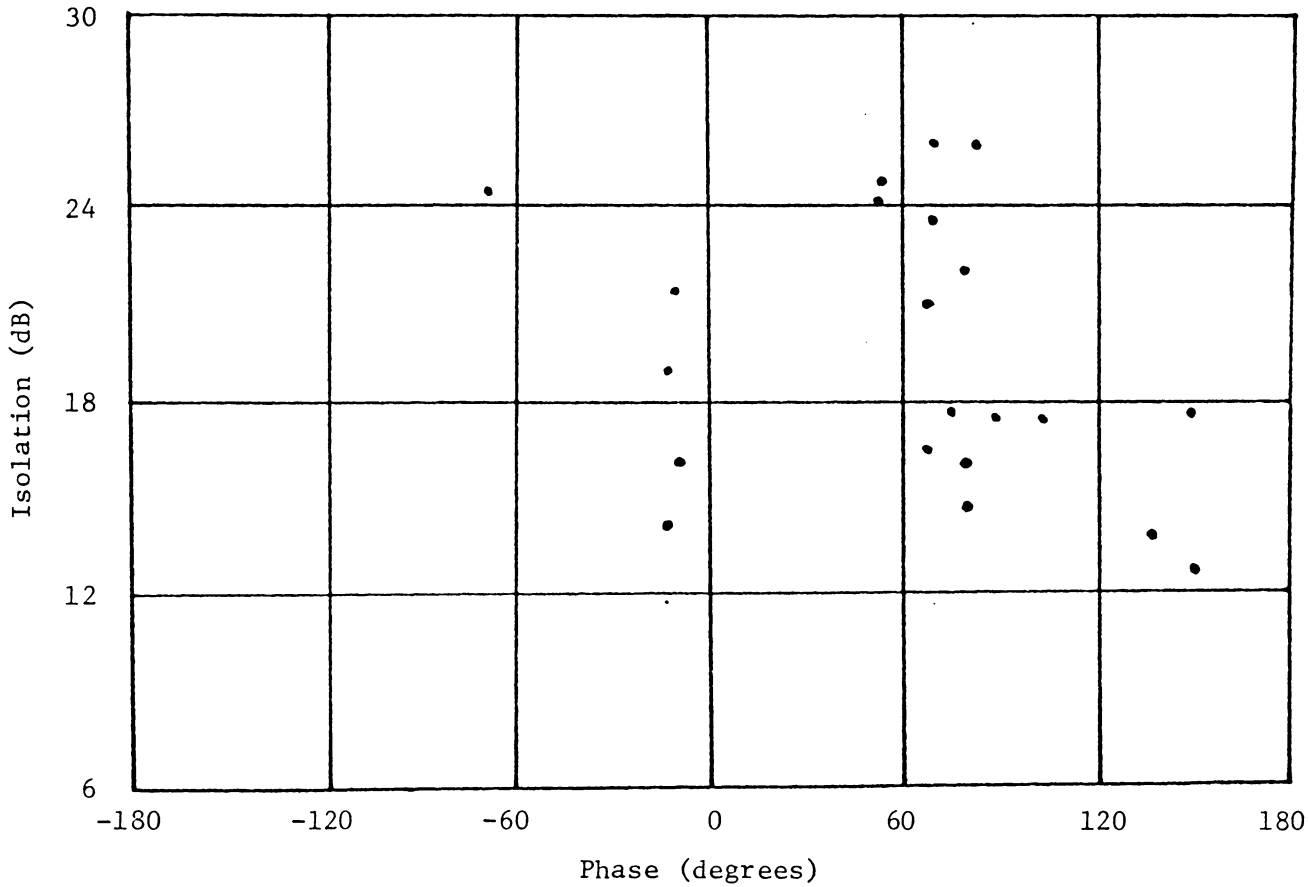

Figure 4.6. Isolation and phase values measured on the SIRIO diversity system for July 15 to December 31, 1980.

theoretical rain models in the literature, either they do not take into account the multiple scattering of the rain medium, or they make unrealistic assumptions, such as that the rain is uniform across the propagation path [33], or that the raindrops that the medium is composed of have all the same shape and canting angle [34]. In the past four years a more realistic model has been developed by Persinger and Stutzman [27] that assumes nonuniform rain across the propagation path. Also, it considers canting angle and shape raindrop distributions. This model considers only first-order multiple scattering. It is our intent in this section to incorporate the more realistic rain medium introduced by Stutzman into the multiple scattering model that was developed in Chapter III.

4.2.1 Scattering Matrix of a Raindrop

The equivolumetric radius of the raindrops varies from 0.1 to 4.0 mm. In the millimeter wave frequencies the raindrop radius is comparable with the free space wavelength and the Rayleigh scattering approximation is not adequate for the calculation of the raindrop scattering matrix. It is necessary, then, to use one of the numerical methods described in Chapter II in order to calculate the raindrop scattering coefficients. In our computation we will use values of scattering coefficients published by Uzunoglou *et al.* [40]. These results have been computed using the Fredholm integral equation method. We will assume that the raindrops are either spherical or oblate spheroids.

Let θ be the canting angle of the oblate raindrop (see Figure

The scattering matrix is then given

$$\underline{f}^{obl} = \frac{1}{2}\begin{bmatrix} f_V(\bar{a})+f_H(\bar{a})+\cos 2\theta[f_H(\bar{a})-f_V(\bar{a})] & [f_V(\bar{a})-f_H(\bar{a})\sin 2\theta \\ [f_V(\bar{a})-f_H(\bar{a})]\sin 2\theta & [f_V(\bar{a})+f_H(\bar{a})+\cos 2\theta[f_V(\bar{a})-f_H(\bar{a}) \end{bmatrix} . \tag{4-51}$$

In this expression, $\bar{a}$ is the equivolumetric radius of the oblate raindrop, $f_V(\bar{a})$ is the scattering coefficient in the direction of the major axis, and $f_H(\bar{a})$ is the scattering coefficient in the plane perpendicular to the direction of the major axis. The quantities $f_V(\bar{a})$, $f_H(\bar{a})$ are expressed in terms of powers of the equivolumetric radius of the raindrop; specifically,

$$f_{\substack{V \\ H}}(\bar{a}) = \sum_{i=0}^{5} \alpha_{i\ \substack{V \\ H}}\, a^{-i} \quad . \tag{4-52}$$

Values of $a_{i\ \substack{V \\ H}}$ were obtained by curve fitting the Uzunoglou [40] results in terms of size, at a specific elevation angle.

4.2.2 Rain Medium Computations

The rain medium is represented by a slab of raindrops of length L. A plane wave $\vec{E}_{ox}$ propagating in the z direction is incident upon the slab. The coherent field propagating inside the rain medium obeys equation (3-40), viz.,

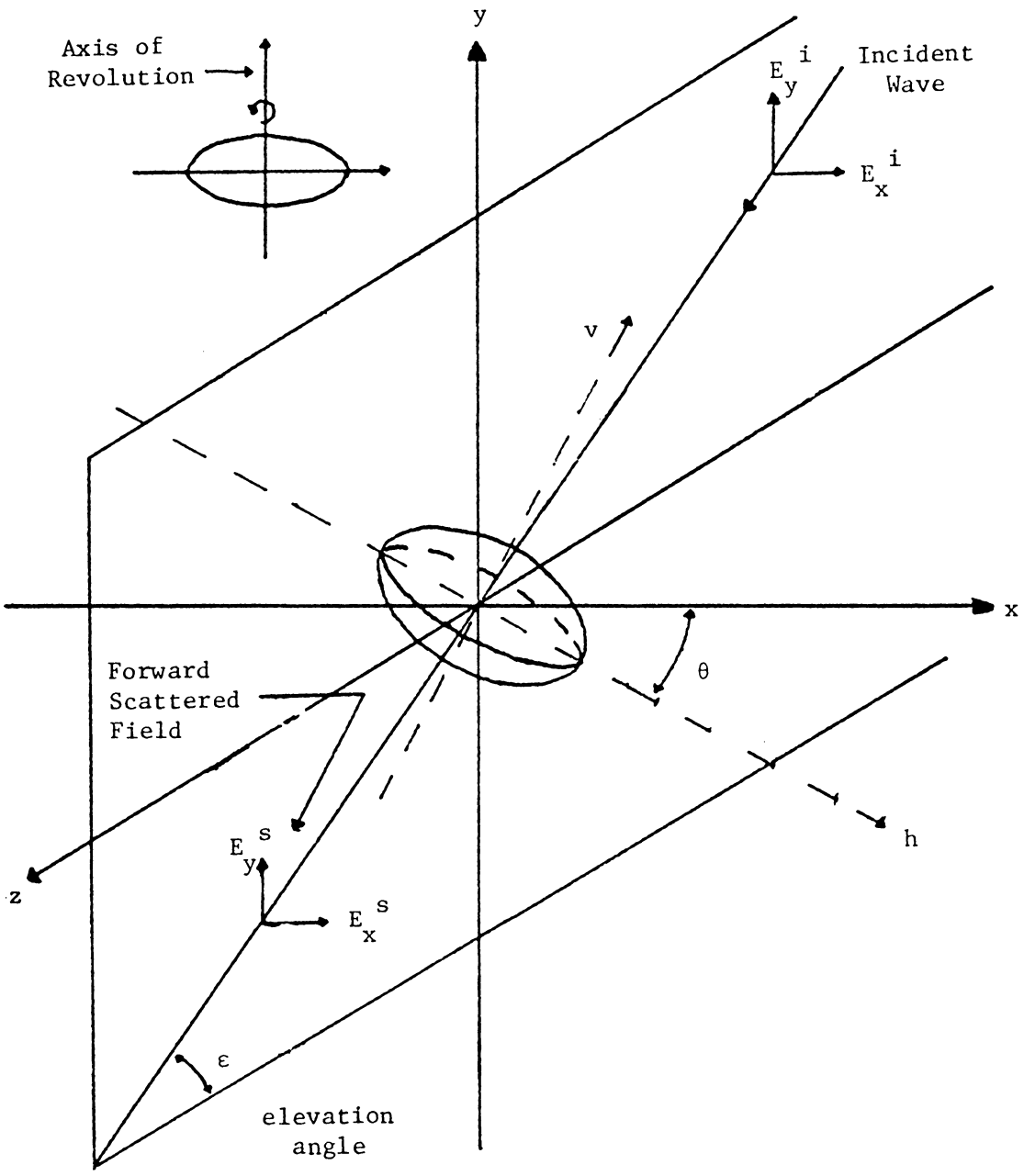

Figure 4.7. Geometry used in deriving the scattering matrix ox an oblate spheroidal raindrop.

$$\langle \underline{E}(z) \rangle = e^{-j\underline{k}(z)} \, \underline{E}_o \, e^{-jk_o z} \quad . \tag{4-53}$$

where

$$\underline{k}(z) = \frac{2\pi}{k_o} \int_{\vec{\omega}} \underline{f}(\vec{\omega}) \, n(\vec{\omega}) \, d\vec{\omega} \quad , \tag{4-54}$$

with

$$\vec{\omega} = (z, s, \bar{a}, \theta) \quad . \tag{4-55}$$

In (4-55), z is the distance in the direction of propagation, s is the shape of the raindrop (spherical or oblate), $\bar{a}$ is the equi-volumetric radius of the individual raindrop, and θ is the raindrop canting angle. The distribution density function $n(\vec{\omega})$ entering into (4-54) is assumed to be statistically independent of θ and s, i.e.,

$$n(\vec{\omega}) = n_o(z, \bar{a}) \, p_1(\theta) \, p_2(s) \quad . \tag{4-56}$$

$p_2(s)$ is a discrete distribution density function, with values p for percentage of spherical raindrops in the rain. The canting angle is Gaussian distributed with average value $\langle\theta\rangle$ and standard deviation σ_θ; so

$$p_1(\theta) = \frac{1}{\sqrt{2\theta} \, \sigma_\theta} \, e^{-(\theta - \langle\theta\rangle)^2 / 2\sigma_\theta^2} \quad . \tag{4-57}$$

For $n_o(z, \bar{a})$ we use the Marshall-Palmer drop size distribution with rain rate as a function of the propagation path, viz.,

$$n_o(z, \bar{a}) = N_o \, e^{-8.2\{R(z)^{-0.21}\}} \quad m^{-3} \, mm^{-1} \quad , \tag{4-58}$$

with N_o = 16,000, and R(z), the rain rate, that varies with respect to z in accordance with the piecewise uniform model of Persinger and Stutzman [1979] as follows:

$$R(z) = \begin{cases} R_o\left[\frac{z}{10}\right]^{-0.66} & 0 \leq z < 0.2L \\ \\ R_o & 0.2\ L \leq z \leq L \end{cases} \qquad (4\text{-}59)$$

Here, R_o is the rain rate at the receiving station at z = L.

The evaluation of the matrix $\underline{k}$ is done as follows:

$$\underline{k} = \frac{2\pi}{k_o} \int_{\vec{\omega}} \underline{f}(\vec{\omega})\ n(\vec{\omega})\ d\vec{\omega}$$

$$= \frac{2\pi}{k_o} \int_o^z dz \int_o^\infty d\bar{a} \int_o d\theta \int ds\ \underline{f}(\bar{a}, s, \theta)\ n_o(z, \bar{a})\ p_1(\theta) p_2(\theta) \quad . \qquad (4\text{-}60)$$

Performing first the integration with respect to s, we obtain

$$\underline{k} = \frac{2\pi}{k_o} \int_o^z dz \int_o^\infty d\bar{a} \int d\theta\ \{p\ \underline{f}^{SPH}(\bar{a}) = (1-p)\ \underline{f}^{OBL}(\bar{a}, \theta)\}\ n_o(z, \bar{a})\ p_1(\theta)\ , \qquad (4\text{-}61)$$

The integral in equation (4-61) over the angle may be performed by evaluating the expressions

$$\langle \sin 2\theta \rangle = \int_{\langle\theta\rangle-\alpha}^{\langle\theta\rangle+\alpha} d\theta\ \sin 2\theta\ p_1(\theta) \quad , \qquad (4\text{-}62a)$$

$$\langle \cos 2\theta \rangle = \int_{\langle\theta\rangle-\alpha}^{\langle\theta\rangle+\alpha} d\theta\ \cos 2\theta\ p_1(\theta) \quad , \qquad (4\text{-}62b)$$

where α is the maximum variation of the canting angle. In Section 4.1.4 it was shown that the integrals in (4-62) can be approximated by

$$\langle \sin 2\theta \rangle = \exp(-2\sigma_\theta^2) \sin 2\langle\theta\rangle \tag{4-63}$$

and

$$\langle \cos 2\theta \rangle = \exp(-2\sigma_\theta^2) \cos 2\langle\theta\rangle \quad . \tag{4-64}$$

Within the framework of this approximation, the average scattering matrix $\underline{k}$ becomes

$$\underline{k} = \frac{2\pi}{k_o} \int_o^z dz \int_o^\infty d\bar{a} \{p\, \underline{f}^{SPH}(\bar{a}) + (1-p) \langle \underline{f}^{OBL}(\bar{a}) \rangle\}\, n_o(z, \bar{a}) \quad , \tag{4-65}$$

where $\langle \underline{f}^{OBL}(\bar{a}) \rangle$ means average of $\underline{f}^{OBL}(\bar{a}, \theta)$ with respect to $\bar{\theta}$, and is obtained from $\underline{f}^{OBL}(\bar{a}, \theta)$ by replacing sin 2θ and cos 2θ with $\langle \sin 2\theta \rangle$ and $\langle \cos 2\theta \rangle$, respectively.

The scattering coefficients f^{SPH}, $f_{\substack{V \\ H}}^{OBL}(\bar{a})$ are expressed, as we mentioned above, in terms of powers of $\bar{a}$ up to the fifth order.

$$f(\bar{a}) = \sum_{n=0}^{5} c_n\, a^{-n} \quad . \tag{4-66}$$

The final evaluation of the matrix $\underline{k}$ is accomplished by performing the indefinite integral

$$\int_o^L dz \int_o d\bar{a}\, f(\bar{a})\, n_o(z, \bar{a}) = \sum_{n=0}^{5} c_n \int_o^L dz \int_o d\bar{a}\, n_o(z, \bar{a})$$

$$= \sum_{n=0}^{5} c_n \int_o^L dz \int d\bar{a}\, \bar{a}^n \{e^{-8.2R(z)^{-0.21}\bar{a}}\} \quad . \tag{4-67}$$

Let $\gamma(z) = -8.2\, R(z)^{-0.21}$. Then, the integration over $\bar{a}$ in Eq. ( ) can be performed. The result is given by

$$\int_o^L dz \int d\bar{a}\, f(\bar{a})\, n_o(z, \bar{a}) = \sum_{n=0}^{5} c_n \int_o^L dz\, e^{\gamma(z)\bar{a}} \left[\sum_{m=1}^{n} \frac{n!}{(n-m)!} \right.$$

$$\left. \frac{\bar{a}^{n-m}}{\gamma(z)^{m+1}} (-1)^m + \frac{a^n}{\gamma(z)} \right] \quad . \tag{4-68}$$

Integrating, finally, over z using the rain rate distribution in Eq. (4-68) we obtain

$$\int_o^L dz \int d\bar{a}\, f(\bar{a})\, n_o(z, \bar{a}) = \sum_{i=1}^{2} \ell_i \sum_{n=0}^{5} c_n \left[\sum_{m=1}^{n} \frac{n!}{(n-m)!} \right.$$

$$\left. \frac{\bar{a}^{n-m}}{\gamma_i^{m+1}} (-1)^m + \frac{a^n}{\gamma_i} \right] \quad , \tag{4-69}$$

where $\ell_1 = 0.2L$, $\ell_2 = 0.8L$ and $\gamma_i = \gamma(\ell_i)$.

The elements of the matrix $\underline{k}$ have been evaluated explicitly. In order to calculate next the depolarization matrix, the quantity

$e^{-j\underline{k}(L)}$ must be computed using the eigenvalue-eigenvector method presented in Section 4.1.4. The calculation of the depolarization matrix for the rain medium will enable us to assess the attenuation and isolation effects that a incident plane wave undergoes when passes through such a channel.

4.1.3 Comparisons of Multiple Scattering Results to First-Order Multiple Scattering

The results derived in Section 4.1.2 have been coded in computer program form. This program is described in Appendix B. Inputs to the program are: frequency, elevation angle, mean and standard deviation of canting angle, rain rate at the receiver, fraction of spherical raindrops and rain medium length. Also the polarization parameters of the incident wave and receive antenna are entered.

Computations have been performed in order to test the model and examine its frequency dependence. In the next pages plots of predicted values of attenuation and isolation versus rain rate are presented at 11, 20, and 30 GHz. The rain medium has uniform rain rate along the entire path and a 5 km length and its composed by 60% oblate and 40% spherical raindrops. The oblate raindrops have a Guassian canting angle distribution with an average of 0° degrees and 12° degrees standard deviation. The polarization of the incident wave is linear with 45° tilted from vertical at a 45° elevation angle. These predicted values are compared with values calculated using a compute-

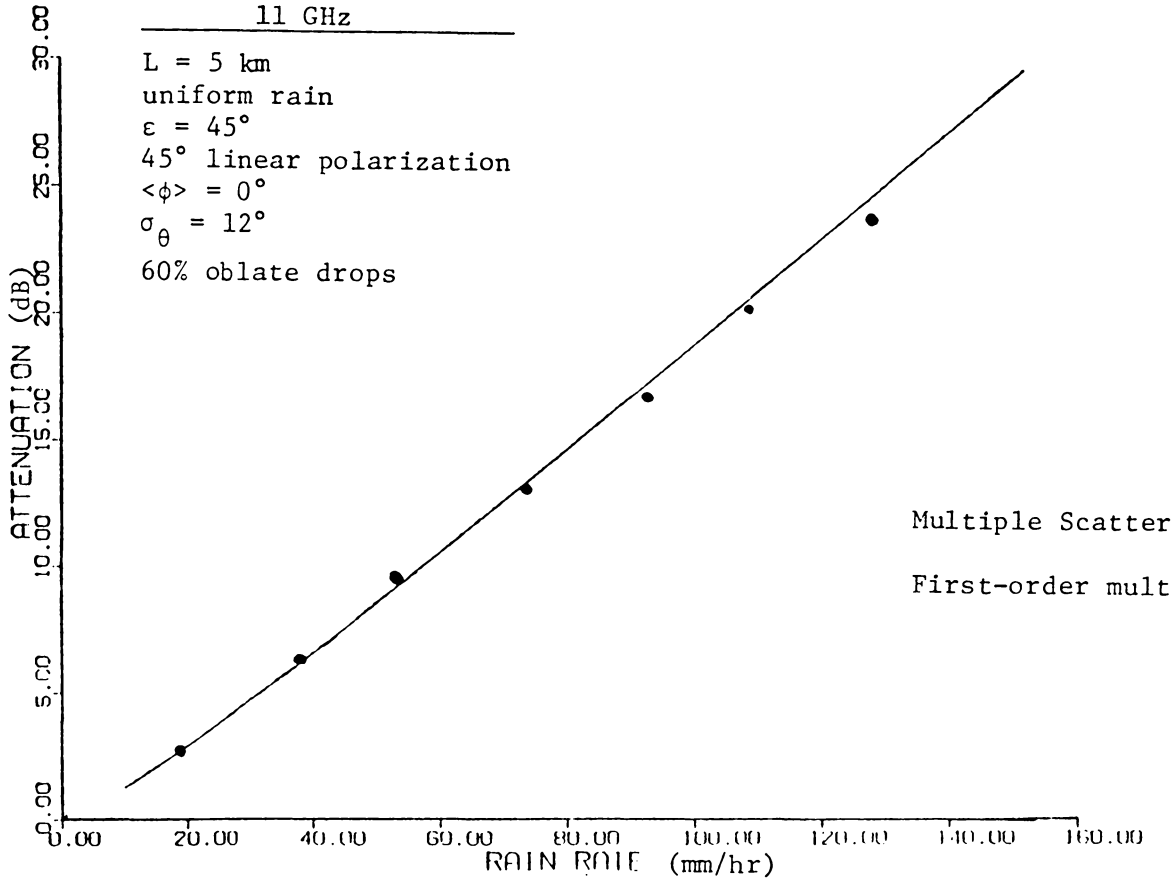

Figure 4.8. Comparison of multiple scattering and first-order multiple scattering calculations at 11 GHz.
a) Attenuation vs rain rate.

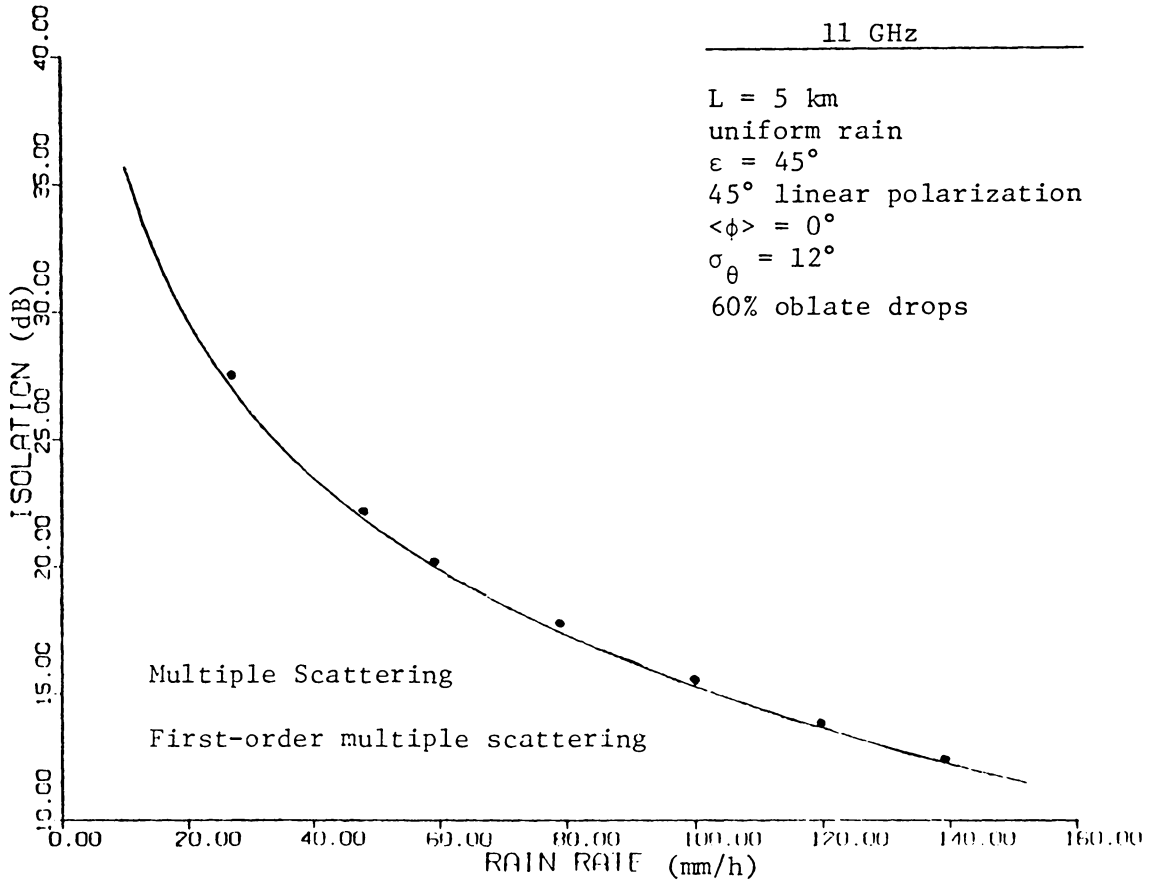

Figure 4.8. Comparison of multiple scattering and first-order multiple scattering calculations at 11 GHz.
b) Isolation versus rain rate.

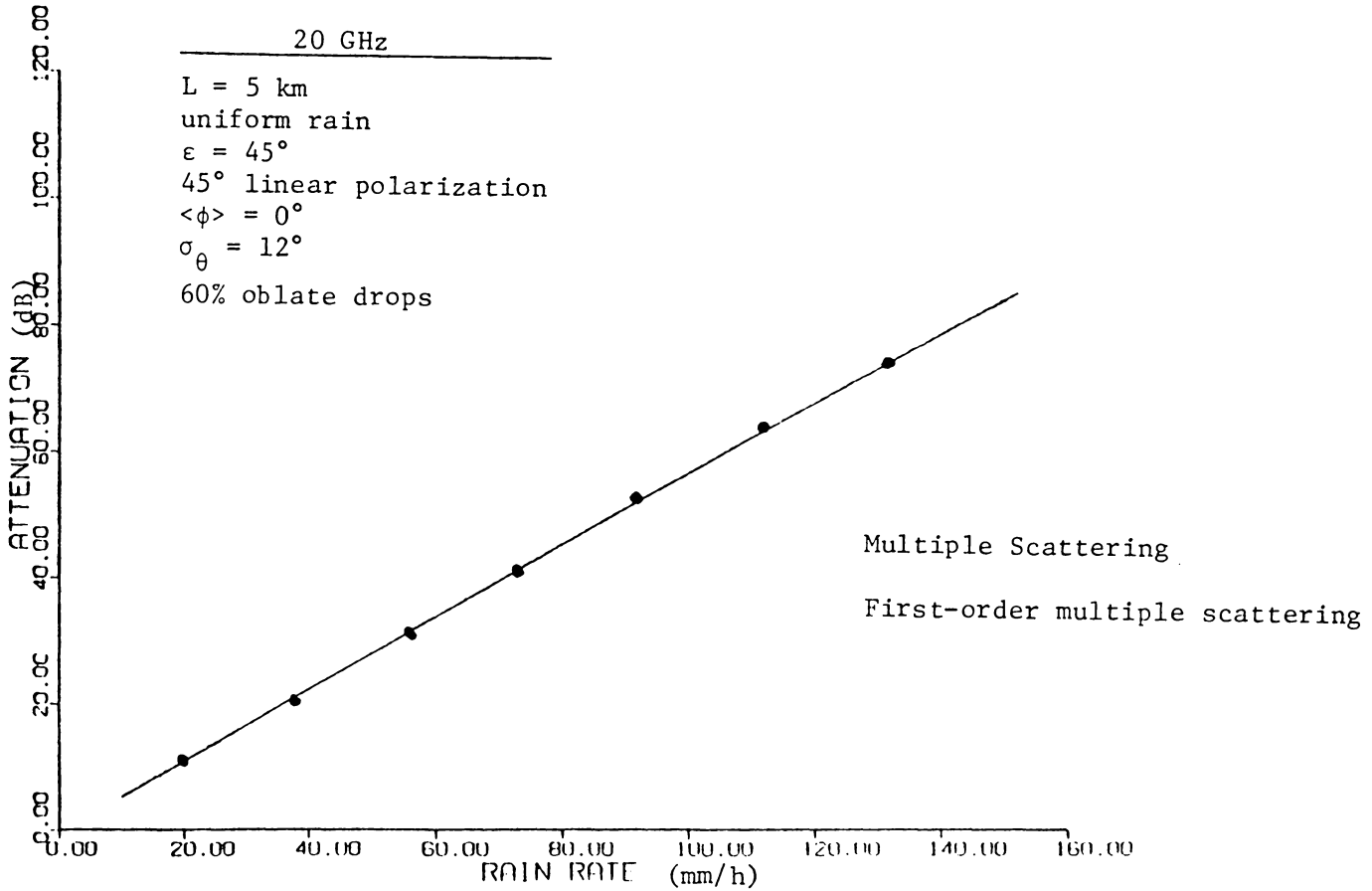

Figure 4.9. Comparison of multiple scattering and first-order multiple scattering calculations at 20 GHz.
a) Attenuation versus rain rate.

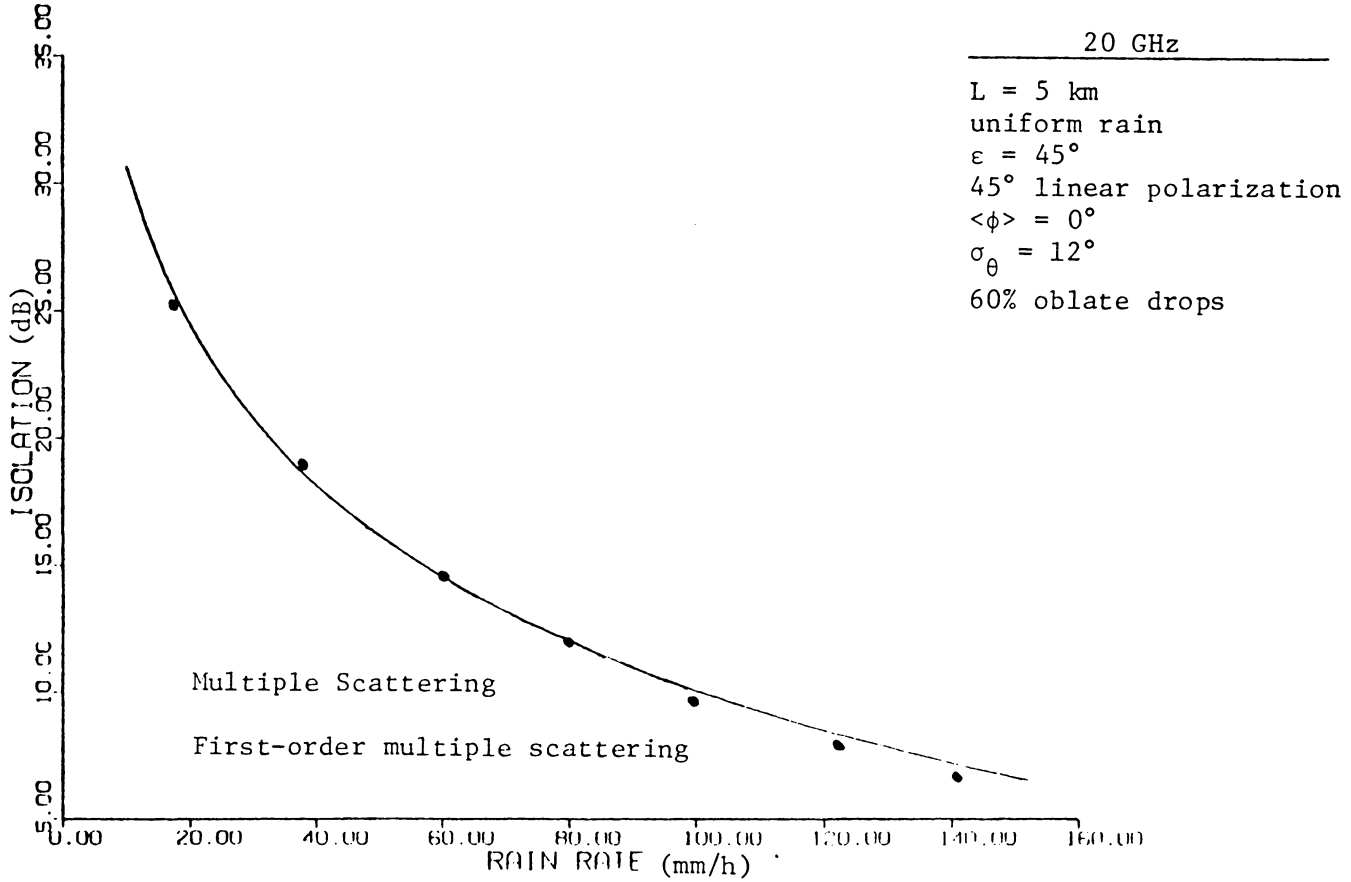

Figure 4.9. Comparison of multiple scattering and first-order multiple scattering calculations at 20 GHz.
b) Isolation versus rain rate.

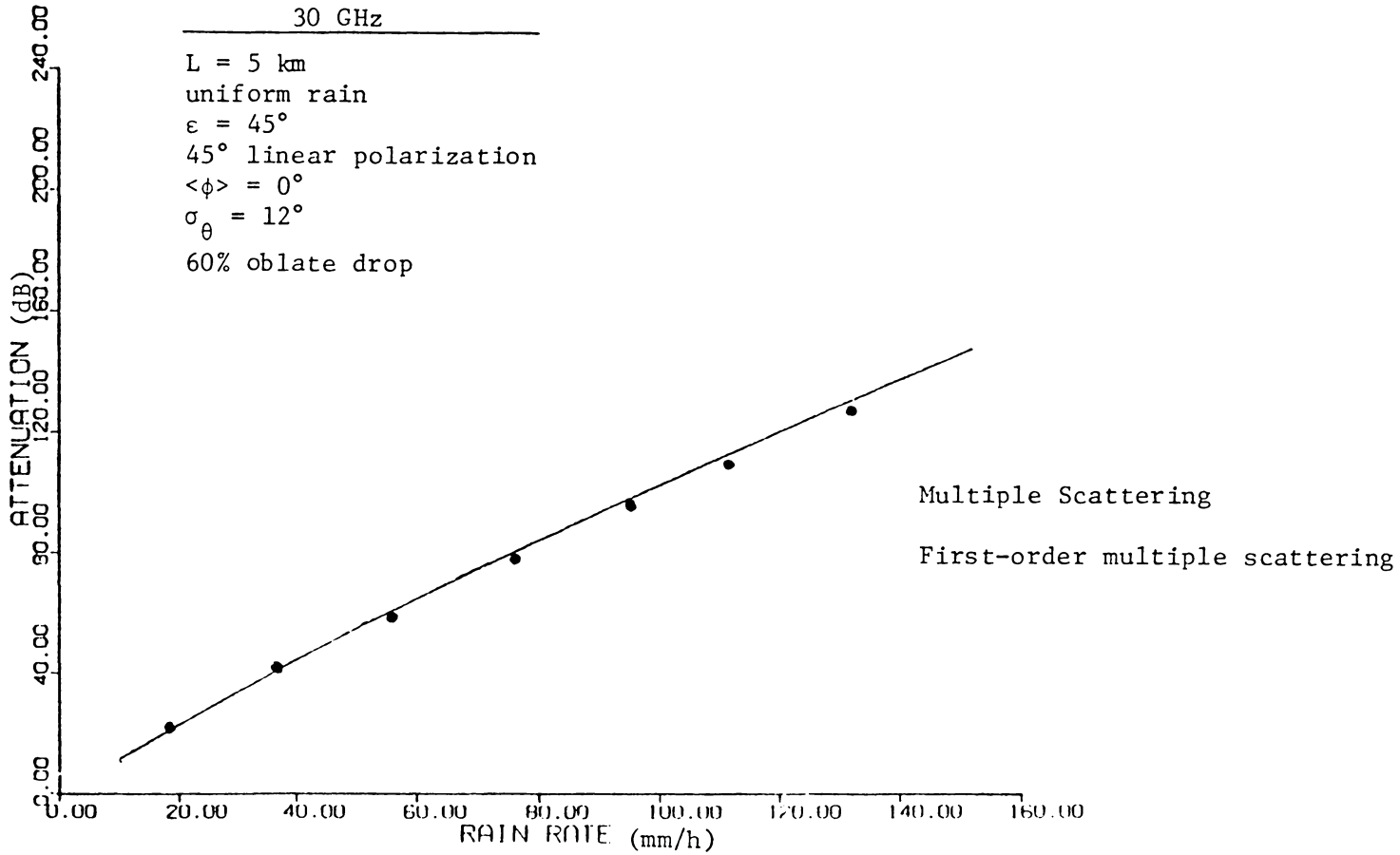

Figure 4.1. Comparison of multiple scattering and first-order multiple scattering calculations at 30 GHz.
a) Attenuation versus rain rate.

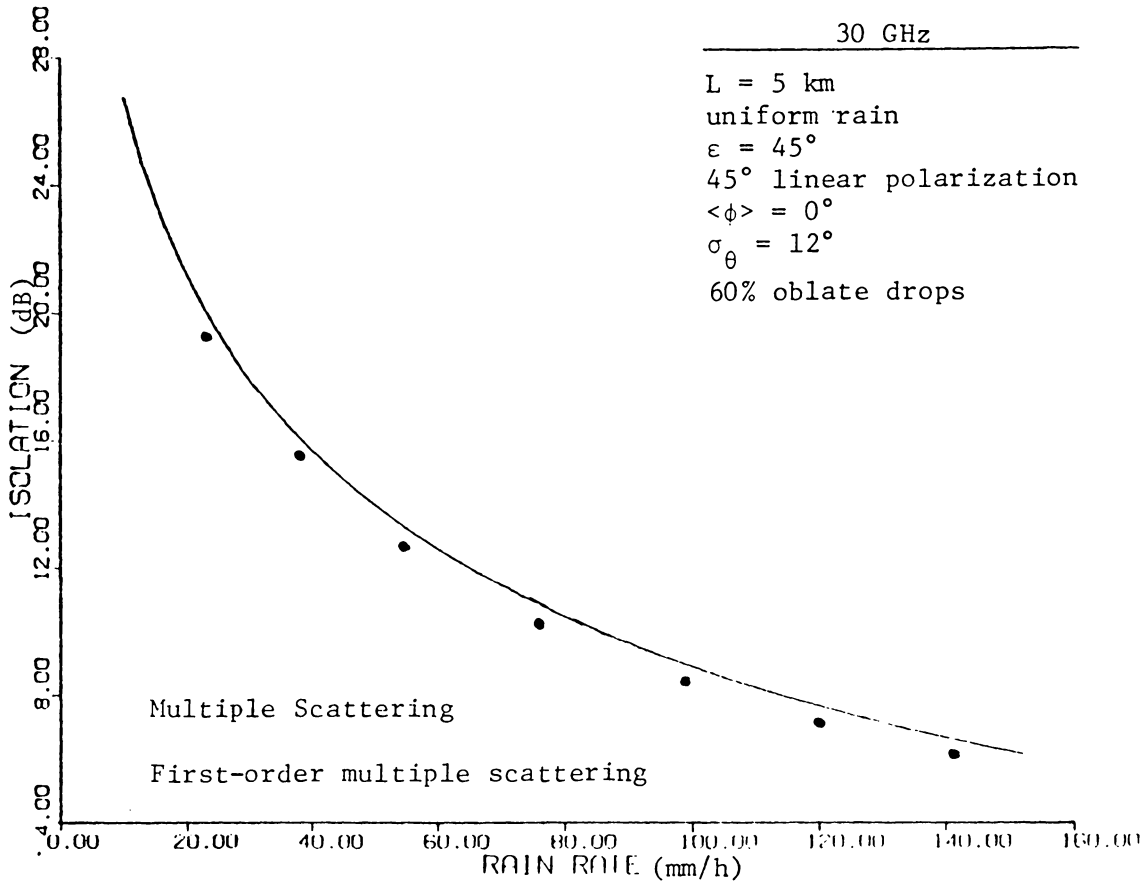

Figure 4.10. Comparison of multiple scattering and first-order multiple scattering calculations at 30 GHz.
b) Isolation versus rain rate.

rized code of first order multiple scattering that was developed by Persinger and Stutzman [27]. The first-order multiple scattering results are presented on the plots by asterisks.

The results that were produced by the two methods are almost identical. At 30 GHz there is a small difference between them. This difference is expected since multiple scattering becomes important at high frequencies. Even if the two models give similar results there is a large difference in computation time. The multiple scattering model is at least 30 times superior to the first-order multiple scattering one. Of course it is quite apparent that for higher frequencies only the multiple scattering model holds, due to the fact that the elements of the $\underline{k}$ matrix are very large and approximations to the exponential matrix are not possible. Unfortunately values for the scattering coefficients for oblate spheroidal raindrops are not available for all sizes, and the comparison of the two models in this frequency region was impossible.

The piecewise uniform rain rate model is used to predict the attenuation and isolation for a COMSTAR receiving terminal (19.04 GHz) at Blacksburg, Virginia. The predicted values from both models (multiple scattering, first-order multiple scattering) are presented in Figure 4.10.

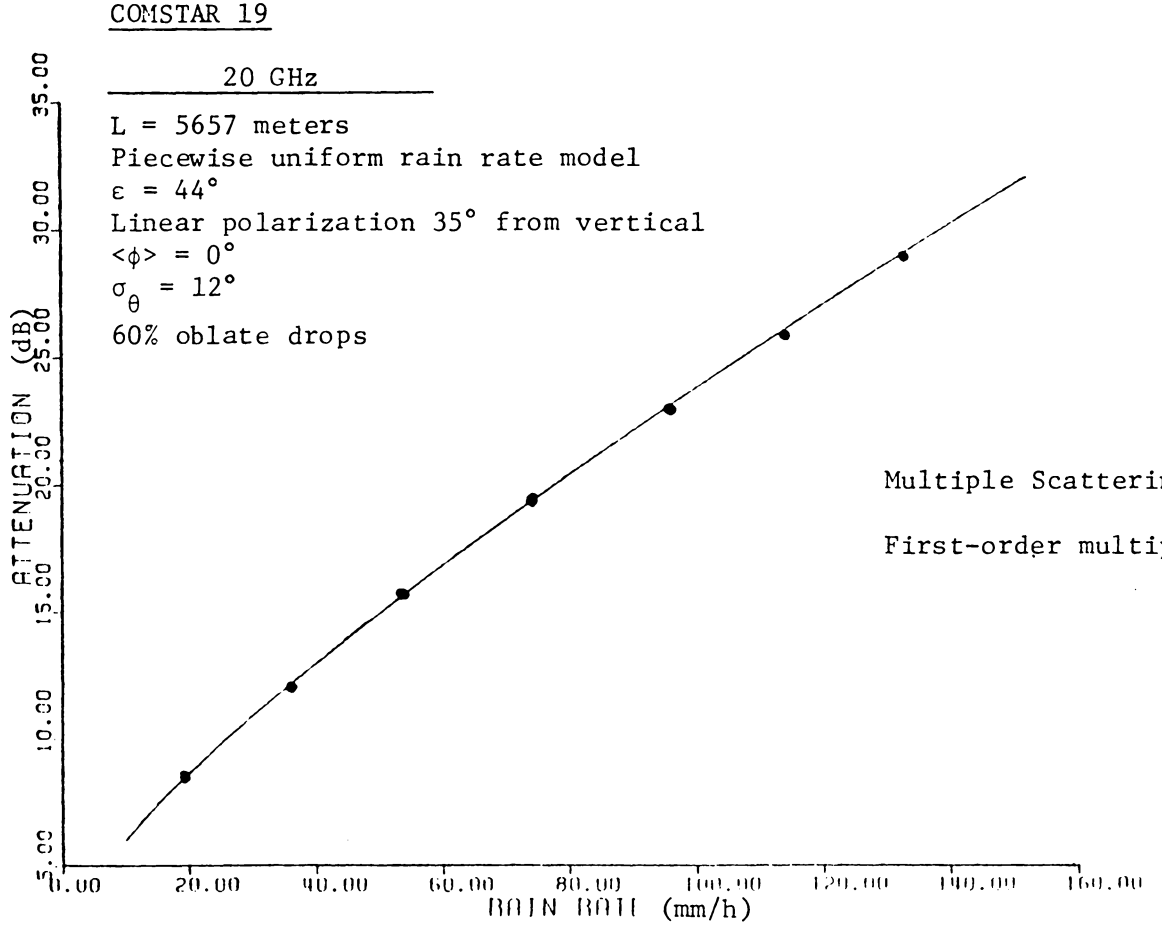

Figure 4.11. Comparison of multiple scattering and first-order multiple scattering calculations for the COMSTAR 19 system.
a) Attenuation versus rain rate.

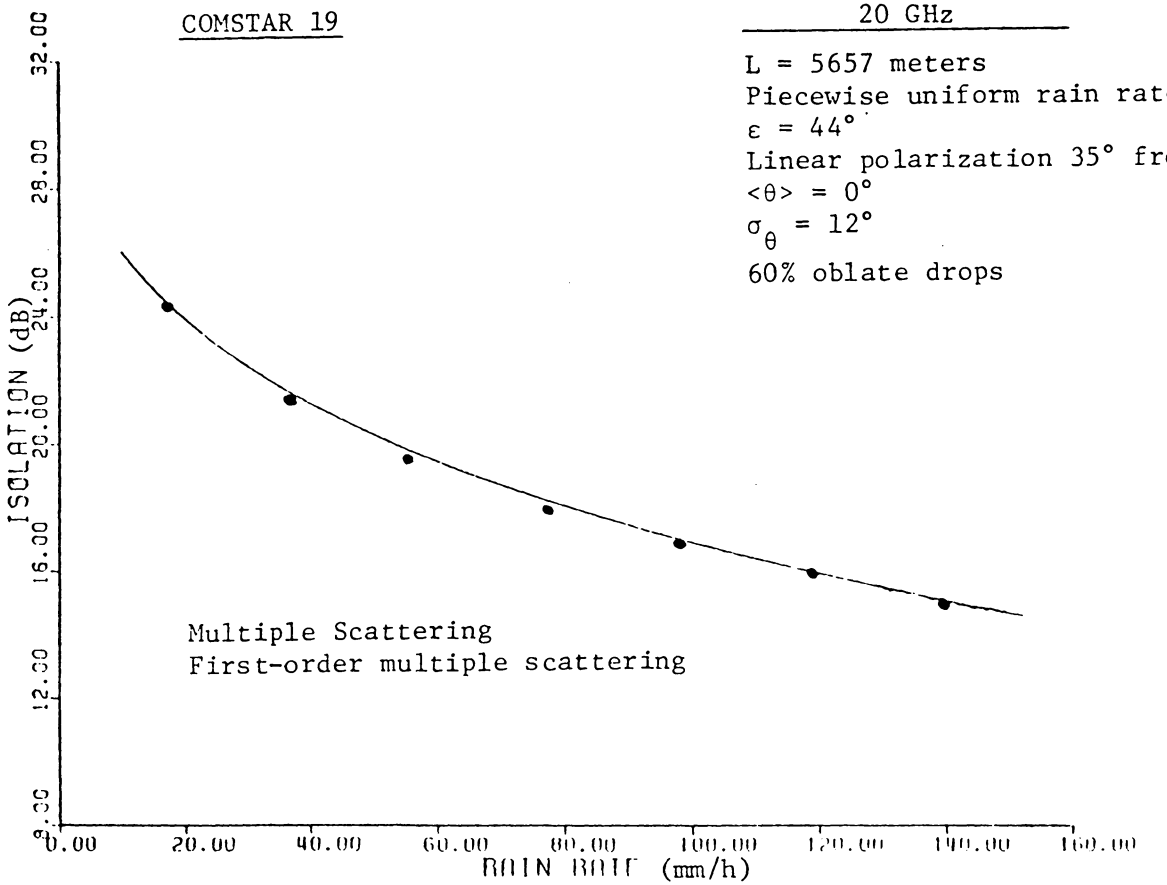

Figure 4.11. Comparison of multiple scattering and first-order multiple scattering calculations for the COMSTAR 19 system.
b) Isolation versus rain rate.

CHAPTER V

TWO-FREQUENCY RADIATIVE TRANSFER EQUATION FOR A RANDOM DISTRIBUTION OF SCATTERERS WITH PAIR CORRELATIONS

In the derivation of the Dyson equation for the coherent electric field in Chapter III it was assumed that the scatterers are uncorrelated. This "perfect gas" assumption is not physically realistic, and there are always correlations among the scatterers.

The primary goal in this part of our study is to derive equations for the coherent scalar field and the incoherent field intensity when there are position correlations between two scatterers, and from these equations to derive a two-frequency radiative transfer equation for the two-frequency incoherent intensity function - a quantity related to the two-frequency mutual coherent function and, hence, to second order pulse statistics. Besides frequency offsets, the resulting transport equation accounts for regular refraction and absorption, and statistical inhomogeneities and anisotropies; furthermore, it is valid under conditions of large-angle scattering and large-scale statistical fluctuations.

The transport theory was first developed in order to study the absorption-, emission-, and scattering-mediated transfer of electromagnetic radiation through stellar atmospheres and turbulent media. This initial development of the theory is heuristic and it lacks mathematical rigor [41]. More recently, however, there have been a number of attempts to systematically derive the radiative transfer equation from basic principles [8-10]. The advantage inherent in a

rigorous electromagnetic development of radiation transport theory is twofold: (1) it provides a clear delineation of the theory's domain of validity; (2) it provides systematic expressions for the transport parameters in terms of prescribed characteristics of the scatterers and the medium in which they are embedded.

The method that we shall follow in order to derive the two-frequency raaiative transfer equation for scalar waves in discrete random channels will be an adaptation of a technique developed recently by Besieris and Kohler [10 see also 9] in connection with scalar waves in continuous random media.

The structure of this chapter is organized as follows: In Section 5.1 the Dyson equation is derived for the coherent electric field. The medium is assumed to be composed of an infinite number of correlated scatterers. In Section 5.2 the two-frequency Bethe-Saltpeter equation is derived for the above medium. In Section 5.3 the Dyson and Bethe-Saltpeter equations are specialized to a tenuous medium consisting of isotropic scatterers. The Bethe-Saltpeter equation is subsequently simplified using a quasihomogeneity assumption, and a transition is effected to a phase space leading, finally, to the generalized transport equation (5-50) under the constraints of small scattering losses, and small difference to sum wavelength ratios. In Section 5.4, the two-frequency radiative transfer equation for the incoherent ray intensity is derived, first for anisotropic and then for isotropic spatial correlation function. Comparisons are also made

with the classical radiation transfer, and with the radiative transfer describing wave propagation in a statistically inhomogeneous and anisotropic absorptive continuous medium. Finally, the connection between "wave" and "photometric" quantities is discussed in Section 5.5.

5.1 The Dyson Equation for a Distribution of Scatterers with Pair Correlations

The electric field at the point $\vec{r}_a$ between the scatterers is governed by equation (3-21), viz.,

$$\vec{E}^a = \vec{E}_i^a + \sum_{j=1}^{N} \bar{\bar{g}}_j^a \cdot \vec{E}_i^j + \sum_{j=1}^{N} \sum_{k=1,k\neq j}^{N} \bar{\bar{g}}_j^a \cdot \bar{\bar{g}}_k^j \cdot \vec{E}_i^k + \sum_{j=1}^{N} \sum_{k=1,k\neq j}^{N} \sum_{\ell=1,\ell\neq k}^{N} \bar{\bar{g}}_j^a \cdot \bar{\bar{g}}_k^j \cdot \bar{\bar{g}}_\ell^k \cdot \vec{E}_i^\ell + \ldots + \ldots \quad (5\text{-}1)$$

Ignoring triple scattering by two scatterers, fourth scattering among three scatterers, and so on, in other words, by using the Twersky procedure, Eq. (5-1) takes the form

$$\vec{E}^a = \vec{E}_i^a + \sum_{j=1}^{N} \bar{\bar{g}}_i^a \cdot \vec{E}_i^j + \sum_{j=1}^{N} \sum_{k=1,k\neq j}^{N} \bar{\bar{g}}_j^a \cdot \bar{\bar{g}}_k^j \cdot \vec{E}_i^k + \sum_{j=1}^{N} \sum_{k=1,k\neq j}^{N} \sum_{\ell=1,\ell\neq k,\ell\neq j}^{N} \bar{\bar{g}}_j^a \cdot \bar{\bar{g}}_k^j \cdot \bar{\bar{g}}_\ell^k \cdot E_i^\ell + \ldots \quad (5\text{-}2)$$

We assume that each scatterer has the same shape, size, orientation distribution and that there is a spatial cross correlation between scatterers. The scatterer correlation function may be defined as

follows:

$$p(\vec{\omega}_j) = \frac{1}{N} p_1(\vec{\gamma}_j)\rho(\vec{r}_j) \quad , \tag{5-3a}$$

$$p(\vec{\omega}_j, \vec{\omega}_k) = \frac{1}{N^2} p_1(\vec{\gamma}_j)p_1(\vec{\gamma}_k)[\rho(\vec{r}_j)\rho(\vec{r}_k) + B'(\vec{r}_j, \vec{r}_k)] \quad , \tag{5-3b}$$

$$p(\vec{\omega}_j, \vec{\omega}_k, \vec{\omega}_\ell) = \frac{1}{N^3} p_1(\vec{\gamma}_j)p_1(\vec{\gamma}_k)p_1(\vec{\gamma}_\ell)$$
$$\times [\rho(\vec{r}_j)\rho(\vec{r}_k)\rho(\vec{r}_\ell) + \rho(\vec{r}_j)B'(\vec{r}_k, \vec{r}_\ell) + \rho(\vec{r}_k)B'(\vec{r}_\ell, \vec{r}_j)$$
$$+ \rho(\vec{r}_\ell)B'(\vec{r}_j, \vec{r}_k) + C(\vec{r}_j, \vec{r}_k, \vec{r}_\ell)] \quad , \tag{5-3c}$$

and so on. Here, $\vec{\gamma}_k = (\phi_k, \bar{a}_k, s_k)$, where γ_k is the orientation angle of the k^{th} scatterer, s_k is a measure of the shape and $\vec{r}_k$ is its position.

We take next the ensemble average of (5-2) using the scatterer correlation functions given in Eq. (5-3). We only consider pair correlations between any two particles and neglect any other contributions from higher order correlations. The coherent field at point $\vec{r}_a$ is given in this case by

$$\langle \vec{E}^a \rangle = \vec{E}_i^{\,a} + \int_{\vec{\omega}_j} \bar{g}_j^{\,a} \cdot \vec{E}_i^{\,j}\, p_1(\vec{\gamma}_j)\rho(\vec{r}_j)d\vec{\omega}_j + \frac{N-1}{N}$$
$$\times \int_{\vec{\omega}_j,\vec{\omega}_k} \bar{g}_j^{\,a} \cdot g_k^{\,j} \cdot \vec{E}_i^{\,k}\, p_1(\vec{\gamma}_k)\, p_1(\vec{\gamma}_j)[\rho(\vec{r}_j)\rho(\vec{r}_k) + B'(\vec{r}_j, \vec{r}_k)$$
$$\times d\vec{\omega}_j\, d\vec{\omega}_k + \frac{(N-1)(N-2)}{N^2} \int_{\vec{\omega}_j,\vec{\omega}_k,} \bar{g}_j^{\,a} \cdot \bar{g}_k^{\,j} \cdot \bar{g}_\ell^{\,k} \cdot \vec{E}_i^{\,\ell}$$

$$\times p_1(\vec{\gamma}_j)p_1(\vec{\gamma}_k)p_1(\vec{\gamma}_\ell)[\rho(\vec{r}_j)\rho(\vec{r}_k)\rho(\vec{r}_\ell) + \rho(\vec{r}_j)$$

$$B'(\vec{r}_k, \vec{r}_\ell) + \rho(\vec{r}_k)B'(\vec{r}_\ell, \vec{r}_j) + \rho(\vec{r}_\ell)B'(\vec{r}_j, \vec{r}_k)]\, d\vec{\omega}_j d\vec{\omega}_k d\vec{\omega}_\ell + \ldots \quad (5\text{-}4)$$

As in Chapter III we make the assumption that the number of the scatterers enclosed in the medium is infinite. Under this assumption, the limits of the quantities $(\frac{N-1}{N})$, $\frac{(N-1)(N-2)}{N}$, etc. reach unity and equation (5-4) may be expressed in the closed form

$$\langle \vec{E}^a \rangle = \vec{E}_i^{\,a} + \int_{\vec{\omega}_j} \bar{g}_j^{\,a} \cdot \langle \vec{E}^j \rangle\, p_1(\vec{\gamma}_j)\rho(\vec{r}_j) d\vec{\gamma}_j\, d\vec{r}_j$$

$$+ \int_{\vec{\omega}_j, \vec{\omega}_k} \bar{g}_j^{\,a} \cdot \langle \bar{G}_k^{\,j} \rangle \cdot \langle \vec{E}^k \rangle\, B'(\vec{r}_j, \vec{r}_k) p_1(\vec{\gamma}_j) p_1(\vec{\gamma}_k)\, d\vec{\omega}_j\, d\vec{\omega}_k \quad , \quad (5\text{-}5a)$$

where the dyadic Green's function $\langle \bar{G}_k^{\,j} \rangle$ obeys the relationship

$$\langle \bar{G}_k^{\,j} \rangle = \bar{g}_k^{\,j} + \int_{\vec{\omega}_\ell} \bar{g}_\ell^{\,j} \cdot \langle \bar{G}_k^{\,\ell} \rangle\, \rho(\vec{r}_\ell) p_1(\vec{\gamma}_\ell)\, d\vec{r}_\ell d\vec{\gamma}_\ell$$

$$+ \int_{\vec{\omega}_\ell, \vec{\omega}_m} \bar{g}_\ell^{\,i} \cdot \langle \bar{G}_m^{\,\ell} \rangle \cdot \langle \bar{G}_k^{\,m} \rangle\, B'(\vec{r}_\ell, \vec{r}_m) p_1(\vec{\gamma}_\ell) p_1(\vec{\gamma}_m)\, d\vec{\omega}_\ell\, d\vec{\omega}_m \quad . \quad (5\text{-}5b)$$

Equation (5-5) is the Dyson equation for the coherent field in a distribution of scatterers with spatial pair correlations. Using the same basic ideas, we will derive, in the next section, the integral equation for the correlation function (field intensity) $\langle \underline{E}^a\, \underline{E}^{b\dagger} \rangle$, where $\underline{E}^{b\dagger}$ denotes the complex conjugate transpose of the column matrix corresponding to the vector $\vec{E}^b$.

5.2 The Two-Frequency Bethe-Saltpeter Equation

From Eq. (5-2) the field $\vec{E}^a$ at point $\vec{r}_a$ is given in the matrix form

$$\underline{E}^a = \underline{E}_i + \sum_{j=1}^{N} \underline{g}_j{}^a \underline{E}_i{}^j + \sum_{j=1}^{N} \sum_{k=1,k\neq j}^{N} \underline{g}_j{}^a \underline{g}_k{}^j E_i{}^k + \sum_{j=1}^{N} \sum_{k=1,k\neq j}^{N}$$

$$\times \sum_{\ell=1,\ell\neq k,\ell\neq j}^{N} \underline{g}_j{}^a \underline{g}_k{}^j \underline{g}^k E_i{}^\ell + \ldots \qquad (5\text{-}6)$$

The field at point $\vec{r}_b$ may be written in the same form, viz.,

$$\underline{E}^b = \underline{E}_i{}^b + \sum_{m=1}^{N} \underline{g}_m{}^b \underline{E}_i{}^m + \sum_{m=1}^{N} \sum_{n=1,n\neq m}^{N} \underline{g}_m{}^b \underline{g}_n{}^m \underline{E}_i{}^n$$

$$\sum_{m=1}^{N} \sum_{n=1,n\neq m}^{N} \sum_{t=1,t\neq n,t\neq m}^{N} \underline{g}_m{}^b \underline{g}_n{}^m \underline{g}_t{}^n \underline{E}_i{}^t + \ldots \qquad (5\text{-}7)$$

Using (5-6) and the complex conjugate transpore of (5-7), we obtain

$$\underline{E}^{a\dagger}\underline{E}^{b\dagger} = \underline{E}_i{}^a \underline{E}_i{}^{b\dagger} + \sum_{j=1}^{N} \underline{g}_j{}^a \underline{E}_i{}^j \underline{E}_i{}^{b\dagger} + \sum_{j=1}^{N} \sum_{k=1,k\neq j}^{N} \underline{g}_j{}^a \underline{g}_k{}^j \underline{E}_i{}^k \underline{E}_i{}^{b\dagger}$$

$$+ \sum_{m=1}^{N} \underline{E}_i{}^a \underline{E}_i{}^{m\dagger} \underline{g}_m{}^{b\dagger} + \sum_{j=1}^{N} \sum_{m=1}^{N} \underline{g}_j{}^a \underline{E}_i{}^j \underline{E}_i{}^{m\dagger} \underline{g}_m{}^{b\dagger} + \sum_{j=1}^{N} \sum_{k=1,k\neq j}^{N}$$

$$\times \sum_{m=1}^{N} \underline{g}_j{}^a \underline{g}_k{}^j \underline{E}_i{}^k \underline{E}_i{}^{m\dagger} \underline{g}_m{}^{b\dagger} + \sum_{m=1}^{N} \sum_{n=1,n\neq m}^{N} \underline{E}_i{}^a \underline{E}_i{}^{n\dagger} \underline{g}_n{}^{m\dagger} \underline{g}_m{}^{b\dagger} +$$

$$\sum_{j=1}^{N} \sum_{m=1}^{N} \sum_{n=1,n\neq m}^{N} \underline{g}_j{}^a \underline{E}_i{}^j \underline{E}_i{}^n \underline{g}_n{}^{m\dagger} \underline{g}_m{}^{b\dagger} + \sum_{j=1}^{N} \sum_{k=1,k\neq j}^{N} \sum_{m=1}^{N} \sum_{n=1,n\neq m}^{N}$$

$$\underline{g}_j{}^a \underline{g}_k{}^j \underline{E}_i{}^k \underline{E}_i{}^{n\dagger} \underline{g}_m{}^{b\dagger} \underline{g}_n{}^{m\dagger} + \ldots \qquad (5\text{-}8)$$

It is important at this point to treat the summations in Eq. (5-8) as follows:

$$\sum_{j=1}^{N}\sum_{m=1}^{N} \underline{g}_j^{\,a}\,\underline{E}_i^{\,j}\,\underline{E}_i^{\,m}\,\underline{g}_m^{\,b\dagger} = \sum_{j=1} \underline{g}_j^{\,a}\,\underline{E}_i^{\,j}\,\underline{E}_i^{\,j\dagger}\,\underline{g}_j^{\,b\dagger} + \sum_{j=1}^{N}\sum_{m=1,m\neq j}^{N}$$

$$\underline{g}_j^{\,a}\,\underline{E}_i^{\,j}\,\underline{E}_i^{\,m\dagger}\,\underline{g}_m^{\,b\dagger} \quad , \tag{5-9}$$

$$\sum_{j=1}^{N}\sum_{k=1,k\neq j}^{N}\sum_{m=1}^{N} \underline{g}_j^{\,a}\,\underline{g}_k^{\,j}\,\underline{E}_i^{\,k}\,\underline{E}_i^{\,m\dagger}\,\underline{g}_m^{\,b\dagger}$$

$$= \sum_{j=1}^{N}\sum_{k=1,k\neq j}^{N}\sum_{m=1,m\neq k,m\neq j}^{N} \underline{g}_j^{\,a}\,\underline{g}_k^{\,j}\,\underline{E}_i^{\,k}\,\underline{E}_k^{\,j\dagger}\,\underline{g}_j^{\,b\dagger}$$

$$+ \sum_{j=1}^{N}\sum_{k=1,k\neq j}^{N} \underline{g}_j^{\,a}\,\underline{g}_k^{\,j}\,\underline{E}_i^{\,k}\,\underline{E}_i^{\,k\dagger}\,\underline{g}_k^{\,b\dagger} \quad . \tag{5-10}$$

The first term on the right-hand side of Eq. (5-9) indicates that the fields at $\vec{r}_a$, $\vec{r}_b$ are scattered from the same scatterer. The second one indicates that the fields at $\vec{r}_a$, $\vec{r}_b$ are scattered from different scatterers. A similar interpretation can be provided for the terms on the right-hand side of Eq. (5-10).

We average next Eq. (5-8) taking into account Eqs. (5-9), (5-10) and using the scatterer correlation functions in Eq. (5-3). An intermediate result for the correlation function $\langle \underline{E}^a\,\underline{E}^{b\dagger} \rangle$ is given by

$$\langle \underline{E}^a\,\underline{E}^{b\dagger} \rangle = \underline{E}_i^{\,a}\,\underline{E}_i^{\,b} + \int_{\vec{\omega}_j} \underline{g}_j^{\,a}\,\underline{E}_i^{\,j}\,\underline{E}_i^{\,b\dagger}\,p_1(\vec{\gamma}_j)\,(\vec{r}_j)\,d\vec{\omega}_j$$

$$+ \int_{\vec{\omega}_m} \underline{E}_i^{\,a}\,\underline{E}_i^{\,m}\,\underline{g}_m^{\,b\dagger}\,p_1(\vec{\gamma}_m)\rho(\vec{r}_m)\,d\vec{\omega}_m + \frac{N-1}{N}\int_{\vec{\omega}_j}\int_{\vec{\omega}_m} \underline{g}_j^{\,a}\,\underline{E}_i^{\,j}\,\underline{E}_i^{\,m\dagger}\,\underline{g}_m^{\,b\dagger}$$

$$\times\ p_1(\vec{\gamma}_j)p_1(\vec{\gamma}_m)[\rho(\vec{r}_j)\rho(\vec{r}_m)+B'(\vec{r}_j,\vec{r}_m)]d\vec{\omega}_j d\vec{\omega}_m + \int_{\vec{\omega}_j} \underline{g}_j{}^{a}\ \underline{E}_i{}^{j\dagger}\ \underline{g}_j{}^{b\dagger}$$

$$\times\ p_1(\vec{\gamma}_j)\rho(\vec{r}_j)\ +\ d\vec{\omega}_j\ +\ \frac{N-1}{N^2}\int_{\vec{\omega}_j}\int_{\vec{\omega}_k} \underline{g}_j{}^{a}\ \underline{g}_k{}^{j}\ \underline{E}_i{}^{k}\ \underline{E}_i{}^{b\dagger}\ p_1(\vec{\gamma}_j)p_1(\vec{\gamma}_k)$$

$$\times\ [\rho(\vec{r}_j)\rho(\vec{r}_k)\ +\ B'(\vec{r}_j,\ \vec{r}_k)]\ d\vec{\omega}_j\ d\vec{\omega}_k\ +\ \frac{N-1}{N}\int_{\vec{\omega}_m}\int_{\vec{\omega}_n}$$

$$\times\ \underline{E}_i{}^{a}\ \underline{E}_i{}^{n\dagger}\ \underline{g}_n{}^{m\dagger}\ \underline{g}_m{}^{\dagger}\ p_1(\vec{\gamma}_m)p_1(\vec{\gamma}_n)\ [\rho(\vec{r}_m)\rho(\vec{r}_n)\ +\ B'(\vec{r}_m,\ \vec{r}_n)]$$

$$\times\ d\vec{\omega}_m\ d\vec{\omega}_n + \frac{N-2}{N^2}\int_{\vec{\omega}_j}\int_{\vec{\omega}_k}\int_{\vec{\omega}_n} \underline{g}_j{}^{a}\ \underline{g}_k{}^{j}\ \underline{E}_i{}^{k}\ \underline{E}_i{}^{m\dagger}\ \underline{g}_m{}^{b\dagger}\ p_1(\vec{\gamma}_j)p_1(\vec{\gamma}_k)$$

$$\times\ p_1(\vec{\gamma}_m)\ [\rho(\vec{r}_j)\rho(\vec{r}_k)\rho(\vec{r}_m)\ +\ \rho(\vec{r}_j)B'(\vec{r}_k,\ \vec{r}_m)\ +$$

$$\rho(\vec{r}_k)B'(\vec{r}_m,\ \vec{r}_j)\ +\ \rho(\vec{r}_m)B'(\vec{r}_j,\ \vec{r}_k)\ d\vec{\omega}_j\ d\vec{\omega}_k\ d\vec{\omega}_m\ +$$

$$\frac{N-1}{N}\int_{\vec{\omega}_j}\int_{\vec{\omega}_k} \underline{g}_j{}^{a}\ \underline{g}_k{}^{j}\ \underline{E}_i{}^{k}\ \underline{E}_k{}^{j\dagger}\ \underline{g}_j{}^{b\dagger}\ p_1(\vec{\gamma}_j)p_1(\vec{\gamma}_k)\ [\rho(\vec{r}_j)\rho(\vec{r}_k)$$

$$+\ B'(\vec{r}_j,\ \vec{r}_k)]\ d\vec{\omega}_j\ d\vec{\omega}_k\ +\ \frac{N-1}{N}\int_{\vec{\omega}_j}\int_{\vec{\omega}_k} \underline{g}_j{}^{a}\ \underline{g}_k{}^{j}\ \underline{E}_i{}^{k}\ \underline{E}_i{}^{k\dagger}\ \underline{g}_k{}^{b\dagger}$$

$$\times\ p_1(\vec{\gamma}_j)p_1(\vec{\gamma}_k)\ [\rho(\vec{r}_j)\rho(\vec{r}_k)\ +\ B'(\vec{r}_j,\ \vec{r}_k)]\ d\vec{\omega}_j\ d\vec{\omega}_k\ +\ \ldots \qquad (5\text{-}11)$$

which, in the limit as N tends to infinity, can be written in the closed form as

$$\langle \underline{E}^{a}\ \underline{E}^{b\dagger}\rangle = \langle \underline{E}^{a}\rangle\ \langle \underline{E}^{b\dagger}\rangle + \int_{\vec{\omega}_j} \langle \underline{G}_j{}^{a}\rangle\ \langle \underline{E}^{j}\ \underline{E}^{j\dagger}\ \langle \underline{G}_j{}^{b\dagger}\rangle$$

$$\times\, p_1(\vec{\gamma}_j)\rho(\vec{r}_j) + \int_{\vec{\omega}_j}\int_{\vec{\omega}_m} \langle \underline{G}_j{}^a \rangle \langle \underline{E}^j\, \underline{E}^{m\dagger} \rangle \langle G_m{}^{b\dagger} \rangle\, B'(\vec{r}_j, \vec{r}_m)$$

$$\times\, p_1(\vec{\gamma}_j)p_1(\vec{\gamma}_m)\, d\vec{\omega}_j\, d\vec{\omega}_m \quad . \tag{5-12}$$

The quantity $\langle \underline{G}_j{}^a \rangle$ entering into the last expression is the near Green's function satisfying the Dyson equation (5-5b).

Equation (5-12) is the Bethe-Saltpeter equation in the ladder approximation. In deriving this equation, as well as the Dyson equation, we only considered pair correlations between particles and neglected any other contributions from higher order correlations.

5.3 Two-Frequency Transport Equation for a Tenuous Medium of Isotropic Scatterers

In the previous section we made no assumptions about the distance between any two scatterers or their scattering properties. In order to simplify our analysis, we will assume, in the following, that the discrete medium is tenuous, and that the scatterers are isotropic. Under these assumptions, the operator $\bar{\bar{g}}_j{}^a$ is a diagonal one, assuming specifically the form

$$\bar{\bar{g}}_j{}^a = f'(\bar{a}_j, k)\, \frac{e^{-jk|\vec{r}_a - \vec{r}_j|}}{|\vec{r}_a - \vec{r}_j|}\, \bar{\bar{I}} = g(\bar{a}_j, k, \vec{r}_a, \vec{r}_j)\bar{\bar{I}} \quad , \tag{5-12}$$

where $\bar{\bar{I}}$ is the unit dyadic and $f'(\bar{a}_j, k)$ is the scattering coefficient of the j^{th} scatterer, depending only on the size of the scatterer and the frequency of operation.

5.1.3 The Dyson and Bethe-Saltpeter Equations

For a tenuous medium of isotropic scatterers the dyadic mean Green's function is rendered diagonal, viz., $\langle\bar{G}\rangle = \langle G\rangle\bar{I}$, where the scalar quantity $\langle G\rangle$ satisfies the Dyson equation

$$\langle G(a', \vec{r}, \vec{r}', k)\rangle = \tilde{g}(a', \vec{r}, \vec{r}', k') + \int_{a'',\vec{r}''} \tilde{g}(a'', \vec{r}, \vec{r}'', k'')$$

$$\times \langle G(\bar{a}', \vec{r}'', \vec{r}', k)\rangle\, p_1(a'')\rho(\vec{r}'')\, da''\, d\vec{r}''$$

$$+ \int_{\bar{a}'',\vec{r}''} \int_{\bar{a}''',\vec{r}'''} \tilde{g}(\bar{a}'', \vec{r}, \vec{r}'', k)\, \langle G(a''', \vec{r}'', \vec{r}''', k)\rangle$$

$$\times \langle G(\bar{a}', \vec{r}'', \vec{r}', k')\rangle\, B'(\vec{r}'', \vec{r}''')p_1(\bar{a}'')p_1(\bar{a}''')\, d\bar{a}''\, d\vec{r}''$$

$$\times d\bar{a}'''\, d\vec{r}''' \quad . \tag{5-14a}$$

As a consequence, each component of the mean field $\langle\vec{E}\rangle$, denoted here by $\langle E\rangle$, satisfies the (scalar) Dyson equation

$$\langle E(\vec{r}, k)\rangle = E_i(\vec{r}, k) + \int_{\bar{a}',\vec{r}'} \tilde{g}(\bar{a}', \vec{r}, \vec{r}', k')\, \langle E(\vec{r}')\rangle$$

$$\times p_1(\bar{a}')\rho(\vec{r}')\, d\bar{a}'\, d\vec{r}' + \int_{\bar{a}',\vec{r}'} \int_{\bar{a}'',\vec{r}''} \tilde{g}(\bar{a}', \vec{r}, \vec{r}', k)\, \langle G(\bar{a}'', \vec{r}', \vec{r}'', k)\rangle$$

$$\times \langle E(\vec{r}'')\rangle\, B(\vec{r}', \vec{r}'')p_1(\bar{a}')p_1(\bar{a}'')\, d\bar{a}'\, d\vec{r}'\, d\bar{a}''\, d\vec{r}'' \quad , \tag{5-14b}$$

and the two-frequency correlation function $\langle E(\vec{r}_1, k_1)E^*(\vec{r}_2, k_2)\rangle$ is governed by the scalar Bethe-Saltpeter equation

$$\langle E(\vec{r}_1, k_1)E^*(\vec{r}_2, k_2)\rangle = \langle E(\vec{r}_1, k_1)\rangle \langle E^*(\vec{r}_2, k_2)\rangle$$

$$+ \int_{\bar{a}',\vec{r}'} \langle G(\bar{a}', \vec{r}_1, \vec{r}', k_1)\rangle \langle E(\vec{r}', k_1)E^*(\vec{r}', k_2)\rangle$$

$$\times \langle G^*(\bar{a}', \vec{r}_2, \vec{r}', k_2)\rangle\, p(\bar{a}')\rho(\vec{r}')\, d\bar{a}'\, d\vec{r}' + \int_{\bar{a}',\vec{r}'} \int_{\bar{a}'',\vec{r}''}$$

$$\times \langle G(\bar{a}', \vec{r}_1, \vec{r}', k)\rangle \langle E(\vec{r}', k_1)E^*(\vec{r}'', k_2)\rangle\, G^*(\bar{a}'', \vec{r}_2, \vec{r}'', k_2)$$

$$\times B(\vec{r}', \vec{r}'')p_1(\bar{a}')p_1(\bar{a}'')\, d\bar{a}'\, d\vec{r}'\, d\bar{a}''\, d\vec{r}'' \quad . \tag{5-15}$$

The Dyson equations for $\langle G\rangle$ and $\langle E\rangle$ [cf. Eqs. (5-13) and (5-14), respectively] and the Bethe-Saltpeter equation for the two-frequency correlation function [cf. Eq. (5-15)] can be brought into forms which are more easily comparable to the corresponding equations for continuous media. Toward this goal, we first perform the integration over the size distribution in Eqs. (5-14)-(5-15), viz.,

$$f = \int f'(\bar{a}', k)\, p_1(\bar{a}')\, d\bar{a} \quad , \tag{5-16}$$

and note that for a narrowband pulse the scattering coefficient is constant, depending only on the prescribed carrier frequency.

Using Eq. (5.16) in conjunction with Eqs. (5-14a) and (5-14b) and operating on the latter two equations with the operator $(\nabla^2 + k^2)$, we obtain

$$(\nabla^2 + k^2 + 4\pi f\, \rho(\vec{r}))\, \langle E(\vec{r}, k)\rangle = -4\pi f \int \langle G(\vec{r}, \vec{r}', k)\rangle$$

$$\langle E(\vec{r}, k)\rangle\, B(\vec{r}, \vec{r}')\, d\vec{r}' \qquad (5\text{-}17a)$$

$$(\nabla^2 + k^2 + 4\pi f\, \rho(\vec{r}))\, \langle G(\vec{r}, \vec{r}', k)\rangle = -4\pi f\, \delta(\vec{r}, \vec{r}')$$

$$- 4\pi f \int dr''\, \langle G(\vec{r}, \vec{r}'', k)\rangle\, \langle G(\vec{r}'', \vec{r}', k)\rangle\, B(\vec{r}, \vec{r}'') \quad . \qquad (5\text{-}17b)$$

These integro-differential expressions are respectively the Dyson equations for $\langle E(\vec{r}, k)\rangle$ and $\langle G(\vec{r}, \vec{r}', k)\rangle$ for the ease of a tenuous medium consisting of discrete pair-correlated scatterers. The functional forms of these two equations are exactly analogous to those derived by Besieris and Kohler [cf. Ref. 10] for a continuous random medium under the assumption of Gaussian statistics for the fluctuating parameters.

We denote next $\langle E(\vec{r}_1, k_1) E^*(\vec{r}_2, k_2)\rangle$ by $\Gamma'(\vec{r}_1, \vec{r}_2, k_1, k_2)$ and operate on Eq. (5-15) with the operator $\nabla_{\vec{r}_1}^2 + k_1^2 + 4f\, \rho(r_1)$ taking, at the same time, into consideration Eqs. (5-17). This procedure results in the expression

$$\{\nabla_{\vec{r}_1}^2 + k_1^2 + 4\pi f\, \rho(\vec{r}_1)\}\, \Gamma'(\vec{r}_1, \vec{r}_2, k_1, k_2) = -4\pi f \int [\langle G(\vec{r}_1, \vec{r}', k_1)\rangle$$

$$\Gamma'(\vec{r}', \vec{r}_2, k_1, k_2) + \Gamma'(\vec{r}_1, \vec{r}', k_1, k_2)\, \langle G^*(\vec{r}_2, \vec{r}', k_2)\rangle]$$

$$B(\vec{r}_1, \vec{r}')\, d\vec{r}' - 4\pi f\, \rho(\vec{r}_1)\, \Gamma'(\vec{r}_1, \vec{r}_1, k_1, k_2)\, \langle G^*(\vec{r}_2, \vec{r}_1, k_2)\rangle \, . \qquad (5\text{-}18)$$

In the same way, we may write

$$\{\nabla_{\vec{r}_2}^2 + k_2^2 + 4\pi f^* \rho(\vec{r}_2)\}\, \Gamma'(\vec{r}_1, \vec{r}_2, k_1, k_2)$$

$$= -4\pi f^* \rho(\vec{r}_2) \langle G(\vec{r}_1, \vec{r}_2, k_1)\rangle\, \Gamma'(\vec{r}_2, \vec{r}_2, k_1, k_2) - 4\pi f^* \times$$

$$\int [\langle G(\vec{r}_1, \vec{r}', k_1)\rangle\, \Gamma'(\vec{r}', \vec{r}_2, k_1, k_2) + \Gamma'(\vec{r}_1, \vec{r}', k_1, k_2) \times$$

$$\langle G^*(\vec{r}_2, \vec{r}', k_2)\rangle]\, B(\vec{r}', \vec{r}_2)\, d\vec{r}' \quad . \tag{5-19}$$

Subtracting, finally, Eq. (5-19) from Eq. (5-18), we obtain

$$\{(\nabla_{\vec{r}_1}^2 - \nabla_{\vec{r}_2}^2) + (k_1^2 - k_2^2) + 4\pi f\, \rho(\vec{r}_1) - 4\pi f\, \rho(\vec{r}_2)\} \times$$

$$\Gamma'(\vec{r}_1, \vec{r}_2, k_1, k_2) = -4\pi\{\pi(\vec{r}_1)\, f\, \Gamma'(\vec{r}_1, \vec{r}_1, k_1, k_2)\, \langle G^*(\vec{r}_2, \vec{r}_1, k_2)\rangle$$

$$- \pi(\vec{r}_2) f^*\, \langle G(\vec{r}_1, \vec{r}_2, k_1)\rangle\, \Gamma'(\vec{r}_2, \vec{r}_2, k_1, k_2)\} - 4\pi \int \times$$

$$[\langle G(\vec{r}, \vec{r}', k_1)\rangle\, \Gamma'(\vec{r}', \vec{r}_2, k_1, k_2) + \Gamma'(\vec{r}_1, \vec{r}', k_1, k_2)\, \langle G^*(\vec{r}_2, \vec{r}', k_2)\rangle]$$

$$[f\, B(\vec{r}_1, \vec{r}') - f^*\, B(\vec{r}', \vec{r}_2)]\, d\vec{r}' \quad . \tag{5-20}$$

This is the ladder approximation of the Bethe-Saltpeter equation for $\Gamma'(\vec{r}_1, \vec{r}_2, k_1, k_2)$ in the case of a tenuous medium of discrete pair-correlated scatterers. Again, this equation is in a functional form which is anologous to the one for a continuous random medium characterized by Gaussian fluctuating parameters [cf. Ref. 10].

5.3.2 The Quasihomogeneous Assumption

In the closed equation for $\Gamma'(\vec{r}_1, \vec{r}_2, k_1, k_2)$ derived in the previous subsection we introduce center-of-mass and difference coordinates and wavenumbers, viz., $\vec{R} = (\vec{r}_1 + \vec{r}_2)/2$, $\vec{r} = \vec{r}_1 - \vec{r}_2$; $k_s = (k_1 + k_2)/2$, $k_d = k_1 - k_2$, and use the notational definitions $\Gamma'(\vec{r}_1, \vec{r}_2, k_1, k_2) = \Gamma(\vec{R}, \vec{r}, k_s, k_d)$, $B'(\vec{r}_1, \vec{r}_2) = B(\vec{R}, \vec{r})$, $\langle G'(\vec{r}_1, \vec{r}_2, k)\rangle = \langle G(\vec{R}, \vec{r}, k)\rangle$. It can be shown, then, that (5-20) can be brought into the form

$$\{2\,\nabla_{\vec{R}} \cdot \nabla_{\vec{r}} + \frac{k_s k_d}{2} + 4\pi[f\,\rho(\vec{R} + 1/2\,\vec{r}) - f^*\,\rho(\vec{R} - 1/2\,\vec{r})]\}$$

$$= -4\pi\,\{(\vec{R} + 1/2\,\vec{r})\, f\, \Gamma(\vec{R} + 1/2\,\vec{r}, 0, k_s, k_d)\, \langle G^*(\vec{R}, -\vec{r}, k_2)\rangle$$

$$- \rho(\vec{R} - 1/2\,\vec{r})\, f^*\, \langle G(\vec{R}, \vec{r}, k_1)\rangle\, \Gamma(\vec{R} - 1/2\,\vec{r}, 0, k_s, k_d)\}$$

$$- 4\pi \int N_1(\vec{R} + \frac{\vec{r}-\vec{r}'}{2}, \vec{r}', k_1)\, \Gamma(\vec{R} - 1/2\,\vec{r}', \vec{r} - \vec{r}', k_s, k_d)\, d\vec{r}'$$

$$+ 4\pi \int \Gamma(\vec{R} - 1/2\,\vec{r}', \vec{r} + \vec{r}', k_s, k_d)\, N_1^*(\vec{R} - 1/2\,(\vec{r} + \vec{r}'), \vec{r}', k_2)\, d\vec{r}'$$

$$+ 4\pi \int \langle G(\vec{R} + \frac{\vec{r}-\vec{r}'}{2}, \vec{r}', k_1)\rangle\, \Gamma(\vec{R} - 1/2\,\vec{r}', \vec{r} - \vec{r}', k_s, k_d) \times$$

$$f^*\, B(\vec{R} - 1/2\,\vec{\lambda}, \vec{r} - \vec{r}')\, d\vec{r}' - 4\pi \int \Gamma(\vec{R} - 1/2\,\vec{r}', \vec{r} + \vec{r}', k_s, k_d) \times$$

$$\langle G^*(\vec{R} - \frac{\vec{r}+\vec{r}'}{2}, \vec{r}', k_2)\rangle\, f\, B(\vec{R} - 1/2\,\vec{r}', \vec{r} + \vec{r}')\, d\vec{r}' \quad ; \qquad (5\text{-}21a)$$

$$N_1(\vec{R} + \frac{\vec{r}-\vec{r}'}{2}, \vec{r}', k_1) = f \langle G(\vec{R} + \frac{\vec{r}-\vec{r}'}{2}, \vec{r}', k_1) \times$$

$$B(\vec{R} + \frac{\vec{r}-\vec{r}'}{2}, \vec{r}') \quad . \tag{5.21b}$$

We consider next smoothly inhomogeneous (or quasihomogeneous) media for which $\Gamma(\vec{R}, \vec{r}, k_s, k_d)$, $B(\vec{R}, \vec{r})$ and $\langle G(\vec{R}, \vec{r}, k)\rangle$ vary slowly with respect to the sum variable $\vec{R}$, and rapidly with respect to the difference variable $\vec{r}$. The quasihomogeneity assumption can be implemented by expanding ρ, N_1, $\langle G\rangle$, and Γ into Taylor series and retaining the dominant terms in (5-21a). As a result, we have the approximate equation

$$\{2 \nabla_{\vec{R}} \cdot \nabla_{\vec{r}} + \frac{k_s k_d}{2} + 4\pi f_R \nabla_{\vec{R}} \rho(\vec{R}) \cdot \vec{r} + 8\pi i f_I \rho(\vec{R})\}$$

$$\Gamma(\vec{R}, \vec{r}, k_s, k_d) + 4\pi\{\rho(\vec{R} + 1/2\ \vec{r})\ f\ \Gamma(\vec{R} + 1/2\ \vec{r}, 0, k_s, k_d) \times$$

$$\langle G^*(\vec{R}_1 - \vec{r}, k_2)\rangle - \rho(\vec{R} - 1/2\ \vec{r})\ f^*\ \langle G(\vec{R}, \vec{r}, k_1)\rangle\ \Gamma(\vec{R} - 1/2\ \vec{r}, 0, k_s, k_d)\}$$

$$+ 4\pi \int_{-\infty}^{\infty} N_1(\vec{R}, \vec{r}', k_1)\ \Gamma(\vec{R}, \vec{r} - \vec{r}', k_s, k_d)\ d\vec{r}' + 2\pi \int_{-\infty}^{\infty} (\vec{r} - \vec{r}') \cdot$$

$$\nabla_{\vec{R}} N_1(\vec{R}, \vec{r}')\ \Gamma(\vec{R}, \vec{r} - \vec{r}', k_s, k_d) - 2\pi \int_{-\infty}^{\infty} \vec{r}'\ N_1(\vec{R}, \vec{r}', k_1) \cdot$$

$$\nabla_{\vec{R}} \Gamma(\vec{R}, \vec{r} - \vec{r}', k_s, k_d)\ d\vec{r}' - 4\pi \int_{-\infty}^{\infty} \Gamma(\vec{R}, \vec{r} + \vec{r}', k_s, k_d)$$

$$N_1^*(\vec{R}, \vec{r}', k_2)\ d\vec{r}' + 2\pi \int_{-\infty}^{\infty} \vec{r} \cdot \nabla_{\vec{R}} \Gamma(\vec{R}, \vec{r} + \vec{r}', k_s, k_d)\ N_1^*(\vec{R}, \vec{r}', k_2) d\vec{r}'$$

$$+ 2\pi \int_{-\infty}^{\infty} \Gamma(\vec{R}, \vec{r} - \vec{r}', k_s, k_d)\ (\vec{r} + \vec{r}') \cdot \nabla_{\vec{R}} N_1^{*}(\vec{R}, \vec{r}', k_2)\, d\vec{r}'$$

$$- 4\pi \int_{-\infty}^{\infty} \langle G(\vec{R}, \vec{r}', k_1) \rangle\, \Gamma(\vec{R}, \vec{r} - \vec{r}', k_s, k_d)\, f^{*}\, B(\vec{R}, \vec{r} - \vec{r}')\, d\vec{r}'$$

$$+ 4\pi \int_{-\infty}^{\infty} \Gamma(\vec{R}, \vec{r} + \vec{r}', k_s, k_d) \langle G^{*}(\vec{R}, \vec{r}', k_2) \rangle\, f\, B(\vec{R}, \vec{r} + \vec{r}')\, d\vec{r}'$$

$$= 0 \quad ; \tag{5-22a}$$

$$f = f_R + j\, f_I \tag{5-22b}$$

5.3.3 Phase-Space Analysis; The Two-Frequency Wigner Distribution Function

It will be convenient in the following to work in a "phase" space $(\vec{R}, \vec{n})$, where $\vec{R}$ is the sum variable introduced in Section 5.3.2, and $\vec{n}$ is the Fourier transform variable that corresponds to the difference coordinate $\vec{r}$. Toward this goal let us introduce the two-frequency Wigner distribution function

$$\tilde{f}(\vec{R}, \vec{n}, k_s, k_d) = \frac{1}{(2\pi)^3} \int_{R^3} d\vec{r}\ \Gamma(\vec{R}, \vec{r}, k_s, k_d)\, e^{-j\vec{n}\cdot\vec{r}} \quad , \tag{5-23}$$

the locally inhomogeneous "spectra"

$$\phi(\vec{R}, \vec{n}) = \int_{R^3} d\vec{r}\ B(\vec{R}, \vec{r})\, e^{-j\vec{n}\cdot\vec{r}} \tag{5-24}$$

$$\tilde{N}_1(\vec{R}, \vec{n}, \cdot) = \int_{R^3} N_1(\vec{R}, \vec{r}, \cdot)\, e^{-j\vec{n}\cdot\vec{r}}\, d\vec{r} \quad , \tag{5-25}$$

and the Fourier transform of the mean Green's function $\langle G(\vec{R}, \vec{r}, \cdot)\rangle$, viz.,

$$\tilde{G}(\vec{R}, \vec{n}, \cdot) = \int_{R^3} d\vec{r}\, \langle G(\vec{R}, \vec{r}, \cdot)\rangle\, e^{-j\vec{n}\cdot\vec{r}}\, d\vec{r} \quad . \tag{5-26}$$

Also we express the locally inhomogeneous spectrum $\tilde{N}_1(\vec{R}, \vec{n}, k)$ in terms of its real and imaginary parts,

$$\tilde{N}_1(\vec{R}, \vec{n}, k) = \tilde{N}_1'(\vec{R}, \vec{n}, k) + j\, N_1''(\vec{R}, \vec{n}, k) \quad .$$

The equation of "evolution" for the two-frequency Wigner distribution function then, may be written as

$$2j\vec{n} \cdot \nabla_{\vec{R}} \tilde{f}(\vec{R}, \vec{n}, k_s, k_d) + \frac{k_s k_d}{2} \tilde{f}(\vec{R}, \vec{n}, k_s, k_d)$$

$$+ 4\pi j\, f_R\, \nabla_{\vec{R}}\, \rho(\vec{R}) \cdot \nabla_{\vec{n}} \tilde{f}(\vec{R}, \vec{n}, k_s, k_d) + 8\pi j\, f_I\, \rho(\vec{R}) \tilde{f}(\vec{R}, \vec{n}, k_s, k_d)$$

$$+ \frac{1}{2\pi^2} \int_{R^3} \{\rho(\vec{R} + 1/2\, \vec{r})\, f\, \Gamma(\vec{R} + 1/2\, \vec{r}, 0, k_s, k_d)\, \langle G^*(\vec{R}, -\vec{r}, k_2)\rangle$$

$$- \rho(\vec{R} - 1/2\, \vec{r})\, f^*\, \langle G(\vec{R}, \vec{r}, k_1)\rangle\, \Gamma(\vec{R} - 1/2\, \vec{r}, 0, k_s, k_d)\}\, e^{-j\vec{n}\cdot\vec{r}}\, d\vec{r}$$

$$+ 4\pi\, \tilde{N}_1(\vec{R}, \vec{n}, k_1)\, \tilde{f}(\vec{R}, \vec{n}, k_s, k_d) + 2\pi j\, \nabla_{\vec{R}} \tilde{N}_1(\vec{R}, \vec{n}, k_1)$$

$$\cdot \nabla_{\vec{n}} \tilde{f}(\vec{R}, \vec{n}, k_s, k_d) - 2\pi j\, \nabla_{\vec{n}} \tilde{N}_1(\vec{R}, \vec{n}, k_1) \cdot \nabla_{\vec{R}} \tilde{f}(\vec{R}, \vec{n}, k_s, k_d)$$

$$+ \frac{1}{2\pi^2} \int_{R^3} d\vec{n}'\, \phi(\vec{R}, \vec{n} - \vec{n}')\, f(\vec{R}, \vec{n}', k_s, k_d) \left[\int_{R^3} f\, \langle G^*(\vec{R}, \vec{r}', k_2)\rangle\right.$$

$$\times e^{j\vec{r}'\cdot\bar{n}} - f^{*} \langle G(\vec{R}, \vec{r}', k_1)\rangle e^{-j\vec{r}'\cdot\vec{n}} d\vec{r}'] = 0 \quad . \tag{5-27}$$

Under the restriction that the ratio of difference to sum wavenumbers is small compared to unity, i.e., $|k_d\ k_s| << 1$, and expanding $\tilde{f}(\vec{R} - 1/2\ \vec{r}, \vec{n}, k_s, k_d)$, $\rho(\vec{R} - 1/2\ \vec{r})$ into Taylor series in terms of r and retaining dominant terms inside the integral of (5-27), the above equation may be further approximated to:

$$2j\vec{n} \cdot \nabla_{\vec{R}} \tilde{f}(\vec{R}, \vec{n}, k_s, k_d) + \frac{k_s k_d}{2} \tilde{f}(\vec{R}, \vec{n}, k_s, k_d) + 4\pi j\ f_R \nabla_{\vec{R}} \rho(\vec{R})$$

$$\cdot \nabla_{\vec{n}} \tilde{f}(\vec{R}, \vec{n}, k_s, k_d) + 8\pi j\ f_I \rho(\vec{R})\ \tilde{f}(\vec{R}, \vec{n}, k_s, k_d)$$

$$+ 8\pi j\ \tilde{N}_1''(\vec{R}, \vec{u}, k_s)\ \tilde{f}(\vec{R}, \vec{n}, k_s, k_d) + 4\pi j\ \nabla_{\vec{R}} \tilde{N}_1'(\vec{R}, \vec{n}, k_s) \cdot$$

$$\nabla_{\vec{n}} \tilde{f}(\vec{R}, \vec{n}, k_s, k_d) - 4\pi j\ \nabla_{\vec{n}} \tilde{N}_1'(\vec{R}, \vec{n}, k_s) \cdot \nabla_{\vec{R}} \tilde{f}(\vec{R}, \vec{n}, k_s, k_d)$$

$$+ \frac{1\pi}{(2\pi)^3} [\int_{R^3} d\vec{n}'\ \{\phi(\vec{R}, \vec{n} - \vec{n}') + \rho(\vec{R})\}\ \tilde{f}(\vec{R}, \vec{n}', k_s, k_d)$$

$$\times \{f\ \tilde{G}^{*}(\vec{R}, \vec{n}, k_s) - f^{*}\ \tilde{G}(\vec{R}, \vec{n}, k_s)\}] = 0 \quad . \tag{5-28}$$

This equation will be written in the next subsection in a more transparent form by exploiting the properties of the mean Green's function $\langle G(\vec{R}, \vec{r}, k)\rangle$ or, equivalently, its Fourier transfor

5.3.4 Generalized Two-Frequency Transport Equation

For smoothly inhomogeneous discrete media, the average Green's function $\langle G(\vec{R}, \vec{r}, k)\rangle$ obeys (cf. Appendix C) the Dyson equation

$$\{\nabla_{\vec{r}}^2 + [k^2 + 4\pi f\, \rho(r)]\}\ \langle G(\vec{R}, \vec{r}, k)\rangle$$

$$= - 4\pi f\, \delta(\vec{r}) - 4\pi \int d\vec{r}'\, N_1(\vec{R}, \vec{r} - \vec{r}', k)\, \langle G(\vec{R}, \vec{r}', k)\rangle\, d\vec{r}' \quad . \tag{5-29}$$

In this expression the complex kernel $N_1(\vec{R}, \vec{r}, k)$ is known as the "mass operator".

The integrodifferential equation (5-29) is of a convolution type; as a consequence, a Fourier transformation with respect to the fast variable $\vec{r}$ yields the formal solution

$$\tilde{G}(\vec{R}, \vec{n}, k) = 4\pi f\{2\, H(\vec{R}, \vec{n}, k)\}^{-1} \tag{5-30}$$

written in terms of the complex "Hamiltonian" of an effective medium, viz.,

$$H(\vec{R}, \vec{n}, k) \equiv H'(\vec{R}, \vec{n}, k) + j\, h''(\vec{R}, \vec{n}, k)$$

$$= \frac{1}{2}\{n^2 - k^2 - 4\pi f_R\, \rho(\vec{R}) - 4\pi\, \tilde{N}_1'(\vec{R}, \vec{n}, k)$$

$$- j[4\pi f_I\, \rho(\vec{R}) + 4\pi\, \tilde{N}_1''(\vec{R}, \vec{n}, k)]\} \quad . \tag{5-31}$$

An insistence on using the exact solution (5-30) in conjunction

with (5-28) would lead us to a radiative transport theory based on complex rays associated with the effective Hamiltonian given in (5-31). Although such a procedure is feasible in principle, it will be avoided in the following development by assuming that the regular and scattering loss terms $4\pi f_I \rho(\vec{R})$, $4\pi \tilde{N}_1''(\vec{R}, \vec{n}, k)$ are small, but not negligible.

The quantities $f \tilde{G}^*(\vec{R}, \vec{n}, k) - f^* \tilde{G}(\vec{R}, \vec{n}, k)$ appear in (5-28) only in the purely scattering integral terms. It is reasonable, then, for their computation to neglect completely the imaginary part of the effective complex Hamiltonian. As a result, $f^* \tilde{G}(\vec{R}, \vec{n}, k)$ simplifies to

$$f^* \tilde{G}(\vec{R}, \vec{n}, k) \simeq 4\pi|f|^2 \{2 H'(\vec{R}, \vec{n}, k)\}^{-1}$$

$$\simeq P\{4\pi|f|^2 [2H'(\vec{R}, \vec{n}, k)]^{-1}\} + j\, 4\pi^2|f|^2 \delta\{H'(\vec{R}, \vec{n}, k)\} \qquad (5\text{-}32)$$

from which we obtain

$$f \tilde{G}^*(\vec{R}, \vec{n}, k) - f^* \tilde{G}(\vec{R}, \vec{n}, k)$$

$$\simeq -j\, 8\pi^2|f|^2 \delta[k^2 - n^2 + 4\pi f_R \rho(\vec{R}) + 4\pi \tilde{N}_1'(\vec{R}, \vec{n}, k)] \quad . \qquad (5\text{-}33)$$

The symbol $P\{\cdot\}$ denotes the principal value of the quantity within the curly bracket.

Under the above assumption, Eq. (5-28) can be rewritten as follows:

$$\vec{n} \cdot \nabla_{\vec{R}} \tilde{f}(\vec{R}, \vec{n}, k_s, k_d) + 2\pi \nabla_{\vec{R}} \rho(\vec{R}) \cdot \nabla_{\vec{n}} \tilde{f}(\vec{R}, \vec{n}, k_s, k_d)$$

$$+ 2\pi \nabla_{\vec{R}} \tilde{N}_1'(\vec{R}, \vec{n}, k_s) \cdot \nabla_{\vec{n}} \tilde{f}(\vec{R}, \vec{n}, k_s, k_d) - 2\pi \nabla_{\vec{n}} \tilde{N}_1'(\vec{R}, \vec{n}, k_s)$$

$$\cdot \nabla_{\vec{R}} \tilde{f}(\vec{R}, \vec{n}, k_s, k_d) + 4\pi f_I \rho(\vec{R}) \tilde{f}(\vec{R}, \vec{n}, k_s, k_d)$$

$$+ 4\pi \tilde{N}_1''(\vec{R}, \vec{n}, k_s) \tilde{f}(\vec{R}, \vec{n}, k_s, k_d) - 2|f|^2 \delta[H(\vec{R}, \vec{n}, k_s)]$$

$$\int_{R^3} d\vec{n}' \{\phi(\vec{R}, \vec{n} - \vec{n}') + \rho(\vec{R})\} \tilde{f}(\vec{R}, \vec{n}', k_s, k_d)$$

$$- j \frac{k_s k_d}{4} \tilde{f}(R, \vec{n}, k_s, k_d) = 0 \quad . \tag{5-34}$$

The effects of deterministic absorption are subsumed in the term $4\pi f_I \rho(\vec{R}) \tilde{f}(\vec{R}, \vec{n}, k_s, k_d)$. On the other hand, absorption due to the randomness of the particles enter into the terms $\tilde{N}_1', ''(\vec{R}, \vec{n}, k_s)$ and $\phi(\vec{R}, \vec{n})$. The interaction between the deterministic absorption and the one due to randomness has been neglected.

Within the framework of the weak absorption approximation, the purely scattering integral term in (5-34) becomes significant only on the energy surface $H'(\vec{R}, \vec{n}, k_s) = 0$. This observation can be used to rewrite (5-34) in a more economical form. Let, specifically, d be the differential of a curvilinear ray that passes the point $\vec{R}$ in the direction of the group velocity $\nabla_{\vec{n}} H'(\vec{R}, \vec{n}, k_s)$. The Hamilton-Zacobi equations corresponding to the Hamiltonian $H'(\vec{R}, \vec{n}, k_s)$ assume, then, the form

$$\frac{d}{d\ell}\vec{R} = \left|\nabla_{\vec{n}} H'(\vec{R}, \vec{n}, k_s)\right|^{-1} \nabla_{\vec{n}} H'(\vec{R}, \vec{n}, k_s) \quad , \tag{5-34a}$$

$$\frac{d}{d\ell}\vec{n} = - \left|\nabla_{\vec{n}} H'(\vec{R}, \vec{n}, k_s)\right|^{-1} \nabla_{\vec{R}} H'(\vec{R}, \vec{n}, k_s) \quad . \tag{5-34b}$$

When these equations are finally used in conjunction with (5-34), we find that the two-frequency Wigner distribution function is governed by the generalized transport equation

$$\left|\nabla_{\vec{n}} H'(\vec{R}, \vec{n}, k_s)\right| \frac{d}{d\ell} \tilde{f}(\vec{R}, \vec{n}, k_s, k_d) + 4\pi f_I \rho(\vec{R}) \tilde{f}(\vec{R}, \vec{n}, k_s, k_d)$$

$$+ 4\pi \tilde{N}_1''(\vec{R}, \vec{n}, k_s) \tilde{f}(\vec{R}, \vec{n}, k_s, k_d) - 2|f|^2 \delta[H'(\vec{R}, \vec{n}, k_s)]$$

$$\int_{R^3} d\vec{n}' \{\phi(\vec{R}, |\vec{n} - \vec{n}'|) + \rho(\vec{R})\} \tilde{f}(\vec{R}, \vec{n}', k_s, k_d) +$$

$$j \frac{k_s k_d}{4} \tilde{f}(\vec{R}, \vec{n}, k_s, k_d) = 0 \quad . \tag{5-35}$$

It must be emphasized that the term "generalized transport equation" is used here rather loosely to distinguish (5-35) from the two-frequency radiative transfer equation for the photometric quantity $I(\vec{R}, \vec{s}, k_s, k_d)$ to be derived in the next section. More, precisely, however, the term should be used in conjunction with the phase-space analog of the two-frequency mutual coherence function [cf. Eq. 5-20]. The phase-space distribution density $f(\vec{R}, \vec{n}, k_s, k_d)$ governed by this equation contains more information than the corresponding one associated with (5-35) since assumptions dealing with

quasihomogeneity, low losses, etc., have not yet been made.

5.4 Two-Frequency Radiative Transfer Equation

5.4.1 Anisotropic Spatial Pair Correlations

In the general case of statistically anisotropic spatial pair correlations of the scatterers we seek a solution to (5-3) in the form

$$\tilde{f}(\vec{R}, \vec{n}, k_s, k_d) = f_o(\vec{R}, \vec{n}, k_s, k_d) + f_1(\vec{R}, \vec{n}, k_s, k_d) \quad . \quad (5\text{-}36)$$

The quantity $f_o(\vec{R}, \vec{n}, k_s, k_d)$ is the coherent part of the two-frequency Wigner distribution, viz.,

$$f_o(\vec{R}, \vec{n}, k_s, k_d) \longleftrightarrow \Gamma_o(\vec{R}, \vec{r}, k_s, k_d)$$

$$= \Gamma_o'(\vec{r}_1, \vec{r}_2, k_1, k_2) \equiv \langle E(\vec{r}_1, k_1) \rangle \langle E^*(\vec{r}_2, k_2) \rangle \quad , \quad (5\text{-}37)$$

and satisfies (cf. Appendix D) the transport equation

$$\left| \nabla_{\vec{n}} H'(\vec{R}, \vec{n}, k_s) \right| \frac{d}{d\ell} f_o(\vec{R}, \vec{n}, k_s, k_d) + 4\pi N_1''(\vec{R}, \vec{n}, k_s)$$

$$\times f_o(\vec{R}, \vec{n}, k_s, k_d) + 4\pi f_I \rho(\vec{R}) f_o(\vec{R}, \vec{n}, k_s, k_d) - j \frac{k_s k_d}{4} f_o(\vec{R}, \vec{n},$$

$$k_s, k_d) = 0 \quad . \quad (5\text{-}38)$$

The incoherent portion of the Wigner distribution function, on the other hand, is chosen (cf. also, Ref.) as follows:

$$f_1(\vec{R}, \vec{n}, k_s, k_d) = k_2 |\nabla_{\vec{n}} H'(\vec{R}, \vec{n}, k_s)| |\nabla_{\vec{n}} H'(\vec{R}, \vec{n}, k_s)|^{-3}$$

$$\times \delta[H'(\vec{R}, \vec{n}, k_s)]\ I(\vec{R}, \vec{s}, k_s, k_d) \quad ; \quad \vec{s} = \frac{\vec{n}}{n} \quad . \tag{5-39}$$

Let, next, $k_{eff}(\vec{R}, \vec{s}, k_s)$ denote the value of n for which $H'(\vec{R}, n\vec{s}, k_s) = 0$, and define an effective index of refraction as follows:

$$n_{eff}(\vec{R}, \vec{s}, k_s) = |\nabla_{\vec{n}} H'(\vec{R}, n, k_s)|/k_s \quad ; \quad n = k_{eff}(\vec{R}, \vec{s}, k_s) \quad . \tag{5-40}$$

Let, finally, $\theta(\vec{R}, \vec{s}, k_s)$ be the angle between the direction of the group velocity $\nabla_{\vec{n}} H'(\vec{R}, \vec{n}, k_s)$ and the phase velocity $\vec{s} = \vec{n}/\vec{n}$. With these definitions in mind, the incoherent intensity function $I(\vec{R}, \vec{s}, k_s, k_d)$ is found to obey the two-frequency radiative transfer equation

$$n_{eff}^2(\vec{R}, \vec{s}, k_s) \frac{d}{d\ell} \{I(\vec{R}, \vec{s}, k_s, k_d) |\cos \theta(\vec{R}, \vec{s}, k_s)|^{-1}$$

$$\times n_{eff}^{-2}(\vec{R}, \vec{s}, k_s)\} = \{-4\pi f_I \rho(\vec{R}) - 4\pi \tilde{N}_1''[\vec{R}, k_{eff}(\vec{R}, \vec{s}, k_s)\vec{s}, k_s]$$

$$+ j \frac{k_s k_d}{4}\} k_s^{-1} n_{eff}^{-1}(\vec{R}, \vec{s}, k_s)\ I(\vec{R}, \vec{s}, k_s, k_d)$$

$$+ 2|f|^2 k_s^{-2} \int_{\Omega} d\Omega(\vec{s}')\ k_{eff}^2(\vec{R}, \vec{s}', k_s)\ n_{eff}(\vec{R}, \vec{s}, k_s)$$

$$\times n_{eff}^{-3}(\vec{R}, \vec{s}', k_s) |\cos \theta(\vec{R}, \vec{s}, k_s)| |\cos \theta(\vec{R}, \vec{s}', k_s)|^{-1}$$

$$\times \{\phi[\vec{R}, k_{eff}(\vec{R}, \vec{s}, k_s)\vec{s} - k_{eff}(\vec{R}, \vec{s}, k_s)\vec{s}'] + \rho(\vec{R})\}$$

$$\times I(\vec{R}, \vec{s}', k_s, k_d) + 2|f|^2 n_{eff}(\vec{R}, \vec{s}, k_s)|\cos\theta(\vec{R}, \vec{s}, k_s)|$$

$$\times \int_{R^3} d\vec{n}' \{\phi[\vec{R}, k_{eff}(\vec{R}, \vec{s}, k_s)\vec{s} - \vec{n}'] + \rho(\vec{R})\} f_o(\vec{R}, \vec{n}', k_s, k_d) \quad , \tag{5-41}$$

where Ω denotes the range of $\vec{s}'$ over the surface of a unit sphere.

Equation (5-41) for the two-frequency incoherent intensity function $I(\vec{R}, \vec{s}, k_s, k_d)$ is the main result of this section. In interpreting this equation, we note the following: The left-hand side of the equation is a convective term; the ray paths correspond to an effective medium determined by the density of the scatterers $\rho(\vec{R})$, the scattering coefficient f and the spatial correlation function of the scatterers. The first and second terms of the right hand side of (5-41) are respectively regular loss and scattering terms; the third term arises because of frequency offsets; the fourth one is the scattering term; finally, the last one is a source term, representing the "feeding" of the incoherent intensity by the coherent part of the Wigner distribution function.

5.4.2 Isotropic Spatial Pair Correlations

For isotropic spatial pair correlations, the quantities $\tilde{N}_1'(\vec{R}, \vec{n}, k_s)$, $\tilde{N}_1''(\vec{R}, \vec{n}, k_s)$, $\phi(\vec{R}, n)$ and, consequently, $H'(\vec{R}, \vec{n}, k_s)$ depend only on the modulus of the wavevector $\vec{n}$, i.e., $n = |\vec{n}|$. In this case, the directions of the group and phase velocities coincide. This is clearly seen from the relationship $\nabla_{\vec{n}} H'(\vec{R}, \vec{n}, k_s) =$

$\vec{n} - 2\pi \nabla_{\vec{n}} \tilde{N}_1'(\vec{R}, n, k_s) = [n - 2\pi \nabla_n \tilde{N}_1'(\vec{R}, n, k_s)]\vec{s}$. Setting then, $\theta = 0$ in (5-41), we find that the latter specializes as follows:

$$n_{eff}^2(\vec{R}, k_s) \frac{d}{d\ell} \{I(\vec{R}, \vec{s}, k_s, k_d)\, n_{eff}^{-2}(\vec{R}, k_s)]$$

$$= \{-4\pi f_I\, \rho(\vec{R}) - 4\pi \tilde{N}_1''[\vec{R}, k_{eff}(\vec{R}, k_s)\vec{s}, k_s] + j \frac{k_s k_d}{4}\}$$

$$\times I(\vec{R}, \vec{s}, k_s, k_d)\, k_s^{-1}\, n_{eff}^{-1}(\vec{R}, k_s) + 2|f|^2\, k_{eff}^2(\vec{R}, k_s) k_s^{-2}$$

$$\times n_{eff}^{-2}(\vec{R}, k_s) \int_\Omega [\phi(\vec{R}, k_{eff}(\vec{R}, k_s)|\vec{s} - \vec{s}'|) + \rho(\vec{R})]$$

$$\times I(\vec{R}, \vec{s}', k_s, k_d)\, d\Omega(\vec{s}') + 2|f|^2 \int \{\phi[\vec{R}, |k_{eff}(\vec{R}, k_s)\vec{s}$$

$$- \vec{n}'|] + \rho(\vec{R})\}\, f_o(\vec{R}, \vec{n}', k_s, k_d)\, d\vec{n}' \quad . \tag{5-42}$$

The two-frequency radiative transfer equation (5-42) is considerably simpler than the equation obtained earlier for anisotropic statistical fluctuations. We note, for example, that the effective wavenumber k_{eff} and the effective refractive index n_{eff} are now independent of $\vec{s}$; furthermore, the scattering integral term on the right-hand side of (5-42) is of a convolution type.

The physical interpretation of the various terms in (5-42) is analogous to that provided in the previous subsection in connection with (5-41).

5.4.3 Comparisons with Classical Radiative Transport Theory

The classical radiation transport equation for a medium of discrete scatterers has the following form:

$$n^2(\vec{R})\,\frac{d}{d\ell}\,[I(\vec{R},\vec{s})n^{-2}(\vec{R})] = -\,\alpha(\vec{R},\vec{s})\,I(\vec{R},\vec{s})$$

$$+\int_{\Omega} d\vec{s}'\;\sigma(\vec{R},\vec{s},\vec{s}')\;I(\vec{R},\vec{s})\quad . \tag{5-43}$$

Here, $I(\vec{R},\vec{s})$ is the ray (or photometric) intensity of the electric field, $d\ell$ is a differential element of a ray passing through the point $\vec{R}$ in the direction $\vec{s}$, $n^2(\vec{R})$ is the regular component of the refractive index in the discrete medium, $\sigma(\vec{R},\vec{s},\vec{s})$ is the scattering coefficient, and finally, $\alpha(\vec{R},\vec{s})$ is the absorption coefficient -- usually the sum of the true absorption and extinction coefficients.

In phenomenological derivations of (5-43) based mostly on energy balance (cf. Refs. -), no "microscopic" interpretation is provided for the scattering and extinction coefficients. On the other hand, the systematic "wave-kinetic" approach used in this thesis to derive Eqs. (5-41) and (5-42) has enabled us to surmount this difficulty.

The radiative transfer equations (5-41) and (5-42) are of the classical form (5-43). However, they differ from the latter on several important aspects which we wish to discuss next.

In (5-42) -- the radiation transport equation for isotropic spatial pair correlations -- we note the following: (1) the effective index of refraction $n^2_{eff}(\vec{R}, k_s)$ contains information about the density

of the scatterers $\rho(\vec{R})$, the average scattering coefficient of the individual scatterer and the spatial pair correlation function; (2) there is clear separation of true absorption and extinction effects in the absorption coefficient, viz.,

$$\alpha(\vec{R}, k_s) = 4\pi f_I \rho(\vec{R}) k_s^{-1} n_{eff}^{-1}(\vec{R}, k_s)$$

$$+ 4\pi \tilde{N}_1''(\vec{R}, k_{eff}(\vec{R}, k_s)\vec{s}, k_s) k_s^{-1} n_{eff}^{-1}(\vec{R}, k_s) \quad , \tag{5-44}$$

with a dependence of the individual terms on the effective wavenumber $k_{eff}(\vec{R}, k_s)$ and the effective index of refraction $n_{eff}(\vec{R}, k_s)$ which is not easily predictable phenomenologically; (3) the term proportional to k_d is missing completely from (5-43). It accounts for frequency offsets and renders the two-frequency incoherent intensity function $I(\vec{R}, \vec{s}, k_s, k_d)$ complex; (4) the scattering coefficient is given explicitly as follows:

$$\sigma(\vec{R}, \vec{s}, \vec{s}', k_s) = 2|f|^2 k_{eff}^2(\vec{R}, k_s) k_s^{-2} n_{eff}^{-2}(\vec{R}, k_s)$$

$$\times [\phi(\vec{R}, k_{eff}(\vec{R}, k_s)|\vec{s} - \vec{s}'|) + \rho(\vec{R})] \quad ; \tag{5-45}$$

(5) the last term, which describes the transformation of the coherent part of the scattered field $f_o(\vec{R}, \vec{n}, k_s, k_d)$ into the incoherent intensity $I(\vec{R}, \vec{s}, k_s, k_d)$, is absent in (5-43). Although such an omission is justified when dealing with purely incoherent fields, it is not acceptable in the study of partially coherent field, such as radio or light wave propagation through rain, smoke, etc.

In (5-41), the effective wavenumber and the effective index of refraction depend on $\vec{s}$ because of the anisotropy of the spatial correlation function. There, also, appears the factor $\cos\theta(\vec{R}, \vec{s}, k_s)$ -- missing from (5-43) -- because of the noncoincidence of the directions of group and phase velocities. The absorption and scattering coefficient can be written down in this case as follows:

$$\alpha(\vec{R}, \vec{s}, k_s) = 4\pi f_I \rho(\vec{R}) k_s^{-1} n_{eff}^{-1}(\vec{R}, \vec{s}, k_s)$$

$$+ 4\pi \tilde{N}_1''(\vec{R}, k_{eff}(\vec{R}, \vec{s}, k_s)\vec{s}, k_s) k_s^{-1} n_{eff}^{-1}(\vec{R}, \vec{s}, k_s) \quad , \tag{5-46}$$

$$\sigma(\vec{R}, \vec{s}, \vec{s}, k_s) = 2|f|^2 k_s^{-2} k_{eff}^2(\vec{R}, \vec{s}', k_s) n_{eff}(\vec{R}, \vec{s}, k_s)$$

$$\times n_{eff}^{-3}(\vec{R}, \vec{s}', k_s)|\cos\theta(\vec{R}, \vec{s}, k_s)||\cos\theta(\vec{R}, \vec{s}', k_s)|^{-1}$$

$$\times \{\phi(\vec{R}, k_{eff}(\vec{R}, \vec{s}, k_s)\vec{s} - k_{eff}(\vec{R}, \vec{s}, k_s)\vec{s}') + \rho(\vec{R})\} \quad . \tag{5-47}$$

5.5 Relationship Between "Wave" and "Photometric" Quantities

Let us briefly retrace several salient features of our development in this chapter. This will enable us to appreciate a useful direct connection between the incoherent intensity $I(\vec{R}, \vec{s}, k_s, k_d)$ and the incoherent part of the two-frequency mutual coherence function.

In order to compute the second-order pulse moment $\langle E(\vec{r}_1, t_1) E^*(\vec{r}_2, t_2)\rangle$ at the receiver site, we must first find the

two-frequency mutual coherence function $\langle E(\vec{r}_1, \omega_1)E^*(\vec{r}_2, \omega_2)\rangle$ and then perform a two-dimensional Fourier transformation with respect to ω_1, ω_2. In the ladder approximation, the two-frequency mutual coherent function obeys the closed Bethe-Saltpeter equation (5-20). The phase-space analog of the two-frequency mutual coherence is the Wigner distribution function $\tilde{f}(\vec{R}, \vec{n}, k_s, k_d)$ [cf. Eq. 5-23] which obeys the generalized two-frequency transport equation (5-35) under the conditions specified in subsections 5.3.3 and 5.3.4. The Wigner distribution is decomposed [cf. Eq. (5-36)] next into a coherent part $f_o(\vec{R}, \vec{n}, k_s, k_d)$ which is governed by the transport equation (5-39), and an incoherent part $f_1(\vec{R}, \vec{n}, k_s, k_d)$ directly expressible in terms of the two-frequency ray intensity $I(\vec{R}, \vec{n}, k_s, k_d)$. The latter obeys Eq. (5-41) for anisotropic spatial pair correlation function and (5-42) for isotropic one.

Not all the successive steps outlined in the previous paragraph need be followed for obtaining information about second-order pulse statistics. If, for example, such information is restricted to the incoherent part of $\langle E(\vec{r}_1, t_1)E^*(\vec{r}_2, t_2)\rangle$, direct usage can be made of the two-frequency ray intensity $I(\vec{R}, \vec{s}, k_s, k_d)$, as explained below.

By virtue of its definition, the quantity $f_1(\vec{R}, \vec{n}, k_s, k_d)$ is the phase-space analog of the incoherent part of the two-frequency mutual coherence function, viz.,

$$f_1(\vec{R}, \vec{n}, k_s, k_d) \longleftrightarrow B_u(\vec{R}, \vec{r}, k_s, k_d) \equiv \Gamma(\vec{R}, \vec{r}, k_s, k_d)$$

$$- \langle E(\vec{R} + 1/2\ \vec{r}, k_s + 1/2\ k_d)\rangle \langle E^*(\vec{R} - 1/2\ \vec{r}, k_s - 1/2\ k_d)\rangle \quad ,$$

or, more explicitly,

$$B_u(\vec{R}, \vec{r}, k_s, k_d) = \frac{1}{(2\pi)^3} \int_{R^3} d\vec{n}\ f_1(\vec{R}, \vec{n}, k_s, k_d)\ e^{\vec{n}\cdot\vec{r}} \quad . \tag{5-48}$$

Recall from (5-39) that in the general case of anisotropic spatial correlation function $f_1(\vec{R}, \vec{n}, k_s, k_d)$ is expressed as

$$f_1(\vec{R}, \vec{n}, k_s, k_d) = k_2 \left|\nabla_{\vec{n}} H'(\vec{R}, \vec{n}, k_s)\right| \left|\nabla_n H'(\vec{R}, \vec{n}, k_s)\right|^{-3}$$

$$\times\ \delta[H'(\vec{R}, \vec{n}, k_s)]\ I(\vec{R}, \vec{s}, k_s, k_d) \quad , \tag{5-49}$$

or equivalent, as

$$f_1(\vec{R}, \vec{n}, k_s, k_d) = k_s^{-2}\ n_{eff}^{-3}(\vec{R}, \vec{s}, k_s) \left|\cos\theta(\vec{R}, \vec{s}, k_s)\right|^{-1}$$

$$\times\ \delta[n - k_{eff}(\vec{R}, \vec{s}, k_s)]\ I(\vec{R}, \vec{s}, k_s, k_d) \quad , \tag{5-50}$$

where use has been made of the notational definitions introduced in subsection 5.4.1.

We substitute next the expression for $f_1(\vec{R}, \vec{n}, k_s, k_d)$ given in (5-50) into (5-48) and carry out the integration over the polar coordinate variable $n = |\vec{n}|$. This operation results in the relationship

$$B_u(\vec{R}, \vec{r}, k_s, k_d) = \int_\Omega d\vec{s}\, k_s^{-2}\, n_{eff}^{-3}(\vec{R}, \vec{s}, k_s)\, k_{eff}^{2}(\vec{R}, \vec{s}, k_s)$$

$$\times \left|\cos\theta(\vec{R}, \vec{s}, k_s)\right|^{-1} I(\vec{R}, \vec{s}, k_s, k_d)\, e^{j\, k_{eff}(\vec{R}, \vec{s}, k_s)\vec{s}\cdot\vec{r}}\,, \qquad (5\text{-}51)$$

which establishes a useful connection between the photometric (a term used originally in the study of incoherent optical radiation) ray intensity $I(\vec{R}, \vec{s}, k_s, k_d)$ and the incoherent part of the two-frequency mutual coherence function. The latter, of course, is a "wave" quantity, directly linked to the stochastic Helmholtz equation.

In the special case of isotropic statistical fluctuations, (5-51) simplifies considerably; specifically

$$B_u(\vec{R}, \vec{r}, k_s, k_d) = k_s^{-2}\, n_{eff}^{-3}(\vec{R}, k_s)\, k_{eff}^{2}(\vec{R}, k_s)$$

$$\int_\Omega d\vec{s}\, I(\vec{R}, \vec{s}, k_s, k_d)\, e^{j\, k_{eff}(\vec{R}, k_s)\vec{s}\cdot\vec{r}}\,. \qquad (5\text{-}52)$$

CHAPTER VI

CONCLUDING REMARKS

Derivations have been presented in the first part of the thesis for the coherent field propagating in a random distribution of scatterers without pair correlations using single, first-order multiple and "complete" multiple scattering formulations. The multiple scattering results have been applied to millimeter wave propagation through precipitation media. It has also been shown that higher-order multiple scattering effects become important for frequencies above 30 GHz.

The above formulations contain several salient features which are important enough to be retraced and discussed: (a) The formulations are vector-valued in nature and allow the incorporation of polarization states of the incident wave and receive antenna, as well as the calculation of the depolarization effects of a tenuous discrete medium; (b) The scatterer distributions in position, size, shape, and orientation angle enter naturally into the model; (c) The formulations allow the density of the scatterers to vary with position. This condition is required in order to evaluate a realistic precipitation medium; (d) Any form of precipitation can be included in the formulations (ice, rain, hail, etc.); (e) The multiple scattering formulation is numerically efficient. This feature will allow in the future the study of isolation and attenuation statistics for various rain rate distributions. Due to large execution time, such a study has been almost impossible [43] on the basis of a first-order multiple

scattering model; (g) The multiple scattering model gives accurate results for systems operating above 30 GHz. Finally, the wave-kinetic procedure leading to (5-41) provides the possibility (1) for ascertaining the domain of validity and (2) for extending the range of applicability (e.g., to account for anisotropic scatterers, depolarization effects, etc.) of the radiative transport theory developed in this thesis.

We shall close this section by mentioning several of the open research areas in propagation through precipitation and random distribution of scatterers. These include:

(i) Computations of isolation and attenuation for rain media with rain rate distributions different than the piecewise unfiorm one that was used in this thesis (e.g., exponential [44]);

(ii) Investigation of precipitation models where the canting angle is not statistically independent of the position;

(iii) Calculation of the incoherent intensity for the rain medium discussed in Section 4.2 using the transport equation (5-41);

(iv) Derivation of the radiative transfer equation for tenuous distributions of anisotropic discrete scatterers, with the depolarization effects of the discrete medium taken into consideration;

(v) Specific applications of the two-frequency radiative transfer equation (5-41) to pulsed wave propagation through precipitation and obcurants.

References

1. L. Rayleigh, Phil. Mag. 41, 279 (1871).

2. L. O. Foldy, Phys. Rev. 67, 107 (1945).

3. M. Lax, Rev. Mod. Phys. 23, 287 (1951).

4. V. Twersky, Proc. Am. Math. Soc. 16, 84 (1969).

5. V. Twersky, J. Math. Phys. 19, 215 (1978).

6. V. N. Bringi, T. A. Seliga, V. K. Varadan, and V. V. Varadan, "Bulk propagation characteristics of discrete random media," in Multiple Scattering of Waves in Random Media, edited by P. L. Chow, W. E. Kohler and G. Papanicolaou (North-Holland Publishing Company, Amsterdam, 1981).

7. Yu. N. Barabanenkov, and V. M. Finkel'berg, Solv. Phys. JETP 26, 587 (1968).

8. K. M. Watson, J. Math. Phys. 10, 688 (1969).

9. Yu. N. Barabanenkov, A. G. Vinogradov, Yu. A. Kravtsov, and V. I. Tatarskii, Izv. VUZ, Radiofix. 15, 1852 (1972).

10. I. M. Besieris and W. E. Kohler, "Two Frequency Radiative Transfer Equation for a Statistically Inhomogeneous and Anisotropic Absorptive Medium" in Multiple Scattering of Waves in Random Media, edited by P. L. Chow, W. E. Kohler and G. Papanicolaou (North-Holland Publishing Company, Amsterdam, 1981).

11. J. Stratton, Electromagnetic Theory (McGraw-Hill Book Co., New York, 1941).

12. M. Kerker, The Scattering of Light (Academic Press, New York, 1969).

13. Lord Rayleigh, Phil. Mag. 44, 28 (1897).

14. D. S. Jones, The Theory of Electromagnetism (Macmillan Company, New York, 1964).

15. W. L. Stutzman, W. P. Overstreet, C. W. Bostian, A. Tsolakis, and E. A. Manus, "Ice Depolarization on Satellite Radio Paths," Final Report for Intelsat Contract, INTEL-123, VPI&SU EE Dept., April 1981.

16. R. Gans, Ann. Phys. 37, 881 (1912).

17. A. Ishimaru, Wave Propagation and Scattering in Random Media (Academic Press, New York, 1978).

18. L. I. Schiff, Quantum Mechanics (McGraw-Hill Co., New York, 1955).

19. T. Oguchi, J. Radio Res. Labs. 33, 467 (1960).

20. J. A. Morrison and T. S. Chu, Bell Syst. Tech. J. 10, 1907 (1973).

21. T. Oguchi and Y. Hosoya, J. de Rech. Atm. 8, 121 (1974).

22. P. M. Morse and H. Feshback, Methods of Theoretical Physics (McGraw-Hill, New York, 1953).

23. A. R. Holt, N. K. Uzunoglou, and B. G. Evans, IEEE Trans. Ant. Prop. 26, 706 (1978).

24. J. W. Shephard, A. R. Holt, and B. G. Evans, IEE Conf. Pub. No. 195 2, 96 (1981).

25. H. C. Van de Hulst, Light Scattering by Small Particles (John Wiley, New York, 1964).

26. W. L. Stutzman, "A Review of Theoretical Modeling of Millimeter Wave Propagation Through Precipitation," Interim Report for NASA Contract NAS5-22577, VPI&SU EE Dept., May 1980.

27. R. R. Persinger, W. L. Stutzman, R. E. Castle, and C. W. Bostian, IEEE Trans. on Ant. and Prop. AP-28, 149 (1980).

28. T. Oguchi, J. Radio Res. Lab. Jpn. 20, 79 (1973).

29. B. G. Evans, and J. Troughten, IEE Conf. Publ. 98, 162 (1973).

30. P. A. Watson and M. Arbabi, Electron. Lett. 8, 282 (1972).

31. C. W. Bostian and J. E. Allnutt, Proc. IEEE 126, 951 (1979).

32. T. Oguchi, Radio Sci. 16, 691 (1981).

33. M. K. Uzunoglu, and B. G. Evans, J. Phys. A. Math. Gen. 11, 767 (1978).

34. G. Brussaard, Radio Sci. 16, 745 (1981).

35. C. Capsoni, and A. Paraboni, Ann. Telecommun. 36, 154 (1981).

36. J. D. Kraus and K. R. Carver, Electromagnetics (McGraw-Hill, New York, 1973).

37. D. J. Cox, H. W. Arnold, and H. H. Hoffman, Radio Sci. 13, 511 (1978).

38. D. A. Bennetts, and F. Rawlins, Quart. J. R. Met. Soc. 107, 477 (1981)

39. W. L. Brogan, Modern Control Theory (Quantum Publishers, New York, 1974).

40. N. K. Uzunoglu, B. G. Evans, and A. R. Holt, Proc. IEE 124, 417 (1977).

41. S. Chandrasekhar, Radiative Transfer (Oxford Univ. Press, 1960).

42. G. C. Pomraning, Radiation Hydrodynamics (Pergamon Press, New York, 1973).

43. S. O. Lane, and W. L. Stutzman, "A Gaussian Rain Cell Model for Prediction of Rain Effects on Millimeter Wave Propagation," Interim Report 1980-2, Contract NAS5-22577, VPI&SU EE Dept., July 1980.

APPENDIX A

ICE PROGRAM

The Ice Program uses the algorithm developed in subsection 4.1.3 to compute the isolation and phase of a plane wave passing through an ice medium. A block diagram of the Ice Program is shown in Fig. A-1. In the following pages a listing of the Ice Program statement is presented.

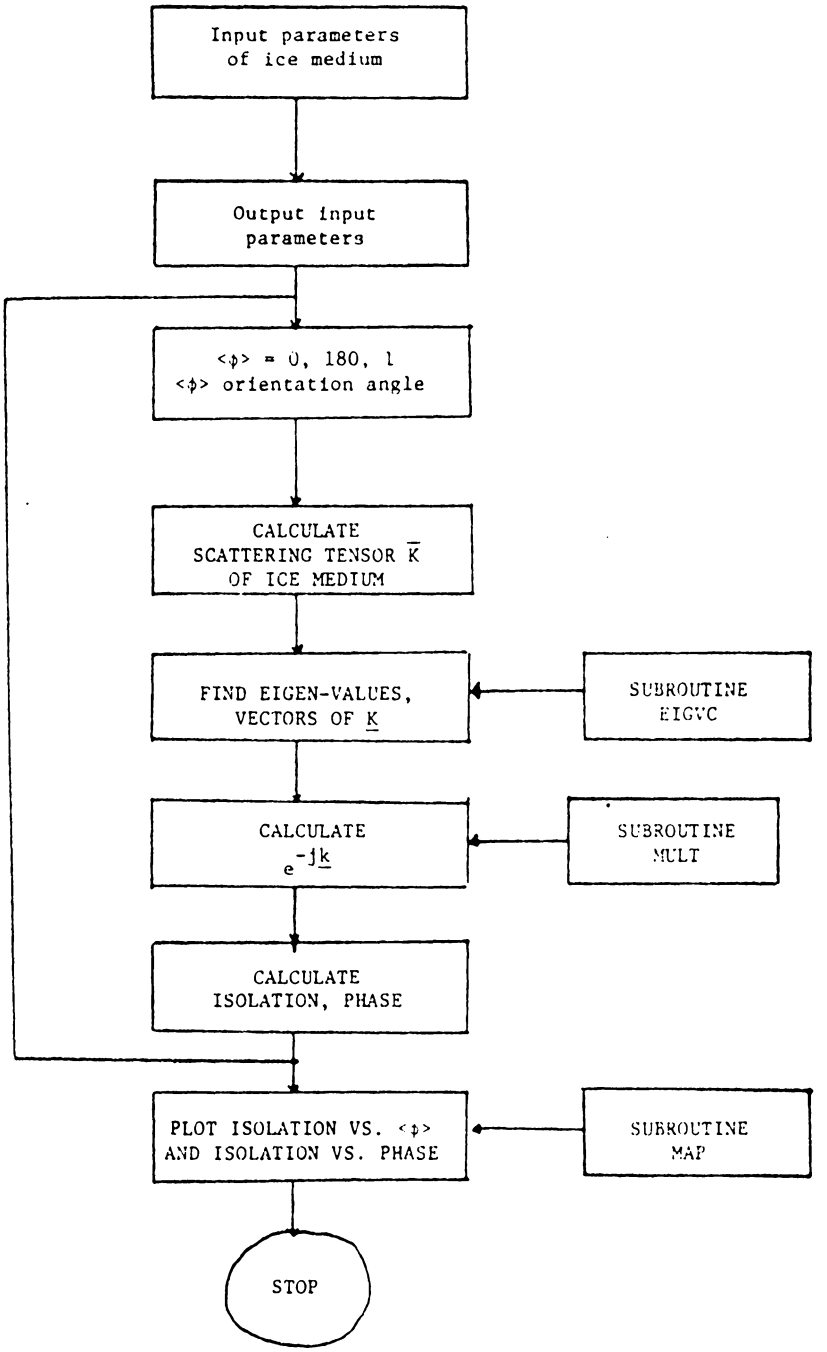

Figure A-1. Block diagram of Ice Program.

```
CCCCCCCCCCCCCCCCCCCCCCCCCCCCCCCCCCCCCCCCCCCCCCCCCCCCCCCCCCCCCCCCCCCCCCC
C
C    THIS PROGRAM CALCULATES THE E VECTOR FIELD THAT COMES OUT
C    FROM A SLAB OF ICE NEEDLES AND ICE PLATES.
C    EI   IS THE INCIDENT FIELD TO THE SLAB
C    IFIV IS THE VECTOR FIELD COMING OUT OF THE SLAB
C    ICO  IS THE ICE CONTENT OF THE CLOUD DEFINED AS THE VOLUME
C         OF THE ICE CRYSTALS PER CUBIC METER OF AIR TIMES
C         THE  LENGHT OF THE CLOUD.
C    PN IS THE PERCENTAGE OF THE ICE NEEDLES IN THE CLOUD
C    DEL IS THE ELEVATION ANGLE OF THE SATELLITE
C    FREQ IS THE FREQUENCY OF THE WAVE IN GHZ
C    SIGM IS THE STANDARD DEVIATION OF THE ORIENTATION
C    ANGLE OF THE ICE NEEDLES
C
CCCCCCCCCCCCCCCCCCCCCCCCCCCCCCCCCCCCCCCCCCCCCCCCCCCCCCCCCCCCCCCCCCCCCCC
      COMPLEX F(2,2),EIGV(2),EIGVC(2,2),WK(2),DIAG(2,2),UNIT(2,2)
     C,WA(2),EI(2,1),EFIN(2,1),EGVC(2,2),MATR1(2,2),MATR2(2,2)
     C,MATR3(2,2)
      COMPLEX JAI,ER,SCPH1,ER1,ISOL
     C,ERO,ELO,MR
      REAL ICO,LAM,ISOLDB,CPH2,SPH2,ISD(182),PHI(182)
```

```
      COMMON ISD,PHI
      PI=3.1415927
      CALL PLOTS(0,0,50)
      MR=(1.78,-0.0024)
      ER=MR**2
      JAI=(0.0,1.0)
C
C   READ IN THE VARIABLES OF THE ICE CLOUD
C
   15 READ(5,999) THE1,DEL1,SIGM1,PN,ICO,FREQ
      IF(THE1.EQ.-1.) GO TO 88
      WRITE(6,91)
 91   FORMAT(1H0,15X,'THE CLOUD PARAMETERS ARE: ')
      WRITE(6,92) PN,ICO,THE1
 92   FORMAT(5X,'PERCENTAGE OF NEEDLES=',F8.3,'CONTENT OF ICE=',
     CE12.3,3X,'THETA IS',F8.3)
      WRITE(6,93) SIGM1
  93  FORMAT(5X,'THE STANDARD DEVIATION OF THE ORIENT ANGLE IS ',
     CF10.3)
      WRITE(6,94)
 94   FORMAT(/,5X,'ISOLATION',5X,'PHASE',5X,'ORIENTATION ANGLE')
C
C   READ THE INCIDENT VECTOR FIELD
C
```

```
      READ(5,97) (EI(J,1),J=1,2),ISTAT
   97 FORMAT(4(F4.1,1X),1X,I1)
      THE=THE1*PI/180.


      DEL=DEL1*PI/180.
      SIGM=SIGM1*PI/180.
      LAM=0.3/FREQ
      AKO=2.0*PI/LAM
      DO 51 IPLOT=1,4
      PN=1.0-IPLOT*0.2
      IF(IPLOT.EQ.1) PN=1.0
      DO 50 IJK=1,180
      PHO=(IJK-1)*PI/180.
C
C   SPH1 IS THE AVER OF SIN(2PHI) CPH1 THE AVER OF COS(2PHI)
C
      CPH1=COS(2.*PHO)*EXP(-2.*(SIGM**2))
      SPH1=SIN(2.*PHO)*EXP(-2.*(SIGM**2))
      OXX=0.5*(CPH1*(SIN(THE)**2-(SIN(DEL)*COS(THE))**2)
     C+SIN(THE)**2+(SIN(DEL)*COS(THE))**2+SIN(2.0*THE)*SPH1
```

```
     C*SIN(DEL))
      OYY=0.5*(CPH1*(COS(THE)**2-(SIN(DEL)*SIN(THE))**2)
     C+COS(THE)**2+(SIN(DEL)*SIN(THE))**2-SPH1*SIN(2.0*THE)*SIN(DEL))
      OXOY=0.25*(SIN(2.0*THE)*(SIN(DEL)**2-1.)-SIN(2.0*THE)*CPH1*(1.0
     C+(SIN(DEL)**2))-2.0*SIN(DEL)*SPH1*COS(2.*THE))
      F(1,1)=0.5*(ER-1.)*(PN*((ER-1.)*OXX+2.)/(ER+1.)
     C+(1.-PN)*((1.-ER)*(COS(THE)*COS(DEL))**2/ER+1.))
      F(1,2)=0.5*(ER-1.)*(PN*OXOY*(ER-1.)/(ER+1.)+
     C(1.-PN)*(1.-ER)*SIN(2.*THE)*(COS(DEL)**2)/(2.*ER))
      F(2,1)=F(1,2)
      F(2,2)=0.5*(ER-1.)*(PN*((ER-1.)*OYY+2.)/(ER+1.)+
     C(1.-PN)*((1.-ER)*((SIN(THE)*COS(DEL))**2)/ER+1.))
C
C   FIND THE EIGEN(VALUES, VECTORS) OF THE SCATTERING MATRIX F
C
      CALL EIGCC(F,2,2,1,EIGV,EIGVC,2,WK,IER1)
C     WRITE(6,96) (EIGV(J), J=1,2)
  96  FORMAT(1X,2(E12.5,E12.5,2X))
      DIAG(1,1)=CEXP(-JAI*EIGV(1)*ICO*AKO)
      DIAG(2,2)=CEXP(-JAI*EIGV(2)*ICO*AKO)
      DO 10 I=1,2
      DO 10 J=1,2
```

```
      IF(I.EQ.J) GO TO 10
      DIAG(I,J)=(0.0,0.0)
   10 CONTINUE
      DO 20 I=1,2
      DO 20 J=1,2
      UNIT(I,J)=(0.0,0.0)
      IF(I.EQ.J) UNIT(I,J)=(1.0,0.0)
   20 CONTINUE
      DO 30 I=1,2
      DO 30 J=1,2
   30 EGVC(I,J)=EIGVC(I,J)
C
C    FIND THE INVERSE OF THE MATRIX OF EIGENVECTORS
C    AND THEN CALCULATE EXP(F*L) * INCIDENT VECTOR FIELD
C
      CALL LEQT1C(EIGVC,2,2,UNIT,2,2,0,WA,IER)
      CALL MULT(EGVC,2,2,DIAG,2,MATR1)



      CALL MULT(MATR1,2,2,UNIT,2,MATR3)
      CALL MULT(MATR3,2,2,EI,2,EFIN)
C     DO 55 J=1,2
```

```
C      WRITE(6,96) (EFIN(I,J),I=1,2)
C 55   CONTINUE
C
C    CALCULATE THE ISOLATION
C    FOR ISTAT=1 EI HORIZ. , ISTAT=2  EI VERTICAL
C    ISTAT=3 EI RHC, ISTAT=4 EI LHC
C
       IF(ISTAT.EQ.1) ISOL=EFIN(2,1)/EFIN(1,1)
       IF(ISTAT.EQ.2) ISOL=EFIN(1,1)/EFIN(2,1)
       IF(ISTAT.LT.3) GO TO 80
       ELO=EFIN(1,1)+JAI*EFIN(2,1)
       ERO=EFIN(1,1)-JAI*EFIN(2,1)
       IF(ISTAT.EQ.3) ISOL=ELO/ERO
       IF(ISTAT.EQ.4) ISOL=ERO/ELO
    80 X1=CABS(ISOL)
       PHASE=180.*ATAN2(AIMAG(ISOL),REAL(ISOL))/PI
       ISOLDB=20.*ALOG10(X1)
       PHO=180.*PHO/PI
       SIGM1=180.*SIGM/PI
       ISD(IJK)=ISOLDB
       PHI(IJK)=PHASE
C      WRITE(6,900) ISOLDB,PHASE,PHO
```

```
   50 CONTINUE
      CALL MAP(IPLOT)
   51 CONTINUE
      CALL PLOT(0.0,0.0,-999)
      GO TO 15
  999 FORMAT(6F10.0)
  900 FORMAT(5X,F8.3,4X,F10.4,6X,F8.4)
   88 CALL PLOT(0.0,0.0,+999)
      STOP
      END
      SUBROUTINE  MULT(A,N,M,B,M1,C)
C
C   THIS SUBROUTINE MULTIPLIES TWO COMPLEX MATRICES
C
      COMPLEX A(N,M),B(M,M1),C(N,M1),SUM
      DO 10 I=1,N
      DO 10 J=1,M1
      SUM=(0.0,0.0)
      DO 20 IJ=1,M
   20 SUM=SUM+A(I,IJ)*B(IJ,J)
   10 C(I,J)=SUM
      RETURN
```

```
      END
      SUBROUTINE TRAN(A,N,M,B)
C
C   THIS SUBROUTINE CALCULATES THE TRANSPOSE OF A MATRIX
C
      COMPLEX A(N,M),B(M,N)
      DO 10 I=1,N
      DO 10 J=1,M



   10 B(J,I)=A(I,J)
      RETURN
      END
      SUBROUTINE MAP(IPLOT)
      REAL ISD(182),PHI(182)
      COMMON ISD,PHI
      IF(IPLOT.NE.1) GO TO 10
C     CALL SCALE(PHI,6.0,180,1)
C     CALL SCALE(ISD,6.0,180,1)
      X1=6.0
      ISD(181)=6.0
```

```
      ISD(182)=6.0
      PHI(181)=-180.0
      PHI(182)=360.0/X1
      CALL PLOT(1.0,1.0,-3)
      CALL AXIS(0.0,0.0,5HPHASE,-5,X1,0.0,PHI(181),PHI(182))
      CALL AXIS(0.0,0.0,9HISOLATION,9,4.0,90.0,ISD(181),ISD(182))
C     CALL NEWPEN(IPLOT)
      CALL LINE(PHI,ISD,180,1,-10,IPLOT)
      RETURN
   10 CALL PLOT(0.0,0.0,-3)
C     CALL NEWPEN(IPLOT)
      CALL LINE(PHI,ISD,180,1,-10,IPLOT)
      RETURN
      END
```

APPENDIX B

RAIN MULTIPLE SCATTERING PROGRAM

The Rain Multiple Scattering Program (RMP) uses the algorithm developed in subsection 4.2.2 to compute the attenuation and isolation that a plane wave undergoes passing through a rain medium. A block diagram of the RMP program is shown in Fig. B-1. In the following pages a listing of the RMP statements is presented.

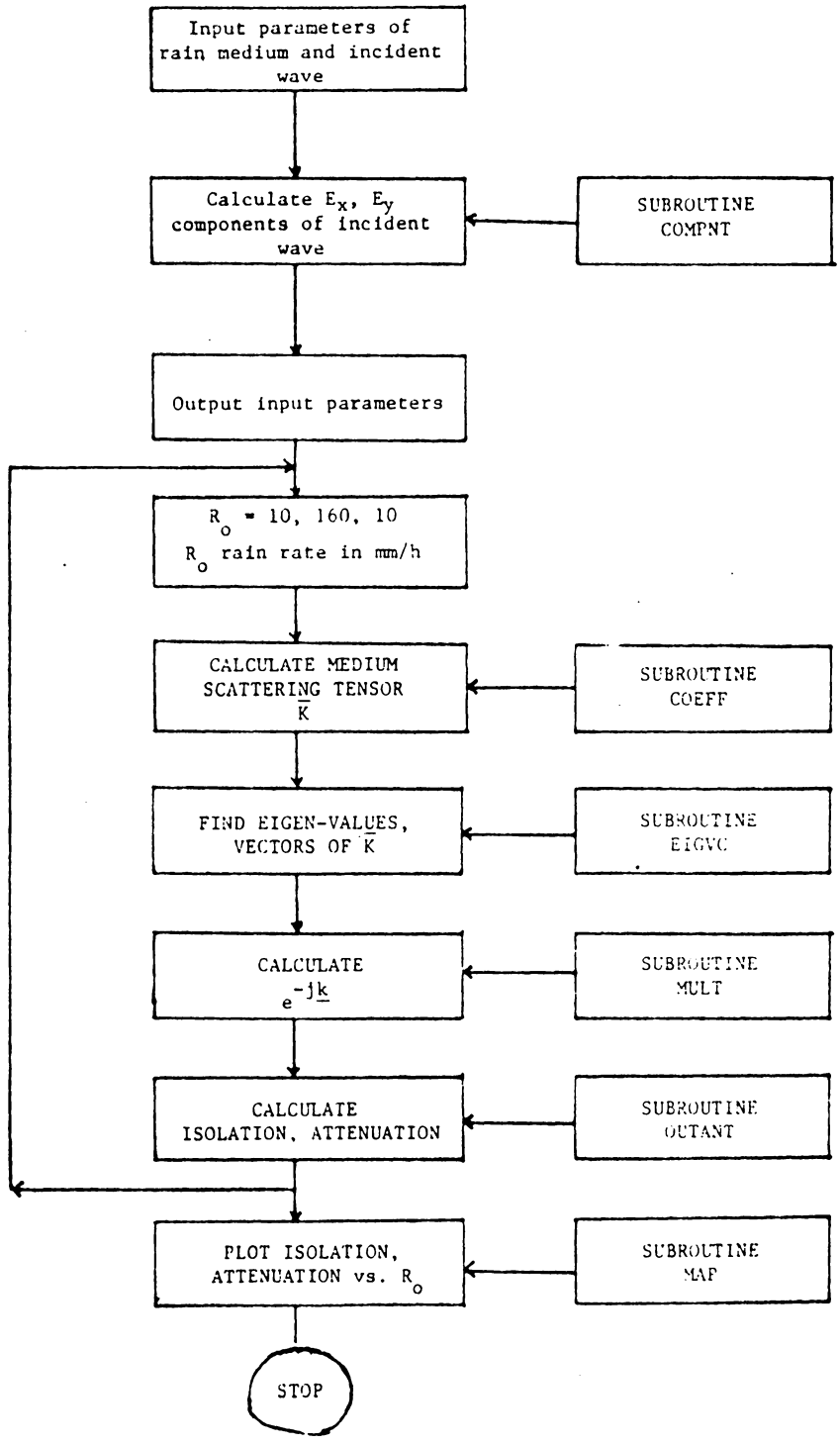

Figure B-1. Block diagram of RMP program.

```
CCCCCCCCCCCCCCCCCCCCCCCCCCCCCCCCCCCCCCCCCCCCCCCCCCCCCCCCCCCCCCCCCCCC
C
C    THIS PROGRAM CALCULATES THE E VECTOR FIELD THAT COMES OUT
C    FROM A RAIN CELL. IT ALSO CALCULATES THE POLARIZATION
C    DIRECTIONS OF THE INCIDENT WAVE THAT WILL PASS THROUGH
C    THE RAIN CELL UNCHANGED.
C    EI  IS THE INCIDENT FIELD TO THE RAIN CELL
C    IFIV IS THE VECTOR FIELD COMING OUT OF THE RAIN CELL
C    L IS THE THICKNESS OF THE RAIN CELL IN METERS
C    LOKANG IS THE ELEVATION ANGLE OF THE SATELLITE
C    FREQ IS THE FREQUENCY OF THE WAVE IN GHZ
C    SIGM IS THE STANDARD DEVIATION OF THE CANTING
C    ANGLE OF THE RAIN DROPS
C    THE IS THE AVERAGE CANTING ANGLE
C
CCCCCCCCCCCCCCCCCCCCCCCCCCCCCCCCCCCCCCCCCCCCCCCCCCCCCCCCCCCCCCCCCCCC
      COMPLEX F(2,2),EIGV(2),EIGVC(2,2),WK(2),DIAG(2,2),UNIT(2,2)
     C,WA(2),EI(2,1),EIIN(2,1),EGVC(2,2),MATR1(2,2),MATR2(2,2)
     C,MATR3(2,2)
      COMPLEX FH,FV,FSH,JAI,SCTHE,DIFF,ER1,ISOL,ATT
     C,ERO,ELO,FV1,FV2,FH1,FH2,DIFF1,DIFF2,FSH1,FSH2
     C,MINUSJ,EXC,EYC,EXX,FYX
```

```
      REAL NO,KO,LOKANG,L,LAM,ISOLDB,ISD(52),RATE(52)
     C,AMODE(6),ATTD(52)
      DATA AMODE/0.0,0.25,1.0,2.0,2.5,3.5/
      COMMON/VAR/ ISD,RATE,ATTD
       COMMON/BLOC1/ MINUSJ,CONV
      COMMON/BLOC2/ VWACM
       MINUSJ=(0.0,-1.0)
      PI=3.1415927
      CONV=PI/180.0
      JAI=(0.0,1.0)
      P1=0.4
      P2=0.6
C
C   READ IN THE VARIABLES OF THE RAIN CELL
C
   15 READ(5,999) LOKANG,THE1,SIGM1,L,NO,FREQ
      IF(LOKANG.EQ.0.) GO TO 88
      READ(5,977) EPSW,TAUW,EPSC,TAUC,EPSX,TAUX
  977 FORMAT(6F10.0)
      WRITE(6,93)
      WRITE(6,92) THE1,SIGM1,L
C
C   READ THE INCIDENT VECTOR FIELD
```

```
C
C     READ(5,91) (EI(J,1),J=1,2),ISTAT
C  91 FORMAT(4(F4.1,1X),1X,I1)
      LOKANG=LOKANG*PI/180.



      THE=THE1*PI/180.
      SIGM=SIGM1*PI/180.
      LAM=0.3/FREQ
      KO=2.*PI/LAM
      CALL COMPNT(EPSW,TAUW,EI(1,1),EI(2,1))
      CALL COMPNT(EPSC,TAUC,EXC,EYC)
      CALL COMPNT(EPSX,TAUX,EXX,EYX)
      EYC=CONJG(EYC)
      EYX=CONJG(EYX)
      VWACM=CABS(EXC*EI(1,1)+EYC*EI(2,1))
      CALL ERROR(SIGM,ER1,2.)
      SCTHE=CLXP(JAI*2.*THE)*ER1*EXP(-2.*(SIGM**2))/2.
C
C   CALCULATE THE AVERAGE OF COS(2.0*THETA) , SIN(2.*THETA)
C
```

```
      CTHE=REAL(SCTHE)
      STHE=AIMAG(SCTHE)
      STHE=0.0
      CTHE=EXP(-2.*(SIGM**2))
      WRITE(6,777) CTHE
777   FORMAT(1X,F15.5)
      IK=9
      DO 50 IJK=1,50
      RO=10.+145.*(IJK-1)/50.
      IK=IK+1
      DO 66 I=1,2
      DO 66 J=1,2
 66   F(I,J)=(0.0,0.0)
      DO 65 J=1,2
      AL=0.8*L
      R=RO*((RO/10.)**(-0.66))
      IF(J.EQ.2) AL=L*0.2
      IF(J.EQ.2) R=RO
      DO 65 I=1,5
      AMODE1=AMODE(I)+0.001
      AMODE2=AMODE(I+1)
      CALL COEF(FREQ,AMODE1,FV1,FH1,FSH1,DIFF1,LOKANG,R)
```

```
      CALL COEF(FREQ,AMODE2,FV2,FH2,FSH2,DIFF2,LOKANG,R)
      FV=FV2-FV1
      FH=FH2-FH1
      FSH=FSH2-FSH1
      DIFF=DIFF2-DIFF1
      F(1,1)=F(1,1)+(P1*FSH+P2*((FH+FV)/2.-DIFF
     C*CTHE/2.))*AL*NO
      F(2,2)=F(2,2)+(P1*FSH+P2*((FV+FH)/2.+DIFF
     C*CTHE/2.))*AL*NO
      F(1,2)=F(1,2)+(P2*DIFF )*AL*NO*STHE/2.
      F(2,1)=F(1,2)
   65 CONTINUE
      F(1,1)=2.*PI*F(1,1)/KO
      F(2,2)=2.*PI*F(2,2)/KO
      F(2,1)=2.*PI*F(2,1)/KO
      F(1,2)=F(2,1)
C
C     FIND THE EIGENVALUES AND EIGENVECTORS OF THEPROPAGATION
C
C     TENSOR F
C
```

```
      CALL EIGCC(F,2,2,1,EIGV,EIGVC,2,WK,IER1)
      DIAG(1,1)=CEXP(-JAI*EIGV(1))
C     DIAG(1,1)=1.-JAI*EIGV(1)
C     DIAG(2,2)=1.-JAI*EIGV(2)
      DIAG(2,2)=CEXP(-JAI*EIGV(2))
      DO 10 I=1,2
      DO 10 J=1,2
      IF(I.EQ.J) GO TO 10
      DIAG(I,J)=(0.0,0.0)
   10 CONTINUE
      DO 20 I=1,2
      DO 20 J=1,2
      UNIT(I,J)=(0.0,0.0)
      IF(I.EQ.J) UNIT(I,J)=(1.0,0.0)
   20 CONTINUE
      DO 30 I=1,2
      DO 30 J=1,2
   30 EGVC(I,J)=EIGVC(I,J)
C
C   FIND THE INVERSE OF THE MATRIX OF EIGENVECTORS
C   AND THEN CALCULATE EXP(F*L) * INCIDENT VECTOR FIELD
C
```

```
      CALL LEQT1C(EIGVC,2,2,UNIT,2,2,0,WA,IER)
      CALL MULT(EGVC,2,2,DIAG,2,MATR1)
      CALL MULT(MATR1,2,2,UNIT,2,MATR3)
      CALL MULT(MATR3,2,2,EI,1,EFIN)
      IF(IK.LT.10) GO TO 150
      WRITE(6,97)  RO,FREQ
97    FORMAT(1X,/,'FOR RAIN RATE',F5.1,'MM /HR AND FREQUENCY',F5.1,
     C' GHZ THE UNDEPOLARIZED POLARIZATION DIRECTIONS ARE:')
      DO 55 J=1,2
      WRITE(6,96) (UNIT(I,J),I=1,2)
96    FORMAT(1X,'(',F5.2,'+JAI',F5.2,') XO  +  (',F5.2,
     C'+JAI',F5.2,') YO')
55    CONTINUE
      IK=0
150   CONTINUE
      CALL OUTANT(EFIN(1,1),EFIN(2,1),EXC,EYC,EXX,EYX,ISOLDB,ATTDB
     C,PHAS)
      ISD(IJK)=ISOLDB
      ATTD(IJK)=ATTDB
      RATE(IJK)=RO
 50   CONTINUE
      CALL MAP
```

```
      WRITE(6,8) (ISD(J),ATTD(J),RATE(J),J=1,20)
    8 FORMAT(5X,3F10.3)
      GO TO 15
  999 FORMAT(3F5.2,F8.2,F12.3,F6.3)
   92 FORMAT(5X,'THE AVERAGE CANTING ANGLE:',F5.2,5X,
     C'THE STANDARD DEV. OF THE CANTING ANGLE:',F5.2,/,
     C5X,'THE EFFECTIVE LENGTH',F8.2)
   93 FORMAT(1H0,15X,'THE VARAIBLESS OF THE RAIN CLOUD ARE'//)
   88 STOP



      END
C
C
      SUBROUTINE  MULT(A,N,M,B,M1,C)
C
C   THIS SUBROUTINE MULTIPLIES TWO COMPLEX MATRICES
C
      COMPLEX A(N,M),B(M,M1),C(N,M1),SUM
      DO 10 I=1,N
      DO 10 J=1,M1
```

```
      SUM=(0.0,0.0)
      DO 20 IJ=1,M
   20 SUM=SUM+A(I,IJ)*B(IJ,J)
   10 C(I,J)=SUM
      RETURN
      END
C
C
      SUBROUTINE ERROR(SIGM,ER,ALFA)
C
C   THIS SUBROUTINE CALCULATES THE ERROR FUNCTION OF
C   A COMPLEX VARIABLE AND IT USES THESE RESULTS TO
C   CALCULATE THE COMPLEX COEFFICIENTS OF THE AVERAGE
C   COS(ALFA* PHI) AND SIN(ALFA* PHI) WHERE PHI IS
C   A RANDOM VARIABLE WITH NORMAL DISTRIBUTION (0,SIGM)
C
      COMPLEX ER,JAI,Z1,Z2,Z,ZS,W1,W2,X3
      JAI=(0.0,1.0)
      Z1=3.3553-JAI*ALFA*SIGM/SQRT(2.)
      Z2=-3.3553-JAI*ALFA*SIGM/SQRT(2.)
      Z=JAI*Z1
      ZS=Z*Z
```

```
      W1=-Z1*((0.4613135/(ZS-0.1901635))+(0.09999216/(ZS-
     C1.7844927))+(0.002883894/(ZS-5.5253437)))
      W2=2.*CEXP(JAI*5.*ALFA*SIGM)
      X3=JAI*AIMAG(Z2*Z2)
      ER=W2*CEXP(-X3)-CONJG(W1)*CEXP(-Z2*Z2)-W1*CEXP(-Z1*Z1)
      RETURN
      END
C
C
      SUBROUTINE MAP
C
C   THIS SUBROUTINE PLOTS ATTENUATION AND
C   ISOLATION VERSUS RAIN RATE
C
      REAL ISD(52),RATE(52),ATTD(52)
      COMMON/VAR/ ISD,RATE,ATTD
      CALL PLOTS(0,0,50)
      CALL SCALE(RATE,8.0,50,1)
      CALL SCALE(ISD,6.0,50,1)
      CALL SCALE(ATTD,6.0,50,1)
      CALL PLOT(2.0,2.0,-3)
      CALL AXIS(0.0,0.0,9HRAIN RATE,-9,8.0,0.0,RATE(51),RATE(52))
```

```
      CALL AXIS(0.0,0.0,9HISOLATION,9,6.0,90.0,ISD(51),ISD(52))



      CALL LINE(RATE,ISD,50,1,0,0)
      CALL PLOT(0.0,0.0,+999)
      CALL PLOTS(0,0,50)
      CALL PLOT(2.0,2.0,-3)
      CALL AXIS(0.0,0.0,9HRAIN RATE,-9,8.0,0.0,RATE(51),RATE(52))
      CALL AXIS(0.0,0.0,11HATTENUATION,11,6.0,90.0,ATTD(51),ATTD(52))
      CALL LINE(RATE,ATTD,50,1,0,0)
      CALL PLOT(0.0,0.0,+999)
      RETURN
      END
C
C
      SUBROUTINE COEF(FREQ,AMODE,FV,FH,FSPH,DIFF,LOKANG,R)
C
C     THIS SUBROUTINE RETURNS TO THE CALLING PROGRAM THE SCATTERING
C     COEFFICIENTS FOR SPHERICAL AND OBLATE RAIN DROPS.
C     THE COEFFICIENTS ARE A FUNCTION OF FREQUENCY AND DROP SIZE
C     AND ELEVATION ANGLE.  THE COEFFICIENTS USED ARE THOSE OF UZUNOGLU,
C     EVANS AND HOLT. THIS IS A MODIFIED VERSION OF THE
```

```
C     SUBROUTINE DEVELOPED BY PRESINGER AND STUTZMAN.
C
      COMPLEX CMPLX
      REAL LOKANG
C
      COMPLEX FV,FH,FSPH,DIFF
      DOUBLE PRECISION U22,U33,U44,U55,AK1,AK2,AK3,AK4,AK5
      AK=-8.2*(R**(-0.21))
      AK1=EXP(AK*AMODE)/AK
C
      IF(AMODE.LT.0.25) AMODE=0.25
      IF(AMODE.LE.0.25) GO TO 100
      IF((INT(FREQ).EQ.11).AND.(AMODE.GT.3.5)) AMODE=3.5
      IF((INT(FREQ).EQ.14).AND.(AMODE.GT.3.5)) AMODE=3.5
      IF((INT(FREQ).EQ.20).AND.(AMODE.GT.3.0)) AMODE=3.0
      IF((INT(FREQ).EQ.30).AND.(AMODE.GT.3.0)) AMODE=3.0
      IF((INT(FREQ).EQ.20).AND.(AMODE.GT.3.0)) GO TO 100
      IF((INT(FREQ).EQ.30).AND.(AMODE.GT.3.0)) GO TO 100
C
      U11=AMODE
      U22=AMODE**2
      U33=AMODE**3
```

```
      U44=AMODE**4
      U55=AMODE**5
      AK2=AK**2
      AK3=AK**3
      AK4=AK**4
      AK5=AK**5
      U1=(U11-1./AK)
      U2=(U22-2.*U11/AK+2.0/AK2)
      U3=(U33-3.*U22/AK+6.*U11/AK2
     C-6.0/AK3)
      U4=(U44-4.*U33/AK+12.*U22/AK2-
     C24.*U11/AK3+24./AK4)
      U5=(U55-5.*U44/AK+20.*U33/AK2
     C-60.*U22/AK3+120.*U11/AK4-120./AK5)


       GO TO 101
  100 U1=AMODE
      U2=(AMODE**2)
      U3=(AMODE**3)
      U4=(AMODE**4)
```

```
      U5=(AMODE**5)
  101 CONTINUE
C
C
C
C     11.0 GHZ COEFFICIENTS
C
      IF(INT(FREQ).NE.11) GO TO 1
C
C     SPHERICAL DROP COEFFICIENTS
C
      IF(AMODE.GT.1.00) GO TO 10
C
      EOR=-0.0020548+0.01638947*U1-0.0417568*U2+0.08832213*U3
      EOI=-0.0025154+0.01928553*U1-0.0456816*U2+0.03655147*U3
      GO TO 11
   10 CONTINUE
C
      EOR=-1.28155706+2.83287718*U1-2.07399678*U2+0.60190887*U3
     1-0.00984194*U4-0.01096165*U5
      EOI=2.60278025-7.52434662*U1+8.14691632*U2-4.12133971*U3
     1+0.99089467*U4-0.08731788*U5
C
```

```
      GO TO 12
   11 CONTINUE
C
C     OBLATE DROP COEFFICIENTS
C
      EV90R=-0.001322+0.01036867*U1-0.025372*U2+0.07072533*U3
      EV90I=-0.0024306+0.01861967*U1-0.0440232*U2+0.03507413*U3
      EH90R=-0.0023684+0.01878307*U1-0.0473704*U2+0.09255573*U3
      EH90I=-0.0030366+0.02320527*U1-0.0546296*U2+0.04299093*U3
      DIFFR=-0.0010464+0.0084144*U1-0.0219984*U2+0.0218304*U3
      DIFFI=-0.000606+0.0045856*U1-0.0106064*U2+0.0079168*U3
C
      GO TO 1000
   12 CONTINUE
C
      EV90R=-0.3653892+0.32540943*U1+0.45280976*U2-0.53907398*U3
     1+0.20309215*U4-0.02432204*U5
      EV90I=2.20618555-6.19251766*U1+6.43873903*U2-3.090414*U3
     1+0.70600211*U4-0.0607173*U5
      EH90R=2.09022706-7.07345119*U1+9.03639726*U2-5.33156215*U3
     1+1.49716423*U4-0.15747063*U5
      EH90I=3.28654422-9.68217951*U1+10.71102231*U2-5.5491184*U3
```

```
     1+1.36694565*U4-0.12512466*U5
      DIFFI=1.08034369-3.48962081*U1+4.2722407*U2-2.45868344*U3
     1+0.66093861*U4-0.06440692*U5
C
      IF(AMODE.GT.2.0) GO TO 120
C
      DIFFR=-0.32599997+0.7531995*U1-0.57039996*U2+0.15039999*U3
      GO TO 1000
C
  120 CONTINUE
C
      DIFFR=11.94200847-14.59334299*U1+5.80600359*U2-0.7346671*U3
C
      GO TO 1000
C
    1 CONTINUE
C
C     14 GHZ COEFFICIENTS
C
```

```
      IF(INT(FREQ).NE.14) GO TO 2
C
C     SPHERICAL DROP COEFFECIENTS
C
      IF(AMODE.GT.1.00) GO TO 20
C
      FOR=-0.001376+0.012776*U1-0.040136*U2+0.128736*U3
      EOI=-0.008796+0.06731467*U1-0.1588*U2+0.12418133*U3
C
      GO TO 21
   20 CONTINUE
C
      EOR=-12.13707993+34.85683676*U1-37.84887378*U2+19.48995359*U3
     1-4.69149894*U4+0.42548477*U5
      EOI=-8.4550178+22.97909617*U1-23.38444001*U2+11.09553161*U3
     1-2.41694538*U4+0.19907664*U5
C
      GO TO 22
   21 CONTINUE
C
C     OBLATE DROP COEFFICIENTS
C
```

```
      EV90R=-0.000248+0.00335467*U1-0.013928*U2+0.10002133*U3
      EV90I=-0.008436+0.06455867*U1-0.152256*U2+0.11893333*U3
      EH90R=-0.000656+0.007656*U1-0.029656*U2+0.122656*U3
      EH90I=-0.010366+0.079154*U1-0.18596*U2+0.143872*U3
      DIFFR=-0.000408+0.00430133*U1-0.015728*U2+0.02263467*U3
      DIFFI=-0.00193+0.01459533*U1-0.033704*U2+0.02493867*U3
C
      GO TO 1000
   22 CONTINUE
C
      EV90R=-4.48493663+12.45481829*U1-12.90182271*U2+6.32901913*U3
     1-1.42805671*U4+0.11875301*U5
      EV90I=-0.1923376+0.3425132*U1-0.196242*U2+0.07468968*U3
C
      IF(AMODE.GT.2.5) GO TO 24
C
      EH90I=1.10278458-3.74696237*U1+4.48042001*U2-2.22964317*U3
     1+0.42010037*U4
      DIFFR=-0.15268404+0.39830845*U1-0.3527577*U2+0.11767014*U3
```

```
      DIFFI=-1.29960041+2.93303524*U1-2.15255009*U2+0.5206384*U3
C
      IF(AMODE.GT.2.00) GO TO 25
C
      EH90R=-1.02599992+2.30733317*U1-1.60799988*U2+0.4266664*U3
C
      GO TO 1000
   24 CONTINUE
C
      EH90I=2.51000033-2.03000022*U1+0.62000004*U2
      DIFFR=-15.85152202+18.27189723*U1-6.68140666*U2+0.79411153*U3
      DIFFI=22.32321586-44.48681458*U1+30.17926125*U2-8.46925565*U3
     1+0.85300427*U4
C
      GO TO 1000
   25 CONTINUE
C
      EH90R=-19.65+20.6567*U1-6.66*U2+0.6933*U3
C
      GO TO 1000
    2 CONTINUE
C
C     20 GHZ COEFFICIENTS
C
```

```
      IF(INT(FREQ).NE.20) GO TO 3
C
C     SPHERICAL DROP COEFFICIENTS
C
      IF(AMODE.GT.1.0) GO TO 30
C
      EOR=0.020296-0.145276*U1+0.297656*U2+0.008224*U3
C
      EOI=-0.015488+0.12709133*U1-0.334568*U2+0.30583467*U3
C
      GO TO 31
   30 CONTINUE
C
      EOR=3.35567152-8.61818659*U1+7.8157989*U2-2.68217917*U3
     1+0.3108073*U4
      EOI=1.85636463-3.70750898*U1+2.19599302*U2-0.25148145*U3
C
      GO TO 32
   31 CONTINUE
C
C     OBLATE COEFFICIENTS
C
```

```
      EV90R=0.02454800-0.17912133*U1+0.384448*U2-0.07447467*U3
      EV90I=-0.013492+0.11190533*U1-0.299032*U2+0.27853867*U3
      EH90R=0.02282-0.16596667*U1+0.34976*U2-0.03061333*U3
      EH90I=-0.015178+0.12623933*U1-0.33848*U2+0.31533867*U3
      DIFFR=0.000072+0.00175467*U1-0.015488*U2+0.03426133*U3
      DIFFI=-0.001686+0.014334*U1-0.039448*U2+0.0368*U3
C
      GO TO 1000
   32 CONTINUE
C
      EV90R=1.56037246-3.97019757*U1+3.66524972*U2-1.24458239*U3
     1+0.14526662*U4
      EV90I=4.77376463-13.63610787*U1+14.83397997*U2
     1-7.66136891*U3+1.96881573*U4-0.19749381*U5
      EH90R=4.63026679-11.97374109*U1+11.0254653*U2
     1-4.0050613*U3+0.50244373*U4
      EH90I=-1.5390057+6.3417866*U1-9.35328879*U2+6.20987895*U3
     1-1.74544867*U4+0.17820925*U5
      DIFFR=3.06989428-8.00354339*U1+7.36021547*U2
```

```
     1-2.76047886*U3+0.3571771*U4
      DIFFI=-6.31274803+19.97783334*U1-24.1872053*U2+13.8712166*U3
     1-3.71425705*U4+0.3757024*U5
C
      GO TO 1000
    3 CONTINUE
C
      IF(INT(FREQ).NE.30) GO TO 2000
C
C     30 GHZ COEFFICIENTS
C
C     SPHERICAL DROP COEFFICIENTS
C
      IF(AMODE.GT.1.0) GO TO 40
C
      EOR=0.028004-0.221564*U1+0.530744*U2+0.022816*U3
      EOI=-0.007072+0.09329866*U1-0.390112*U2+0.55688533*U3
C
      GO TO 41
   40 CONTINUE
C
      EOR=-1.95096901+3.4107597*U1-0.82790307*U2-0.39982485*U3
```

```
     1+0.1291964*U4
      EOI=5.77798866-16.3876166*U1+16.10102407*U2-6.06482662*U3
     1+0.82747918*U4
C
      GO TO 42
   41 CONTINUE
C
C     OBLATE DROP COEFFICIENTS
C
      EV90R=0.03542-0.2838733*U1+0.7038*U2-0.15834666*U3
      EV90I=0.013876-0.064756*U1-0.026904*U2+0.290784*U3
      EH90R=0.031652-0.252652*U1+0.614952*U2-0.049952*U3
      EH90I=-0.000532+0.04746533*U1-0.299512*U2+0.50957867*U3
      DIFFR=-0.003768+0.03122133*U1-0.088848*U2+0.10839467*U3
      DIFFI=-0.014408+0.11222133*U1-0.272608*U2+0.21879467*U3
C
      GO TO 1000
   42 CONTINUE
C
      EV90R=3.93161268-10.97208846*U1+11.43870068*U2
     1-4.78953064*U3+0.69447892*U4
      EV90I=3.12729055-9.08249632*U1+9.16246329*U2
```

```
     1-3.47227982*U3+0.47789632*U4



      EH90R=-6.97583584+16.79179963*U1-13.53607686*U2
     1+4.63811854*U3-0.57535653*U4
      EH90I=-1.39373246+1.72736066*U1-0.14076091*U2+0.05474057*U3
      DIFFR=-10.90744851+27.76388807*U1-24.97477753*U2
     1+9.42764918*U3-1.26983545*U4
      DIFFI=5.33984552-17.20920477*U1+20.7812541*U2
     1-11.64360435*U3+3.07942984*U4-0.30370378*U5
C
 1000 CONTINUE
C
      ALPH=1.576796-LOKANG
      CSLA=0.001*COS(ALPH)**2
      SNLA=0.001*SIN(ALPH)**2
      EVR=CSLA*EQR+SNLA*EV90R
      EVI=-CSLA*EQI-SNLA*EV90I
      EHR=CSLA*EQR+SNLA*EH90R
      EHI=-CSLA*EQI-SNLA*EH90I
      DIFFR=-SNLA*DIFFR
```

```
      DIFFI=SNLA*DIFFI
      EOR=0.001*EOR
      EOI=-0.001*EOI
C
      FV=CMPLX(FVR,FVI)*AK1
      FH=CMPLX(FHR,FHI)*AK1
      FSPH=CMPLX(EOR,EOI)*AK1
      DIFF=CMPLX(DIFFR,DIFFI)*AK1
C
      GO TO 3000
C
 2000 WRITE(6,2001)
 2001 FORMAT(//,3X,'FREQUENCY NOT ALLOWED, ONLY 11,14,20,30 GHZ ALLOWED'
     1)
C
      STOP
 3000 CONTINUE
C
      RETURN
      END
C
C
```

```
      SUBROUTINE OUTANT(EXN,EYN,EXC,EYC,EXX,EYX,ISOL1,ATTEN1,PHASE1)
C
C     THIS SUBROUTINE TAKES THE X AND Y COMPONENTS OF THE WAVE EXITING
C     THE RAIN CELL (EXN,EYN) AND USES THE COMPLEX VECTOR METHOD
C     TO COMPUTE VALUES FOR ATTENUATION, ISOLATION, AND PHASE AS A
C     RESULT OF THE RAIN MEDIUM AND POLARIZATION MISMATCH EFFECTS OF THE
C     RECEIVE ANTENNA
C     THIS DATA IS STORED IN PROGRAM MEMORY FOR LATER OUTPUT
C     THIS SUBROUTINE WAS WRITTEN BY PRESINGER.
C
      REAL ISOL1
      COMMON/BLOC1/MINUSJ,CONV
      COMMON/BLOC2/ VWACM
      COMPLEX MINUSJ
      COMPLEX  EXC,EYC,EXX,EYX



      COMPLEX  VWPAC,VWPAX
      COMPLEX  EXN,EYN
      REAL  VWPACM,VWPAXM
C
```

```
      VWPAC=EXN*EXC + EYN*EYC
      VWPAX=EXN*EXX + EYN*EYX
C
C
      VWPACR=REAL(VWPAC)
      VWPACI=AIMAG(VWPAC)
      VWPACM=CABS(VWPAC)
      VWPACR=ATAN2(VWPACI,VWPACR)
      VWPACP=VWPACR/CONV
C
      VWPAXR=REAL(VWPAX)
      VWPAXI=AIMAG(VWPAX)
      VWPAXM=CABS(VWPAX)
      IF(VWPAXM.EQ.0.0) GO TO 10
      VWPAXR=ATAN2(VWPAXI,VWPAXR)
      VWPAXP=VWPAXR/CONV
      IF(VWPAXM.LE.0.000001) VWPAXP=0.0
C
      ISOL1=20.*ALOG10(VWPACM/VWPAXM)
      GO TO 11
   10 CONTINUE
      VWPAXP=0.0
```

```
      ISOL1=999.99
   11 CONTINUE
C
      PHASE1=VWPAXP-VWPACP
C
      IF(PHASE1.LT.0.0) PHASE1=PHASE1+360.0
C
      ATTEN1=20.*ALOG10(VWACM/VWPACM)
C
      RETURN
      END
C
C
      SUBROUTINE COMPNT(EPS,TAU,EX,EY)
C
C     THIS SUBROUTINE RETURNS THE X AND Y COMPONENTS GIVEN AN EPSILON
C     AND TAU (IN DEGREES) DESCRIBING AN ARBITRARY POLARIZATION STATE
C
      COMPLEX  EX,EY
      COMPLEX MINUSJ
      COMMON/BLOC1/MINUSJ,CONV
C
```

```
      EPSR=EPS*CONV
      TAUR=TAU*CONV
C
      IF(ABS(EPSR).EQ.(45.*CONV)) GO TO 1
      IF(EPSR.EQ.0.) GO TO 2
      IF(TAUR.EQ.0.) GO TO 3
      IF(TAUR.EQ.(90.*CONV)) GO TO 4
C
      T1=TAN(2.*EPSR)
      T2=SIN(2.*TAUR)
      DELTR=ATAN2(T1,T2)
      GAMR=0.5*ARCOS(COS(2*EPSR)*COS(2*TAUR))
      GO TO 100
    1 DELTR=2.*EPSR
      GAMR=45.*CONV
      GO TO 100
    2 DELTR=0.
      GAMR=TAUR
      GO TO 100
```

```
    3 DELTR=SIGN(1.,EPSR)*90.*CONV
      GAMR=ABS(EPSR)
      GO TO 100
    4 DELTR=SIGN(1.,EPSR)*90.*CONV
      GAMR=90.*CONV-ABS(EPSR)
  100 CONTINUE
C
      EX=COS(GAMR)
      EY=SIN(GAMR)*CEXP(-MINUSJ*DELTR)
C
      RETURN
      END
```

APPENDIX C

DERIVATION OF THE DYSON EQUATION FOR $G(R, r, k)$ in THE CASE OF SMOOTHLY INHOMOGENEOUS DISCRETE MEDIA

From Eq. (5-17) $\langle G'(\vec{r}_1, \vec{r}_2, k)\rangle$ obeys the equation

$$\{\nabla^2_{\vec{r}_1} + k^2 + 4\pi f\, \rho(\vec{r}_1)\}\, \langle G'(\vec{r}_1, \vec{r}_2, k)\rangle$$

$$= -4\pi f\, \delta(\vec{r}_1 - \vec{r}_2) - 4\pi \int_{R^3} N_1'(\vec{r}_1, \vec{r}', k)\, \langle G'(\vec{r}', \vec{r}_2, k)dr'\rangle \qquad \text{(C-1)}$$

The kernel $N_1'(\vec{r}_1, \vec{r}', k)$ in (C-1) is called the "mass operator", and is defined [cf., also, Eq. (5.22b) as follows:

$$N_1'(\vec{r}_1, \vec{r}', k) = f\, \langle G'(\vec{r}_1, \vec{r}', k)\rangle\, B(\vec{r}_1, \vec{r}') \qquad \text{(C-2)}$$

Our specific intent in this Appendix is to show that (C-1) simplifies to (5-29) in the case of smoothly inhomogeneous media. Toward this end, we introduce in (C-1) the center-of-mass and difference coordinates $\vec{R} = (\vec{r}_1 + \vec{r}_2)/2$, $\vec{r} = \vec{r}_1 - \vec{r}_2$:

$$\{\nabla^2_{\vec{r}} + 1/2\, \nabla^2_{\vec{R}} - \nabla_{\vec{R}}\, \nabla_{\vec{r}} + k^2 + 4\pi f\, \rho(\vec{R} + 1/2\, \vec{r})\}\, \langle G(\vec{R}, \vec{r}, k)\rangle$$

$$= -4\pi f\, \delta(\vec{r}) - 4\pi \int_{R^3} d\vec{r}_1'\, N_1'(\vec{R} + 1/2\, \vec{r}, \vec{r}_1', k)\, \langle G'(\vec{r}_1', \vec{R} - 1/2\, \vec{r}, k)\rangle$$

(C-3)

We resort, also, to the change of variable $\vec{r}_1' = \vec{R} + 1/2\, \vec{r} - \vec{r}'$. The latter bring (C-3) into the convenient form

$$\{\nabla^2_{\vec{r}} + \frac{1}{4}\nabla^2_{\vec{R}} - \nabla_{\vec{R}} \cdot \nabla_{\vec{r}} + k^2 + 4\pi f\, \rho(\vec{R} + 1/2\, \vec{r})\} \langle G(\vec{R}, \vec{r}, k)\rangle$$

$$= -4\pi f\, \delta(\vec{r}) - 4\pi \int d\vec{r}'\, N_1(\vec{R} + (\vec{r} - \vec{r}')/2, \vec{r}', k)\, \langle G(\vec{R} - 1/2\, \vec{r}', \vec{r} - \vec{r}', k)\rangle$$

(C-4)

Finally, we invoke the quasihomogeneity condition (cf. Sec. 5.3.2), u under which $\rho(\vec{R} + 1/2\, \vec{r})$, $N_1(\vec{R} + (\vec{r} - \vec{r}')/2, \vec{r}', k)$, $\langle G(\vec{R} - 1/2\, \vec{r}', \vec{r} - \vec{r}', k)\rangle$ are slowly varying functions of $\vec{R}$ and fast varying functions of $\vec{r}$. Retaining only dominant terms, (C-4) simplifies in this case to the Dyson equation (5-29), viz.,

$$\nabla^2_{\vec{r}}\, \langle G(\vec{R}, \vec{r}, k)\rangle + [k^2 + 4\pi f\, \rho(\vec{R})]\, \langle G(\vec{R}, \vec{r}, k)\rangle$$

$$= -4\pi f\, \delta(\vec{r}) - 4\pi \int_{R^3} d\vec{r}'\, N_1(\vec{R}, \vec{r} - \vec{r}', k)\, \langle G(\vec{R}, \vec{r}', k)\rangle \quad . \qquad \text{(C-5)}$$

APPENDIX D

DERIVATION OF THE TRANSPORT EQUATION FOR $f_o(\vec{R}, \vec{n}, k_s, k_d)$

Consider the stochastic lossy Helmholtz equation (5-17) at two spatial points $\vec{r}_1$, $\vec{r}_2$ and wavenumbers k_1, k_2. We have, then,

$$\{\nabla_{\vec{r}_1}^2 + k_1^2 + 4\pi f\, \rho(\vec{r}_1)\} \langle E(\vec{r}_1, k_1)\rangle$$

$$+ 4\pi \int_{R^3} d\vec{r}'\, N_1(\vec{r}_1, \vec{r}', k_1) \langle E(\vec{r}', k_1)\rangle = 0 \quad , \tag{D-1a}$$

$$\{\nabla_{\vec{r}_2}^2 + k_2^2 + 4\pi f\, \rho(\vec{r}_2)\} \langle E(\vec{r}_2, k_2)\rangle$$

$$+ 4\pi \int_{R^3} d\vec{r}'\, N_1(\vec{r}_2, \vec{r}', k_1) \langle E(\vec{r}, k_2)\rangle = 0 \quad . \tag{D-1b}$$

We recall next from (5.4.2) the definition

$$\Gamma_o'(\vec{r}_1, \vec{r}_2, k_1, k_2) = \langle E(\vec{r}_1, k_1)\rangle \langle E^*(\vec{r}_2, k_3)\rangle \quad , \tag{D-2}$$

and use it in conjunction with (D-1) in order to obtain the equation

$$(\nabla_{\vec{r}_1} - \nabla_{\vec{r}_2})\, \Gamma_o'(\vec{r}_1, \vec{r}_2, k_1, k_2) + (k_1^2 - k_2^2) + 4\pi\{f\, \rho(\vec{r}_1)$$

$$- f^*\, \rho(\vec{r}_2)\}\, \Gamma_o'(\vec{r}_1, \vec{r}_2, k_1, k_2) + 4\pi \int_{R^3} d\vec{r}'\, N_1'(\vec{r}_1, \vec{r}', k_1)$$

$$\Gamma_o'(\vec{r}', \vec{r}_2, k_1, k_2) - 4\pi \int d\vec{r}'\, N_1^*(\vec{r}_2, \vec{r}', k_2)\, \Gamma_o'(\vec{r}_1, \vec{r}', k_1, k_2)$$

$$= 0 \quad , \tag{(D-3)}$$

which is analogous to (5-21).

Our subsequent steps are identical to those followed in subsections 5.3.2 and 5.3.3. They lead ultimately to the transport equation

$$2j\vec{n} \cdot \nabla_{\vec{n}} f_o(\vec{R}, \vec{n}, k_s, k_d) + k_s k_d f_o(\vec{R}, \vec{n}, k_s, k_d)$$

$$+ 4\pi j f_R \nabla_{\vec{R}} \rho(\vec{R}) \cdot \nabla_{\vec{n}} f(\vec{R}, \vec{n}, k_s, k_d) + 8\pi j f_I \rho(\vec{R}) f(\vec{R}, \vec{n}, k_s, k_d)$$

$$= -4\pi \tilde{N}_1(\vec{R}, \vec{n}, k_1) f_o(\vec{R}, \vec{n}, k_s, k_d) + 4\pi \tilde{N}_1^*(\vec{R}, \vec{n}, k_2) f_o(\vec{R}, \vec{n}, k_s, k_d)$$

$$- 4\pi j \nabla_{\vec{R}} \tilde{N}_1(\vec{R}, \vec{n}, k_1) \cdot \nabla_{\vec{n}} f_o(\vec{R}, \vec{n}, k_s, k_d)$$

$$+ 4\pi j \nabla_{\vec{n}} \tilde{N}_1(\vec{R}, \vec{n}, k_1) \cdot \nabla_{\vec{R}} f(\vec{R}, \vec{n}, k_s, k_d) \qquad \text{(D-4)}$$

for $f_o(\vec{R}, \vec{n}, k_s, k_d) \longleftrightarrow \Gamma_o(\vec{R}, \vec{r}, k_s, k_d)$. Equation (D-4) can be brought into desired form (5-38) if the definition of the effective Hamiltonian $H'(\vec{R}, \vec{n}, k_s)$ is taken into consideration.

The vita has been removed from the scanned document

MULTIPLE SCATTERING OF ELECTROMAGNETIC WAVES BY RANDOM DISTRIBUTIONS OF PARTICLES WITH APPLICATIONS TO RADIO WAVE PROPAGATION THROUGH PRECIPITATION

by

Anastasios I. Tsolakis

(ABSTRACT)

The Twersky procedure is used to derive the vector Foldy-Lax-Twersky integral equation (Dyson equation) for the coherent field in a random distribution of particles. The above equation is applied to ice depolarization and rain attenuation and depolarization. Twersky's procedure is then extended in order to derive a vector-valued Dyson equation and a tensor-valued two-frequency Bethe-Saltpeter equation for waves propagating in a distribution of spatially pair correlated absorptive scatterers. From these equations a systematic transition is made to a two-frequency radiative transfer equation suitable forpusled scalar waves in the presence of a tenuous distribution of absorptive isotropic discrete scatterers with pair correlations.